Thesis

学 位 論 文

Transport Phenomena in the d-p Model

d-p 模 型 に お け る 輸 送 現 象

1994

Isao Sawada
沢 田 功

Department of Physics,
Nagoya University, Nagoya 464-01, Japan

主　論　文

Thesis

学 位 論 文

Transport Phenomena in the d-p Model

d-p 模 型 に お け る 輸 送 現 象

1994

Isao Sawada
沢 田　功

Department of Physics,
Nagoya University, Nagoya 464-01, Japan

Acknowledgements

First of all, I thank Prof. Yoshihiro Kuroda for his patient discussions and encouragements throughout this work from the very beginning.

I thank Prof. Tamifusa Matsuura for his educational advice for years and Dr. Yoshiaki Ōno for his valuable information and discussions on this work.

I acknowledge the stimulating discussions with Prof. Shin-ichi Uchida, University of Tokyo, on the generalized Drude analyses (GDA) of the optical spectra of high-T_c superconductors.

I am grateful to Dr. Kazuhiro Sano, Mie University, and Dr. Akio Tokumitu, Nagoya City University, for their advice on the numerical calculations, Dr. D. S. Hirashima, University of Tsukuba, for his useful discussions on this work, and Dr. Hideo Yoshioka and Mr. Munehiro Azami for their constant encouragements.

This work is supported by Grant-in-Aid for Scientific Research on Priority Areas, Science of High-T_c Superconductivity from the Ministry of Education, Science and Culture.

Finally, this thesis is dedicated to my parents, Takashi (隆) and Akiko (彰子), on the occasion of the 30th anniversary of their married life, my lovely sister, Ritsuko (律子), and my grandmother, Kazu Inoue (井上カヅ), on the occasion of the 90th anniversary of her life.

Abstract

We develop an approximation procedure to calculate the optical conductivity $\sigma(\omega)$ and the electronic Raman scattering intensity in the d-p model by including terms of the leading order in the expansion from the large limit of the spin-orbital degeneracy N at $T \lesssim T_0$, where the well-defined quasi-particle states called *ingap states* emerge inside the charge transfer gap upon hole doping to the half-filled case. In above, T_0 is the coherence temperature of $0.2\omega_0$, where ω_0 is a half of the band width of the *ingap states* at $T = 0$ and is proportional to the doped hole concentration δ at $\delta \lesssim 0.1$. The *ingap states* are shown to contribute to the Drude components in $\sigma(\omega)$ with the intensity also proportional to δ at $\delta \lesssim 0.1$, as has been observed in experiments. Both of the ω- and the T-dependences in $\sigma(\omega)$ are found to be scaled well by ω_0. The generalized Drude analyses (GDA) of $\sigma(\omega)$ show that both of the optical mass $m_{\rm opt}(\omega)$ and the optical scattering rate $\tau^*_{\rm opt}(\omega)^{-1}$ are only weakly ω-dependent in contradiction to the experimental observations, which seems to suggest that the *ingap states* at $T \lesssim T_0$ do not account for the anomalous optical properties of high-T_c superconductors. We show that the ω-dependence of the quasi-particle scattering rate plays a crucial role for determining the ω-dependence of the optical mass $m_{\rm opt}(\omega)$ and comment on the confusion regarding GDA seen among physicists.

Key words: d-p model, slave-boson, $1/N$-expansion, ingap states,
optical conductivity, electronic Raman scattering, generalized Drude analyses

Contents

Chapter 1

Introduction

Discovery of high-T_c superconducting cuprates [1)] has taken physicists to an intriguing field of solid state physics. That is physics of strongly correlated system. In this chapter, we overview some experimental aspects of such a fascinating field and outline the present theoretical study.

We briefly discuss the electronic states of the representative perovskite $La_{2-x}Sr_xCuO_4$ as a function of x in the electron-representation. The electronic configurations of the compound with $x = 0$, i.e., La_2CuO_4, are composed of the closed electronic shells, $La^{3+}(5p^6)$ and $O^{2-}(2p^6)$, and the open electronic shell, $Cu^{2+}(3d^9)$. The Cu $3d_{x^2-y^2}$ state, which is the highest in energy because of the crystal field splitting of the five-fold degenerate $3d$ states, is singly occupied. Then the system is expected to be conductor from the simple band theory, but it behaves as an antiferromagnetic insulator. This is because the intraatomic Coulomb repulsion at the Cu sites, U, is much larger than the band width. Since the energy levels line to be $\epsilon_d < \epsilon_p < \epsilon_d + U$, not $\epsilon_p < \epsilon_d < \epsilon_d + U$, with the Cu $3d_{x^2-y^2}$-level ϵ_d and the O $2p_\sigma$-level ϵ_p, it is also called the charge transfer insulator.

Substituting $Sr^{2+}(4p^6)$ ions for $La^{3+}(5p^6)$ ions yields the hole doped compound with $x > 0$ and these holes are expected to fill the Bloch band consisting of $2p_\sigma$ orbitals. However, because of strong correlation effects the doped holes in CuO_2 layers form a coherent band called *ingap states* that emerge inside the charge transfer gap $\Delta = \epsilon_d + U - \epsilon_p$ with intensity increasing with x. Though the superconducting compounds are obtained in the region $0.06 \lesssim x \lesssim 0.25$ with the maximum $T_c \simeq 39K$, their metallic phases are reported,

irrespective of x, to show anomalous properties compared with the conventional metals. The anomalous properties stated below are in common with other superconducting Y-, B_i-, and Tl-based cuprates.

Among those are: (1) The in-plane resistivity increases approximately linearly with temperature T over the wide temperature range in the normal phases. [2) – 6)] The linear-in-T behavior reminds us of the Bloch-Grüneisen formula at $T \gtrsim 0.25\Theta_D$ with Debye temperature Θ_D. However, the temperature range of that is much wider than this. We note that the T^2-behavior is observed in heavy fermion compounds at low temperatures well below the Fermi temperature. (2) The Drude components of the optical conductivity decrease much slowly with frequency ω as $\omega^{-\alpha}$ with $\alpha < 2$ compared with the conventional Drude tail, ω^{-2}. [7) – 15)] (3) The electronic Raman scattering intensities show anomalously broad peaks extended up to several thousands of cm^{-1} irrespective of polarization geometries. [16) – 21)] As far as the intraband transitions in the conventional metals are concerned, the Fermi liquid theory predicts that the electronic Raman scattering should extend at most up to few hundreds of cm^{-1} for the parallel polarization geometries, while, no scattering for the crossed polarization geometries. (4) And other transport coefficients such as the Hall coefficient and the thermoelectric power show the strong T-dependences up to few times of room temperature [22, 23)] and so on.

Thus, it has been widely believed that the 2D-electronic systems in CuO_2 layers play most crucial roles to bring about high-T_c superconductivity and show numbers of anomalous properties in the metallic states compared with the conventional superconducting materials. [24, 25)] The understanding of these anomalous properties is thought to be crucial clues to uncover the mechanism of high-T_c superconductivity. Various types of approaches have been presented so far to promote such understanding but unfortunately no conclusive solution to explain these anomalous properties in a unified manner has been obtained yet. [26) – 39)]

In the present study, we investigate transport properties of the normal phase of the simplest d-p model simulating the 2D-electronic system in CuO_2 layers, which is described in the hole-picture with the fundamental parameters such as the Cu $3d_{x^2-y^2}$-level ϵ_d, the O $2p_\sigma$-level ϵ_p, the transfer integral between the adjacent Cu and O sites, t_{pd}, and the

intraatomic Coulomb repulsion at the Cu sites, U. Furthermore, we assume U to be infinity to exclude the Cu^{3+}-states and introduce the auxiliary bosons to describe the hole-empty states, i.e., the Cu^{1+}-states. We impose the strict local constraints [40] which guarantee the equivalence between the original infinite-U model and the modified version in the auxiliary boson representation. We employ the perturbation expansion from the large limit of the spin-orbital degeneracy N ($1/N$-expansion method).

Some extensive studies on the single particle properties of the same model as described above have been done by several authors. [41) – 46)] Jichu et al. [41, 42)] have studied the properties at $T = 0$ and found that upon hole doping at the half-filled case (the ionic $Cu^{2+}O^{2-}$-states) in the d-p model the coherent quasi-particle states (called *ingap states*) emerge inside the charge transfer gap $\Delta = \epsilon_p - \epsilon_d$, that the integrated intensity and the band width of the ingap states are increasing with the doped hole concentration δ, and that the Fermi surface is determined by the Luttinger's sum rule which results in the Fermi level almost in the midst of the band. Hirashima et al. [44)] have found that the system is insulating at the half-filled case with $\delta = 0$ when Δ is equal to or larger than a certain critical value, Δ_c. These findings are very specific to such highly correlated states as the ingap states.

Ōno et al. [51)] have studied the properties at finite temperatures by solving numerically a set of the self-consistent equations (SCE) for the single-particle Green's functions obtained within the approximation to the leading order in the $1/N$-expansion. What they have found are: There exist the two characteristic energies in the system, ω_0 and T_0, where ω_0 is the binding energy of the slave bosons at $T = 0$, which corresponds to the Kondo temperature T_K in the Kondo lattice model and is proportional to δ at $\delta \lesssim 0.1$, and T_0 is the coherence temperature of $0.2\omega_0$. At low temperatures $T < T_0$, the ingap states are well-defined and behave as Fermi liquid. At high temperatures $T > \omega_0$, the p-holes are scattered incoherently by the d-holes which behave as localized spins and the quasi-particle picture completely collapse. At intermediate temperatures, $T_0 < T < \omega_0$, the crossover phenomena between the two limiting cases are observed and the system shows several anomalous behaviors. For example, the p-hole scattering rate at the chemical potential $\mu(T)$ is proportional to $(T - T_0)$.

In the present study, we investigate the transport properties of the ingap states at $T \lesssim T_0$ in order to examine how the quasi-particle picture for the ingap state is going to collapse as the temperature increases. We develop an approximation procedure to determine the single-particle properties at $T \lesssim T_0$ and calculate the optical conductivity $\sigma(\omega)$ and the electronic Raman scattering intensity $I(\omega)$ in the d-p model by including terms of the leading order in the $1/N$-expansion.

What we find are: the *ingap states* are shown to contribute to the Drude components in $\sigma(\omega)$ with the intensity also proportional to δ at $\delta \lesssim 0.1$, as has been observed in experiments. Both of the ω- and the T-dependences in $\sigma(\omega)$ are found to be scaled well by ω_0. The generalized Drude analyses (GDA) of $\sigma(\omega)$ show that both of the optical mass $m_{\rm opt}(\omega)$ and the optical scattering rate $\tau^*_{\rm opt}(\omega)^{-1}$ are only weakly ω-dependent in contradiction to the experimental observations, which seems to suggest that the *ingap states* at $T \lesssim T_0$ do not account for the anomalous optical properties of high-T_c superconductors. We show that the ω-dependence of the quasi-particle scattering rate plays a crucial role for determining the ω-dependence of the optical mass $m_{\rm opt}(\omega)$ and comment on the confusion regarding GDA seen among physicists.

In Ch.2, we present the model and review the results obtained by the earlier studies regarding the single-particle Green's functions, which are needed to calculate the transport coefficients. In Ch.3, using an approximation justified in the low temperature limit, we calculate the single-particle properties at $T \lesssim T_0$. In Ch.4, we derive the formulae to calculate the transport coefficients such as optical conductivity and electronic Raman scattering of the leading order in the $1/N$-expansion and present their numerical results. Finally, we summarize and discuss the results obtained in the present study in Ch.5.

Chapter 2

Model and Formulation

Here we review the model and the formulation for determining the single-particle Green's functions given in the earlier studies [41) - 46)] and to be used in the present study. We employ the simplest 2D d-p model in the slave-boson representation, which is given in the hole-picture by

$$H = H_p + H_d + H_{dp}, \tag{2.0.1}$$

with

$$H_p \equiv \epsilon_p \sum_{\mathbf{k}} \sum_{\sigma} c^{\dagger}_{\mathbf{k}\sigma} c_{\mathbf{k}\sigma} + \epsilon_p \sum_{\mathbf{k}} \sum_{\sigma} c^{0\dagger}_{\mathbf{k}\sigma} c^{0}_{\mathbf{k}\sigma}, \tag{2.0.2}$$

$$H_d \equiv \epsilon_d \sum_{i} \sum_{\sigma} d^{\dagger}_{i\sigma} d_{i\sigma}, \tag{2.0.3}$$

$$H_{dp} \equiv N_{\rm L}^{-\frac{1}{2}} \sum_{i} \sum_{\mathbf{k}} \sum_{\sigma} \Big(\mathrm{e}^{-\mathrm{i}\mathbf{k}\cdot\mathbf{R}_i} t_{\mathbf{k}} c^{\dagger}_{\mathbf{k}\sigma} d_{i\sigma} b^{\dagger}_{i} + h.c. \Big), \tag{2.0.4}$$

where $c^{\dagger}_{\mathbf{k}\sigma}$ and $c^{0\dagger}_{\mathbf{k}\sigma}$ are the creation operators for the O-$2p_\sigma$ hole of the bonding and non-bonding orbitals. [†] The operators $b^{\dagger}_{i}$ and $d^{\dagger}_{i\sigma}$ create the slave-boson representing a Cu $3d_{x^2-y^2}$ hole-empty state (Cu^{1+}-state) and the pseudo-fermion representing a Cu $3d_{x^2-y^2}$ singly occupied state (Cu^{2+}-state), respectively. The total number of the unit cells is $N_{\rm L}$. The atomic energies of the p- and d- holes, $\epsilon_p = \epsilon^0_p - \mu(T)$ and $\epsilon_d = \epsilon^0_d - \mu(T)$, are measured

[†]The non-bonding orbitals are unoccupied and can be removed out of the problem at $T = 0$,[41, 42, 44)] while, at finite temperatures, they are partly occupied and must be taken into account in order to determine the temperature dependence of physical quantities as seen in Ch.3.

relative to the chemical potential. The transfer energy, $t_{\mathbf{k}}$, is given by

$$t_{\mathbf{k}} \equiv \sqrt{W(\mathbf{k})} = 2t_{pd}\sqrt{1-(\cos k_x a + \cos k_y a)/2}, \tag{2.0.5}$$

with the transfer integral between the adjacent Cu and O sites, t_{pd}, and the lattice constant a. This model (2.0.1) is equivalent to the original infinite-U d-p model as long as it is treated within the physical space where the following local constraints hold:

$$\hat{Q}_i \equiv b_i^\dagger b_i + \sum_\sigma d_{i\sigma}^\dagger d_{i\sigma} = 1, \quad (i = 1, 2, \cdots, N_{\rm L}). \tag{2.0.6}$$

The expectation value of an operator $\hat{O}$ calculated within the physical space, i.e., under the local constraints, eq.(2.0.6), is given by [40, 47]

$$\langle \hat{O} \rangle = \lim_{\{\lambda_i\}\to\infty} \langle \hat{O} \prod_i \hat{Q}_i \rangle_\lambda \; / \; \langle \prod_i \hat{Q}_i \rangle_\lambda, \tag{2.0.7}$$

where $\langle \hat{A} \rangle_\lambda$ is calculated in the grand canonical ensemble for the Hamiltonian H_λ:

$$\langle \hat{A} \rangle_\lambda \equiv {\rm Tr}[{\rm e}^{-\beta H_\lambda}\hat{A}] \; / \; {\rm Tr}[{\rm e}^{-\beta H_\lambda}], \tag{2.0.8}$$

with

$$H_\lambda \equiv H + \sum_i \lambda_i \hat{Q}_i. \tag{2.0.9}$$

For calculating $\langle \hat{A} \rangle_\lambda$, we employ the perturbation expansion from the large limit of the spin-orbital degeneracy N using the Feynman diagrams ($1/N$-expansion method). See the references [47], [48], and [49] for the details of the $1/N$-expansion method. Following the procedure mentioned above we calculate the single-particle Green's functions within the approximation to the leading order in the $1/N$-expansion. Then, the explicit forms of the p-hole, the slave-boson and the pseudo-fermion Green's functions are given, respectively, by

$$G_p(\mathbf{k}, {\rm i}\omega_n) \simeq [\, {\rm i}\omega_n - \epsilon_p - \Sigma(\mathbf{k}, {\rm i}\omega_n)\,]^{-1}, \tag{2.0.10}$$

$$B_i({\rm i}\nu_n) \simeq [\, {\rm i}\nu_n - \lambda_i - \Pi_i({\rm i}\nu_n)\,]^{-1}, \tag{2.0.11}$$

$$F_{i\sigma}({\rm i}\omega_n) \simeq [\, {\rm i}\omega_n - \epsilon_d - \lambda_i\,]^{-1}, \tag{2.0.12}$$

where the self-energy parts are given by

$$\Sigma(\mathbf{k}, {\rm i}\omega_n) \equiv W(\mathbf{k}) P({\rm i}\omega_n), \tag{2.0.13}$$

$$\Pi_i({\rm i}\nu_n) \equiv \frac{1}{N_{\rm L}} \sum_{\mathbf{k}} \sum_\sigma W(\mathbf{k})\, T \sum_{\omega_{n'}} F_{i\sigma}({\rm i}\omega_{n'} + {\rm i}\nu_n) G_p(\mathbf{k}, {\rm i}\omega_{n'}), \tag{2.0.14}$$

with

$$P(\mathrm{i}\omega_n) \equiv \lim_{\lambda_i\to\infty}[\, -T\sum_{\nu_{n'}} F_{i\sigma}(\mathrm{i}\omega_n+\mathrm{i}\nu_{n'})B_i(\mathrm{i}\nu_{n'}) \,/\, \langle\hat{Q}_i\rangle_\lambda \,], \tag{2.0.15}$$

$$\langle\hat{Q}_i\rangle_\lambda \equiv \langle\hat{n}_{b_i}\rangle_\lambda + \sum_\sigma \langle\hat{n}_{d_{i\sigma}}\rangle_\lambda. \tag{2.0.16}$$

In above, $\langle\hat{n}_{b_i}\rangle_\lambda \equiv \langle b_i^\dagger b_i\rangle_\lambda$ and $\langle\hat{n}_{d_{i\sigma}}\rangle_\lambda \equiv \langle d_{i\sigma}^\dagger d_{i\sigma}\rangle_\lambda$, which are given with the most dominant terms in the $1/N$-expansion by

$$\langle\hat{n}_{b_i}\rangle_\lambda \simeq -T\sum_{\nu_n} B_i(\mathrm{i}\nu_n), \tag{2.0.17}$$

$$\langle\hat{n}_{d_{i\sigma}}\rangle_\lambda \simeq T\sum_{\omega_n} F_{i\sigma}(\mathrm{i}\omega_n) - \frac{1}{N_{\mathrm{L}}}\sum_{\mathbf{k}} W(\mathbf{k})T^2\sum_{\omega_n}\sum_{\nu_{n'}} F_{i\sigma}(\mathrm{i}\omega_n+\mathrm{i}\nu_{n'})^2\; G_p(\mathbf{k},\mathrm{i}\omega_n)\; B_i(\mathrm{i}\nu_{n'}). \tag{2.0.18}$$

Eqs. (2.0.10)-(2.0.18) constitute a set of self-consistent equations (SCE) to be solved, which are diagrammatically shown in Fig.1. Now we perform the analytic continuation from these equations to the following integral equations:

$$\mathrm{Im}P(\omega+\mathrm{i}0^+) = \mathrm{Im}B_i(\epsilon_d+\lambda_i-\omega+\mathrm{i}0^+)(\mathrm{e}^{\beta\omega}+1) \,/\, \Psi_Q(T), \tag{2.0.19}$$

$$\mathrm{Im}\Pi_i(\epsilon_d+\lambda_i-\omega+\mathrm{i}0^+) = \frac{1}{N_{\mathrm{L}}}\sum_\sigma\sum_{\mathbf{k}} W(\mathbf{k})\mathrm{Im}G_p(\mathbf{k},\omega+\mathrm{i}0^+)f(\omega), \tag{2.0.20}$$

$$\mathrm{Im}G_p(\mathbf{k},\omega+\mathrm{i}0^+) = \frac{W(\mathbf{k})\mathrm{Im}P(\omega+\mathrm{i}0^+)}{[\,\omega-\epsilon_p-W(\mathbf{k})\mathrm{Re}P(\omega)\,]^2 + [\,W(\mathbf{k})\mathrm{Im}P(\omega+\mathrm{i}0^+)\,]^2}, \tag{2.0.21}$$

$$\mathrm{Im}B_i(\epsilon_d+\lambda_i-\omega+\mathrm{i}0^+) = \frac{\mathrm{Im}\Pi_i(\epsilon_d+\lambda_i-\omega+\mathrm{i}0^+)}{[\,\epsilon_d-\omega-\mathrm{Re}\Pi_i(\epsilon_d+\lambda_i-\omega)\,]^2 + [\,\mathrm{Im}\Pi_i(\epsilon_d+\lambda_i-\omega+\mathrm{i}0^+)\,]^2}, \tag{2.0.22}$$

with

$$\mathrm{Re}P(\omega) = -\frac{1}{\pi}\,\mathrm{P}\int_{-\infty}^{\infty}\mathrm{d}\omega'\frac{1}{\omega-\omega'}\,\mathrm{Im}P(\omega'+\mathrm{i}0^+), \tag{2.0.23}$$

$$\mathrm{Re}\Pi_i(\epsilon_d+\lambda_i-\omega) = \frac{1}{\pi}\,\mathrm{P}\int_{-\infty}^{\infty}\mathrm{d}\omega'\frac{1}{\omega-\omega'}\,\mathrm{Im}\Pi_i(\epsilon_d+\lambda_i-\omega'+\mathrm{i}0^+), \tag{2.0.24}$$

and

$$\Psi_Q(T) \equiv \lim_{\{\lambda_i\}\to\infty}[\,\mathrm{e}^{\beta(\lambda_i+\epsilon_d)}\langle\hat{Q}_i\rangle_\lambda\,] \tag{2.0.25}$$

$$= N + \frac{\beta}{\pi}\int_{-\infty}^{\infty}\mathrm{d}\omega\left[\frac{\pi}{2} - \arctan\Big(\frac{\epsilon_d-\omega-\mathrm{Re}\Pi_i(\epsilon_d+\lambda_i-\omega)}{\mathrm{Im}\Pi_i(\epsilon_d+\lambda_i-\omega+\mathrm{i}0^+)}\Big)\right]\mathrm{e}^{\beta\omega}, \tag{2.0.26}$$

where $f(\omega) \equiv (e^{\beta\omega}+1)^{-1}$ is the Fermi distribution function and $\beta \equiv 1/T$.

In the low temperature limit, the solution of the SCE (2.0.10)-(2.0.18) or (2.0.19)-(2.0.26) were obtained by Jichu et al..[41, 42] The procedure is as follows: First we assume that, at $T = 0$, the p-hole Green's function is given by

$$G_p(\mathbf{k}, i\omega_n) = \left[i\omega_n - \epsilon_p - \frac{bW(\mathbf{k})}{i\omega_n - \omega_0} \right]^{-1} = \sum_{\gamma=\pm} \frac{A_\gamma(\mathbf{k})}{i\omega_n - E_\gamma(\mathbf{k})}, \tag{2.0.27}$$

with

$$E_\gamma(\mathbf{k}) \equiv \frac{1}{2}\left(\epsilon_p + \omega_0 + \gamma\sqrt{(\epsilon_p - \omega_0)^2 + 4bW(\mathbf{k})} \right), \tag{2.0.28}$$

$$A_\gamma(\mathbf{k}) \equiv \frac{1}{2}\left(1 + \gamma \frac{\epsilon_p - \omega_0}{\sqrt{(\epsilon_p - \omega_0)^2 + 4bW(\mathbf{k})}} \right), \tag{2.0.29}$$

where ω_0 is the binding energy of the resonance state of the slave-boson and b is the residue of the resonance state, which will be determined self-consistently. From eq.(2.0.27), the density of states per spin for the p-holes is given by

$$\rho_{p\sigma}(\omega) = \frac{|\omega-\omega_0|}{b}\, R\left(\frac{(\omega-\epsilon_p)\,(\omega-\omega_0)}{b} \right), \tag{2.0.30}$$

where

$$R(W) \equiv \frac{1}{N_L} \sum_{\mathbf{k}} \delta\big(W - W(\mathbf{k})\big), \tag{2.0.31}$$

is the density of the mixing weight, which shows the 2D van Hove singularity at $W = (2t_{pd})^2 = 1$. In eq.(2.0.30), $\rho_{p\sigma}(\omega)$ has finite intensity for $E_\gamma^{bot} \le \omega \le E_\gamma^{top}$ with $\gamma = \pm$, where E_γ^{bot} and E_γ^{top} are the lower and the upper band edges of $E_\gamma(\mathbf{k})$ in eq.(2.0.28), respectively. Substituting eq.(2.0.27) into eq.(2.0.20), we obtain

$$\mathrm{Im}\Pi_i(\epsilon_d+\lambda_i-\omega+i0^+) = -2\pi \frac{(\omega-\epsilon_p)\,(\omega-\omega_0)}{b}\, \rho_{p\sigma}(\omega)\, \theta(-\omega). \tag{2.0.32}$$

By using eqs.(2.0.24) and (2.0.32), $\mathrm{Re}\Pi_i(\epsilon_d+\lambda_i-\omega)$ is calculated as

$$\mathrm{Re}\Pi_i(\epsilon_d+\lambda_i-\omega) = \frac{2}{b}\, \mathrm{P} \int_{-\infty}^{\infty} d\omega' \frac{(\omega'-\epsilon_p)\,(\omega'-\omega_0)}{\omega' - \omega}\, \rho_{p\sigma}(\omega')\, \theta(-\omega'). \tag{2.0.33}$$

Substituting eqs.(2.0.32) and (2.0.33) into eq.(2.0.22), we obtain the spectral function of the slave-boson at $T = 0$:

$$-\frac{1}{\pi}\mathrm{Im}B_i(\epsilon_d+\lambda_i-\omega+i0^+) = b\,\delta(\omega-\omega_0) + d\,\delta(\omega-\omega_d) + C(\omega), \tag{2.0.34}$$

where the 1st term of in the rhs of eq.(2.0.34) represents the resonance state with the binding energy $\omega_0(>0)$ and the residue b determined by

$$\mathrm{Re}[\ B_i(\epsilon_d+\lambda_i-\omega_0)^{-1}\ ] = \epsilon_d - \omega_0 - \mathrm{Re}\Pi_i(\epsilon_d+\lambda_i-\omega_0) = 0, \tag{2.0.35}$$

$$\frac{1}{b} = -\frac{\mathrm{d}}{\mathrm{d}\omega}\mathrm{Re}[\ B_i(\epsilon_d+\lambda_i-\omega)^{-1}\ ]\Big|_{\omega=\omega_0} = 1+\frac{\mathrm{d}}{\mathrm{d}\omega}\mathrm{Re}\Pi_i(\epsilon_d+\lambda_i-\omega)\Big|_{\omega=\omega_0}, \tag{2.0.36}$$

and the 2nd term represents the atomic d-state with the renormalized energy $\omega_d(<\epsilon_d<0)$ and the residue d determined by

$$\mathrm{Re}[\ B_i(\epsilon_d+\lambda_i-\omega_d)^{-1}\ ] = \epsilon_d - \omega_d - \mathrm{Re}\Pi_i(\epsilon_d+\lambda_i-\omega_d) = 0, \tag{2.0.37}$$

$$\frac{1}{d} = -\frac{\mathrm{d}}{\mathrm{d}\omega}\mathrm{Re}[\ B_i(\epsilon_d+\lambda_i-\omega)^{-1}\ ]\Big|_{\omega=\omega_d} = 1+\frac{\mathrm{d}}{\mathrm{d}\omega}\mathrm{Re}\Pi_i(\epsilon_d+\lambda_i-\omega)\Big|_{\omega=\omega_d}. \tag{2.0.38}$$

In eq.(2.0.34), $C(\omega)$ represents the continuous spectrum, which comes from the local charge and spin fluctuations on the Cu site and has finite intensity for $E_-^{bot}\le\omega\le 0$ as seen from eq.(2.0.32). The spectral function of the slave-boson satisfies the following sum rule:

$$b+d+\int_{-\infty}^{+\infty} C(\omega)\mathrm{d}\omega = 1. \tag{2.0.39}$$

Using eqs.(2.0.32) and (2.0.35), eq.(2.0.26) is rewritten as

$$\Psi_Q(T\to 0) = N+\mathrm{e}^{\beta\omega_0}-\frac{\beta}{\pi}\int_{-\infty}^{0}\mathrm{d}\omega\left[\frac{\pi}{2}+\arctan\Big(\ \frac{\epsilon_d-\omega-\mathrm{Re}\Pi_i(\epsilon_d+\lambda_i-\omega)}{\mathrm{Im}\Pi_i(\epsilon_d+\lambda_i-\omega+\mathrm{i}0^+)}\ \Big)\right]\mathrm{e}^{\beta\omega}. \tag{2.0.40}$$

In the low temperature limit, $\Psi_Q(T)$ diverges as $\Psi_Q(T)\to\mathrm{e}^{\beta\omega_0}$ because of $\omega_0>0$. Substituting eqs.(2.0.34) and (2.0.40) into eq.(2.0.19) and using eq.(2.0.23), we obtain at $T=0$,

$$\mathrm{Im}P(\omega+\mathrm{i}0^+) = -\pi\ b\ \delta(\omega-\omega_0), \tag{2.0.41}$$

$$\mathrm{Re}P(\omega) = \frac{b}{\omega-\omega_0}. \tag{2.0.42}$$

Substituting these results into eq.(2.0.21) leads to eq.(2.0.27). Thus, eqs.(2.0.27)-(2.0.42) are proved to be self-consistent.

Next we calculate the average number of the p- and d-holes of the leading order in the $1/N$-expansion. Using eqs.(2.0.7), (2.0.10) and (2.0.18), we obtain

$$n_p \equiv \frac{1}{N_{\mathrm{L}}}\sum_\sigma\sum_{\mathbf{k}}\langle c^\dagger_{\mathbf{k}\sigma}c_{\mathbf{k}\sigma}\rangle = \frac{1}{N_{\mathrm{L}}}\sum_\sigma\sum_{\mathbf{k}}[\ T\sum_{\omega_n}G_p(\mathbf{k},\mathrm{i}\omega_n)\mathrm{e}^{\mathrm{i}\omega_n 0^+}\ ], \tag{2.0.43}$$

$$n_d \equiv \lim_{\lambda_i\to\infty}[\ \sum_\sigma\langle d^\dagger_{i\sigma}d_{i\sigma}\rangle_\lambda/\langle\hat{Q}_i\rangle_\lambda\ ] = n_d^0+\Delta n_d^{(0)}, \tag{2.0.44}$$

with

$$n_d^0 \equiv \sum_\sigma \lim_{\lambda_i\to\infty}[\, T\sum_{\omega_n} F_{i\sigma}(\mathrm{i}\omega_n)/\langle\hat{Q}_i\rangle_\lambda \,] = 2/\Psi_Q(T), \tag{2.0.45}$$

$$\begin{aligned}\Delta n_d^{(0)} &\equiv \sum_\sigma \lim_{\lambda_i\to\infty}\left[\, T\sum_{\nu_n} B_i(\mathrm{i}\nu_n)\,\frac{\mathrm{d}}{\mathrm{d}(\mathrm{i}\nu_n)}\Pi_i(\mathrm{i}\nu_n)\;/\;\langle\hat{Q}_i\rangle_\lambda\,\right]\\ &= \frac{1}{N_\mathrm{L}}\sum_\sigma\sum_{\mathbf{k}}\left[\, -T\sum_{\omega_n} G_p(\mathbf{k},\mathrm{i}\omega_n)\,\frac{\mathrm{d}}{\mathrm{d}(\mathrm{i}\omega_n)}\Sigma(\mathbf{k},\mathrm{i}\omega_n)\,\right],\end{aligned} \tag{2.0.46}$$

where n_d^0 is the contribution of the bare pseudo-fermions while $\Delta n_d^{(0)}$ is the lowest order correction in the $1/N$-expansion. The former represents the incoherent part of the d-holes which behaves as localized magnetic moments, while the latter represents the coherent part which is described as quasi-particles. At $T=0$, $n_d^0=0$ and then

$$n_d = \Delta n_d^{(0)} = b\,\frac{\mathrm{d}}{\mathrm{d}\omega}\mathrm{Re}\Pi_i(\epsilon_d{+}\lambda_i{-}\omega)\,\Big|_{\omega=\omega_0} = 1-b. \tag{2.0.47}$$

In deriving eq.(2.0.47), eqs.(2.0.34), (2.0.40) and (2.0.36) are used. Combining eqs.(2.0.43) and (2.0.44), we obtain the total hole number, $n_p{+}n_d{=}1{+}\delta$ with the doped hole concentration δ,

$$1+\delta = \frac{1}{N_\mathrm{L}}\sum_\sigma\sum_{\mathbf{k}}\left[\, -T\sum_{\omega_n}\frac{\mathrm{d}}{\mathrm{d}(\mathrm{i}\omega_n)}\log\{G_p(\mathbf{k},\mathrm{i}\omega_n)^{-1}\}\,\right] \;+\; n_d^0. \tag{2.0.48}$$

At $T=0, n_d^0=0$ and Im $\Sigma(\mathbf{k},0+\mathrm{i}0^+)=0$ and hence eq.(2.0.48) reduces to

$$1+\delta = \frac{1}{N_\mathrm{L}}\sum_\sigma\sum_{\mathbf{k}}\theta\big(-\epsilon_p{-}\mathrm{Re}\Sigma(\mathbf{k},0)\big) = \frac{1}{N_\mathrm{L}}\sum_\sigma\sum_{\mathbf{k}}\theta\big(-E_{-}(\mathbf{k})\big). \tag{2.0.49}$$

This is nothing but the Luttinger sum rule. We refer to the quasi-particles defined by $E_{-}(\mathbf{k})$ as *ingap states*. We note that ω_0 and b are proportional δ at $\delta \ll 1$, where the ingap states have the band width proportional to δ as given in eq.(2.0.28) with the Fermi level almost in the midst of the band forming the large Fermi surface.

Finally we calculate the physical d-hole Green's function defined by

$$G^d_{ij\sigma}(\mathrm{i}\omega_n) \equiv \lim_{\lambda_i,\lambda_j\to\infty}\left[\,\int_0^\beta \mathrm{d}\tau \mathrm{e}^{\mathrm{i}\omega_n\tau}(-)\langle T_\tau[b_i^\dagger(\tau)d_{i\sigma}(\tau)d_{j\sigma}^\dagger(0)b_j(0)]\rangle_\lambda\big/\langle\hat{Q}_i\hat{Q}_j\rangle_\lambda\,\right]. \tag{2.0.50}$$

To the lowest order in the $1/N$-expansion, its Fourier transform at $T=0$ is given by

$$G_d(\mathbf{k},\mathrm{i}\omega_n) = P(\mathrm{i}\omega_n) + P(\mathrm{i}\omega_n)W(\mathbf{k})G_p(\mathbf{k},\mathrm{i}\omega_n)P(\mathrm{i}\omega_n) \tag{2.0.51}$$

$$= b\left[\,\mathrm{i}\omega_n-\omega_0-\frac{bW(\mathbf{k})}{\mathrm{i}\omega_n-\epsilon_p}\,\right]^{-1} = \sum_{\gamma=\pm}\frac{b(1-A_\gamma(\mathbf{k}))}{\mathrm{i}\omega_n-E_\gamma(\mathbf{k})}, \tag{2.0.52}$$

with $E_\gamma(\mathbf{k})$ and $A_\gamma(\mathbf{k})$ defined in eqs.(2.0.28) and (2.0.29). The diagrammatic description is shown in Fig.2. Eq.(2.0.52) describes the itinerant component of the d-hole Green's function, which yields the density of states per spin for the itinerant component of the d-holes:

$$\rho_{d\sigma}(\omega) = |\omega - \epsilon_p| \; R\Big(\frac{(\omega-\epsilon_p)\;(\omega-\omega_0)}{b}\Big). \tag{2.0.53}$$

From eq.(2.0.53) and using eqs.(2.0.33) and (2.0.36), we obtain the average number of the itinerant d-holes:

$$n_d^{itin} = b\;(1-b). \tag{2.0.54}$$

The localized d-holes are from the corrections of $O(1/N)$ to the localized component of the d-hole Green's function and given by [52]

$$n_d^{local} = \Big[\; d + \int_{-\infty}^{+\infty} C(\omega)\mathrm{d}\omega \;\Big]\,(1-b). \tag{2.0.55}$$

Taking account of the sum rule for the spectral function of the slave-boson, eq.(2.0.39), we confirm that the total number of the d-holes per site, $n_d^{itin} + n_d^{local} = 1 - b$, certainly coincides with n_d given in eq.(2.0.47).

Chapter 3

Single-Particle Properties at Finite Temperatures

3.1 Results of the previous studies

The formulation for determining the single-particle properties is given in the previous section. Now, to calculate the transport properties, we need more explicit forms of the information about the single-particle properties. In fact, those are available in the low temperature limit thanks to the quite extensive studies done by several authors. [41, 42, 44, 45, 46] However, as is well known, many anomalous properties of high-T_c superconductors have been observed in the metallic phases at $T \gtrsim T_c$. In order to investigate those characteristics of the experimental observations, it is essential to study the properties of the d-p model at finite temperatures, especially at $T \gtrsim T_0$. For that aim we need to solve a set of the self-consistent equations, eqs.(2.0.19)-(2.0.26), at $T \gtrsim T_0$, but it is possible only through the tremendous amount of numerical calculations. Such study has been done by Ōno et al. [51] very recently.

They have solved numerically a set of the self-consistent equations (SCE) at finite temperatures by employing a simlified model for $R(W)$ defined in eq.(2.0.31),

$$R_0(W) = \begin{cases} \dfrac{1}{W_0} & 0 \le W \le W_0 \qquad \text{with} \qquad W_0 \equiv 2(2t_{pd})^2 \\ 0 & \text{otherwise,} \end{cases} \tag{3.1.1}$$

instead of the one given in the original 2D d-p model. They have checked the validity of the simplified model, eq.(3.1.1), for $R(W)$ by solving eqs.(2.0.35) and (2.0.36) with use of eq.(3.1.1) in eq.(2.0.33) at $T = 0$ to obtain ω_0 and b and comparing the results with those obtained for the original 2D d-p model to find the remarkable agreement. Then they have believed that the simplified model given by eq.(3.1.1) still keeps the essential feature of the d-p model. For the numerical calculations they have chosen such values for the parameters included in the model as $2t_{pd} = 1$, $\epsilon_p^0 = 3$ and $\epsilon_d^0 = 0$, i.e., the charge transfer gap $\Delta \equiv \epsilon_p^0 - \epsilon_d^0 = 3$. With this set of the parameters the system is an insulator at the half-filled case at $T = 0$ because of $\Delta_c = 2.45$ and the ingap states emerge inside the charge transfer gap upon hole doping.

They have found the two characteristic energies, ω_0 and T_0, in the system, where T_0 is called the coherence temperature of $0.2\omega_0$ and ω_0 is proportional to δ at $\delta \lesssim 0.1$ with the doped hole concentration δ. At low temperatures $T < T_0$, a new coherent band (ingap band) behaves as Fermi liquid with a large Fermi surface determined by the Luttinger sum rule. At high temperatures $T > \omega_0$, the the chemical potential stay away outside the ingap band and the doped holes sit almost in the O-$2p$ band forming a small Fermi surface, while the d-holes behave like spin-$\frac{1}{2}$ localized moments. At intermediate temperatures $T_0 < T < \omega_0$, the crossover phenomena between the two limiting cases are observed. The ingap band becomes quasi-coherent and the p-hole scattering rate at the chemical potential $\mu(T)$ due to the incoherent scattering is proportional to $(T - T_0)$. We thus expect that the normal state anomalies observed in the experiments for high-T_c superconductors may be due to the anomalous properties of the ingap states at the intermediate temperatures. However, unfortunately, the solutions of SCE have been given only numerically and the data points, particularly at energies near the resonance state of the slave-boson, are not dense enough to be used for calculating the transport coefficients accurately. Here we present a method to avoid such difficulties at $T \lesssim T_0$.

3.2 Low temperature approximation (LTA)

In the low temperature limit, $T \ll \omega_0$, the spectral function of the slave-boson of the leading order in the $1/N$-expansion is given by [48, 49, 50]

$$-\frac{1}{\pi}\mathrm{Im}B_i(\epsilon_d+\lambda_i-\omega+\mathrm{i}0^+) \;=\; b(T)\;\delta\Big(\omega-\omega_0(T)\Big) \;+\; C(\omega), \tag{3.2.1}$$

where the binding energy $\omega_0(T)$ and the residue $b(T)$ is determined by eqs.(2.0.35) and (2.0.36) with $\mathrm{Re}\Pi_i$ calculated at finite temperatures. The continuous spectrum $C(\omega)$ has finite intensity for $\omega \lesssim T \ll \omega_0(T)$ as seen from eqs.(2.0.22) and (2.0.20). Using eqs.(2.0.20) and (2.0.35) in eq.(2.0.26), we obtain

$$\Psi_Q(T) \;=\; N \;+\; \mathrm{e}^{\beta\omega_0(T)}. \tag{3.2.2}$$

Substituting eqs.(3.2.1) and (3.2.2) into eq.(2.0.19) and using eq.(2.0.23), we obtain

$$\mathrm{Im}P(\omega+\mathrm{i}0^+) \;=\; -\pi\,\Big(\;b(T)\;\delta(\omega-\omega_0(T)) + C(\omega)\;\Big)\frac{1+\mathrm{e}^{\beta\omega}}{N+\mathrm{e}^{\beta\omega_0(T)}} \tag{3.2.3}$$

$$\simeq\; -\pi\;q(T)\;\delta\Big(\omega-\omega_0(T)\Big), \tag{3.2.4}$$

$$\mathrm{Re}P(\omega) \;\simeq\; \frac{q(T)}{\omega-\omega_0(T)}, \tag{3.2.5}$$

with

$$q(T) \;=\; b(T)\;\frac{1+\mathrm{e}^{\beta\omega_0(T)}}{N+\mathrm{e}^{\beta\omega_0(T)}}. \tag{3.2.6}$$

In deriving eqs.(3.2.4) and (3.2.5), as the 0-th order approximation, we have neglected the terms carrying a factor $C(\omega)(\mathrm{e}^{\beta\omega}+1)/(N+\mathrm{e}^{\beta\omega_0(T)})$, which is at most of $O(C(\omega)/(N+\mathrm{e}^{\beta\omega_0(T)}))$ for $\omega \lesssim T \ll \omega_0(T)$ and can be safely neglected. Within the same approximation, the densities of states per spin for the p-holes and the itinerant component of the d-holes at $T \ll \omega_0$ are given by

$$\rho^T_{p\sigma}(\omega) \;=\; \frac{|\omega-\omega_0(T)|}{q(T)}\;R_0\Big(\frac{(\omega-\epsilon_p)\;(\omega-\omega_0(T))}{q(T)}\Big), \tag{3.2.7}$$

$$\rho^T_{d\sigma}(\omega) \;=\; |\omega-\epsilon_p|\;R_0\Big(\frac{(\omega-\epsilon_p)\;(\omega-\omega_0(T))}{q(T)}\Big). \tag{3.2.8}$$

These are derived from eqs.(2.0.30) and (2.0.53) where ω_0 and b are replaced by $\omega_0(T)$ and $q(T)$, respectively.

As a step to improve the approximation, we include perturbationally effects of the terms carrying the small factor of $O(C(\omega)/(N+e^{\beta\omega_0(T)}))$ in eq.(3.2.3), which primarily furnishes the quasi-particles with finte lifetime and plays the main role to determine the transport properties of the system. In order to avoid the difficulties in the numerical calculations as mentioned above, we only take the main term in the perturbation expansion with respect to the small factor of $O(C(\omega)/(N+e^{\beta\omega_0(T)}))$. Then we obtain an analytic form of $C(\omega)$ and its corresponding corrections for $\mathrm{Im}P(\omega+i0^+)$, while $\mathrm{Re}P(\omega)$ is still given by eq.(3.2.5). Using these results, we calculate the transport coefficients such as the optical conductivity and the electronic Raman scattering intensity. This approximation procedure (Low Temparature Approximation (LTA)) is not only justified in the low temperature limit, $T \ll \omega_0$, but also turns out to be a plausible approximation even at $T \lesssim T_0$.

3.3 Single-particle properties within LTA

Using eqs.(3.1.1) and (3.2.7), we perform the k-summation in eq.(2.0.20) analytically to obtain

$$\mathrm{Im}\Pi_i^{\mathrm{LTA}}(\epsilon_d+\lambda_i-\omega+i0^+) = -2\pi \frac{(\omega-\epsilon_p)\ (\omega-\omega_0(T))}{q(T)} \rho_{p\sigma}^T(\omega)\ f(\omega), \qquad (3.3.1)$$

which is finite for $E_-^{bot}(T) \leq \omega \leq E_-^{top}(T)=\omega_0(T)$, because $f(\omega)$ is practically zero for $\omega \geq E_+^{bot}(T)=\epsilon_p \gg \omega_0$ at $T \lesssim T_0$. This function reduces to eq.(2.0.32) in the low temperature limit. Substituting eq.(3.3.1) to eq.(2.0.24) yields

$$\mathrm{Re}\Pi_i^{\mathrm{LTA}}(\epsilon_d+\lambda_i-\omega) = \frac{2}{q(T)}\ \mathrm{P}\int_{-\infty}^{\infty} d\omega' \frac{(\omega'-\epsilon_p)\ (\omega'-\omega_0(T))}{\omega'-\omega} \rho_{p\sigma}^T(\omega')\ f(\omega'). \qquad (3.3.2)$$

Substituting eq.(3.3.2) to eq.(2.0.35), we obtain the solution for $\omega_0(T)$ in LTA, $\omega_0^{\mathrm{LTA}}(T)$. The numerical results for $\omega_0^{\mathrm{LTA}}(T)$, together with the solutions of SCE and those in the mean field approximation (MF) [51] are shown in Fig.3. The solution $\omega_0^{\mathrm{LTA}}(T)$ does not recover the input value for $\omega_0(T)$ correctly at $T \gtrsim T_0$, where the approximation procedure (LTA) breaks down. In order to avoid trivial complexities in the numerical calculations, we adjust $\mathrm{Re}\Pi_i^{\mathrm{LTA}}$ by adding a small artifact number so that eq.(2.0.35) may yield the solution, $\omega_0^{\mathrm{LTA}}(T)=\omega_0(T)$. Substituting eqs.(3.3.1) and (3.3.2) to eq.(2.0.22), we obtain the same form as eq.(2.0.34), where ω_0 and b are replaced by $\omega_0(T)$ and $b(T)$, respectively, and

$C^{\rm LTA}(\omega)$ is explicitly given by

$$C^{\rm LTA}(\omega) = \frac{{\rm Im}\Pi_i^{\rm LTA}(\epsilon_d+\lambda_i-\omega+{\rm i}0^+)}{[\ \epsilon_d-\omega-{\rm Re}\Pi_i^{\rm LTA}(\epsilon_d+\lambda_i-\omega)\ ]^2+[\ {\rm Im}\Pi_i^{\rm LTA}(\epsilon_d+\lambda_i-\omega+{\rm i}0^+)\ ]^2}. \qquad (3.3.3)$$

Then eq.(3.2.3) is rewritten as

$${\rm Im}P(\omega+{\rm i}0^+) = -\pi\ q(T)\ \delta\Big(\omega-\omega_0(T)\Big)\ -\pi\ \frac{1+{\rm e}^{\beta\omega}}{N+{\rm e}^{\beta\omega_0(T)}}\ C^{\rm LTA}(\omega). \qquad (3.3.4)$$

The numerical results for ${\rm Im}B_i(\omega+{\rm i}0^+)$ for $\delta = 0.1$ at $T = 0.0$, † 0.010, 0.015 and 0.025 together with the solutions of SCE at $T = 0.010, 0.025$ are shown in Fig.4(a). These results show that LTA reproduces the overall features of the solutions of SCE reasonably well at $T = 0.010$ while not so much at $T = 0.025$. On the other hand, T_0 is estimated through the relation, $T_0 \simeq 0.2\omega_0$ [51] with $\omega_0 = 0.048$ for $\delta = 0.1$. Thus LTA may be regarded to be a plausible approximation to the solutions of SCE at $T \lesssim T_0$. Although LTA seems to be a rather poor approximation as seen in Fig.4(a), it produces the single-particle densities of states obtained by the solutions of SCE reasonably well as confirmed by comparing eqs.(3.2.7) and (3.2.8) with the corresponding numerical results of SCE shown in Fig.4(b). Therefore LTA is expected to be used as a plausible approximation even up to $T \simeq 0.025 \sim 2T_0$.

The numerical results for ${\rm Im}B_i(\omega+{\rm i}0^+)$ for $\delta = 0.1$, 0.2, 0.3, and 0.4 as functions of ω/ω_0 at $T \sim T_0 \sim 0.2\omega_0$ are shown in Fig.4(c). Note that $\omega_0 = 0.084$, 0.110 and 0.129 for $\delta = 0.2$, 0.3 and 0.4, respectively. These results show that both of the ω- and the T-dependences of the single-particle properties are scaled rather well by ω_0 or T_0, which is shown in Fig.4(d) as a function of δ.

Substituting eqs.(3.2.3) and (3.2.5) into eq.(2.0.10), we obtain

$$G_p(\mathbf{k},\omega+{\rm i}0^+) = \Big[\ \omega-\epsilon_p-{\rm Re}\Sigma(\mathbf{k},\omega)-{\rm i}{\rm Im}\Sigma(\mathbf{k},\omega+{\rm i}0^+)\ \Big]^{-1} \qquad (3.3.5)$$

$$\simeq \frac{A_-(\mathbf{k})}{\omega-E_-(\mathbf{k})+{\rm i}[\ 2\tau_{\rm ingap}(\mathbf{k})\ ]^{-1}}+\frac{A_+(\mathbf{k})}{\omega-E_+(\mathbf{k})+{\rm i}0^+}, \qquad (3.3.6)$$

$$[\ 2\tau_{\rm ingap}(\mathbf{k})\ ]^{-1} \equiv -A_-(\mathbf{k})\ {\rm Im}\Sigma(\mathbf{k},E_-(\mathbf{k})+{\rm i}0^+), \qquad (3.3.7)$$

†In the low temperature limit, because the fermi factor $f(\omega)$ in eq.(3.3.1) reduces to $\theta(-\omega)$, eq.(3.3.3) is non-zero only for $\omega \leq 0$ and hence the 2nd term in the rhs of eq.(3.3.4) vanishes.

with $E_\gamma(\mathbf{k})$ and $A_\gamma(\mathbf{k})$ given in eqs.(2.0.28) and (2.0.29) where ω_0 and b are replaced by $\omega_0(T)$ and $q(T)$, respectively. In deriving eq.(3.3.6), we have expanded eq.(3.3.5) around the pole, $\omega = E_-(\mathbf{k})$.

Rewriting $W(\mathbf{k})$ in eq.(2.0.13) in terms of $E_-(\mathbf{k})$ by using eq.(2.0.28), we obtain

$$-\mathrm{Im}\Sigma(\mathbf{k},\omega{+}\mathrm{i}0^+) \;=\; \pi\,\frac{(E_-(\mathbf{k}){-}\epsilon_p)\;(E_-(\mathbf{k}){-}\omega_0(T))}{q(T)}\;\frac{1+\mathrm{e}^{\beta\omega}}{N+\mathrm{e}^{\beta\omega_0(T)}}\;C^{\mathrm{LTA}}(\omega). \qquad (3.3.8)$$

Thus, in the leading order in the $1/N$-expansion, the p-holes are scattered only by the continuum $C^{\mathrm{LTA}}(\omega)$ in the slave-boson spectra. We have neglected the 1st term in the rhs of eq.(3.2.3), since it vanishes at $\omega{=}E_-(\mathbf{k})$ because of the factor, $(E_-(\mathbf{k}){-}\omega_0(T))\;\delta(\omega{-}\omega_0(T))$. The numerical results for $\mathrm{Im}\Sigma(\mathbf{k},\, E_-(\mathbf{k}){+}\mathrm{i}0^+)$ for $\delta = 0.1$ at $T = 0.010$, 0.015 and 0.025 are shown in Fig.5. We note that $\mathrm{Im}\Sigma(\mathbf{k},\, E_-(\mathbf{k}){+}\mathrm{i}0^+)$ shown in Fig.5 is roughly proportional to ω at $\omega \simeq 0$ with a slope increasing with T.

Substituting eq.(3.3.8) into eq.(3.3.7), the quasi-particle scattering rate is given by

$$\frac{1}{2\tau_{\mathrm{ingap}}(\mathbf{k})} \;=\; \pi\,\frac{(E_-(\mathbf{k}){-}\epsilon_p)\;(E_-(\mathbf{k}){-}\omega_0(T))^2}{q(T)\;(2E_-(\mathbf{k}){-}\epsilon_p{-}\omega_0(T))}\;\frac{1+\mathrm{e}^{\beta E_-(\mathbf{k})}}{N+\mathrm{e}^{\beta\omega_0(T)}}\;C^{\mathrm{LTA}}(E_-(\mathbf{k})), \qquad (3.3.9)$$

which is proportional to $(E_-(\mathbf{k}){-}\omega_0(T))^2$ at $E_-(\mathbf{k}) \lesssim \omega_0(T)$. The numerical results for $\delta = 0.1$ at $T = 0.010$, 0.015 and 0.025 are shown in Fig.6. We note that $A_-(\mathbf{k})$ in eq.(3.3.7) is the wave-function renormalization factor for the *ingap states* and estimated to be $q(T)W(\mathbf{k})/(\epsilon_p - \omega_0(T))^2$ with $q(T) \ll 1$ and of $O(0.1)$ at most in the present cases.

The T-dependences of the p-hole scattering rate at $|\mathbf{k}| = \mathrm{k_F}$ for $\delta = 0.1$, 0.2, 0.3 and 0.4 at $T \lesssim 2T_0$ are shown in Fig.7. The results show that the T-dependences are scaled rather well by ω_0 or T_0. Unfortunately, these results do not well reproduce the results of SCE, which are proportional to $(T - T_0)$ at the intermediate temperatures, $T_0 \lesssim T \lesssim \omega_0$. This means that the higher order corrections in power of the small factor of $O(C(\omega)/(N{+}\mathrm{e}^{\beta\omega_0(T)}))$ in the slave-boson spectra play crucial roles to determine the T-dependence at $T \gtrsim T_0$.

Substituting eq.(3.3.6) into eq.(2.0.51), we obtain

$$G_d(\mathbf{k},\omega{+}\mathrm{i}0^+) \;=\; P(\omega{+}\mathrm{i}0^+) \;+\; P(\omega{+}\mathrm{i}0^+)W(\mathbf{k})G_p(\mathbf{k},\omega{+}\mathrm{i}0^+)P(\omega{+}\mathrm{i}0^+) \qquad (3.3.10)$$

$$\simeq\; \frac{q(T)\;(1{-}A_-(\mathbf{k}))}{\omega - E_-(\mathbf{k}) + \mathrm{i}[\;2\tau_{\mathrm{ingap}}(\mathbf{k})\;]^{-1}} \;+\; \frac{q(T)\;(1{-}A_+(\mathbf{k}))}{\omega - E_+(\mathbf{k}) + \mathrm{i}0^+}. \qquad (3.3.11)$$

Eqs.(3.3.6) and (3.3.11) together with eq.(3.3.8) yield the densities of states per spin for the p-holes and for the itinerant component of the d-holes consistent with eqs.(3.2.7) and (3.2.8).

Chapter 4

Transport Coefficients

4.1 General formulae

Here we derive the formulae for caluculating the optical conductivity and the electronic Raman scttering intensity. The electronic current operator with wave vector $\mathbf{q} \to \mathbf{0}$ in the d-p model, eq.(2.0.1), is given by [53]

$$\mathbf{J} = \frac{e}{\hbar} N_{\mathrm{L}}^{-\frac{1}{2}} \sum_{i} \sum_{\mathbf{k}} \sum_{\sigma} \Big(\mathrm{e}^{-\mathrm{i}\mathbf{k}\cdot\mathbf{R}_i} \nabla_{\mathbf{k}} t_{\mathbf{k}} \, c^{\dagger}_{\mathbf{k}\sigma} d_{i\sigma} b^{\dagger}_{i} + h.c. \Big). \tag{4.1.1}$$

Then the optical conductivity $\sigma(\omega) = \sigma^{'}(\omega) + \mathrm{i}\sigma^{''}(\omega)$ is given by

$$\sigma(\omega) = -\frac{1}{\mathrm{i}\omega} \Big(\chi_{JJ}(\omega + \mathrm{i}0^{+}) - \chi_{JJ}(0 + \mathrm{i}0^{+}) \Big), \tag{4.1.2}$$

where $\chi_{JJ}(\omega + \mathrm{i}0^{+})$ is the retarded current current response function given by the analytic continuation of the temperature Green's function,

$$\begin{aligned} \chi_{JJ}(\mathrm{i}\omega_n) &= \frac{1}{N_{\mathrm{L}}} \int_0^{\beta} \mathrm{d}\tau \mathrm{e}^{\mathrm{i}\omega_n \tau} (-) \Big\langle \mathrm{T}_{\tau} [\mathbf{J}^{\dagger}(\tau) \, \mathbf{J}(0)] \Big\rangle \\ &= \frac{1}{N_{\mathrm{L}}} \sum_{\mathbf{k}\mathbf{k}^{'}} \sum_{\sigma\sigma^{'}} \sum_{\alpha=\pm} \mathbf{V}(\mathbf{k}) \, \mathbf{V}(\mathbf{k}^{'}) K_{\alpha}(\mathbf{k}^{'}, \mathbf{k}, \mathrm{i}\omega_n), \end{aligned} \tag{4.1.3}$$

with

$$\mathbf{V}(\mathbf{k}) \equiv \sum_{\mu=\mathbf{x},\mathbf{y}} \frac{e}{\hbar} \big(\hat{\mu} \cdot \nabla_{\mathbf{k}} t_{\mathbf{k}} \big) \, \hat{\mu}, \tag{4.1.4}$$

$$K_{+}(\mathbf{k}^{'}, \mathbf{k}, \mathrm{i}\omega_n) \equiv \frac{1}{N_{\mathrm{L}}} \sum_{ij} \mathrm{e}^{-\mathrm{i}\mathbf{k}\cdot\mathbf{R}_i} \mathrm{e}^{\mathrm{i}\mathbf{k}^{'}\cdot\mathbf{R}_j} \lim_{\lambda_i, \lambda_j \to \infty} \Big[\int_0^{\beta} \mathrm{d}\tau \mathrm{e}^{\mathrm{i}\omega_n \tau}$$

$$\times \quad (-)\langle \mathrm{T}_\tau[b_j(\tau)d^\dagger_{j\sigma'}(\tau)c_{\mathbf{k}'\sigma'}(\tau)c^\dagger_{\mathbf{k}\sigma}(0)d_{i\sigma}(0)b^\dagger_i(0)]\rangle_\lambda \Big/ \langle \hat{Q}_i\hat{Q}_j\rangle_\lambda \Big], \quad (4.1.5)$$

$$K_-(\mathbf{k}',\mathbf{k},\mathrm{i}\omega_n) \equiv \frac{1}{N_\mathrm{L}}\sum_{ij}\mathrm{e}^{\mathrm{i}\mathbf{k}\cdot\mathbf{R}_i}\mathrm{e}^{-\mathrm{i}\mathbf{k}'\cdot\mathbf{R}_j}\lim_{\lambda_i,\lambda_j\to\infty}\Big[\int_0^\beta \mathrm{d}\tau \mathrm{e}^{\mathrm{i}\omega_n\tau}$$

$$\times \quad (-)\langle \mathrm{T}_\tau[c^\dagger_{\mathbf{k}'\sigma'}(\tau)d_{j\sigma'}(\tau)b^\dagger_j(\tau)b_i(0)d^\dagger_{i\sigma}(0)c_{\mathbf{k}\sigma}(0)]\rangle_\lambda \Big/ \langle \hat{Q}_i\hat{Q}_j\rangle_\lambda \Big], \quad (4.1.6)$$

and with the unit vectors, $\hat{\mathbf{x}}$ and $\hat{\mathbf{y}}$, parallel to the x- and the y-axis, respectively. More explicitly we find

$$\sigma'(\omega) = \frac{1}{\omega}\frac{1}{N_\mathrm{L}}\sum_{\mathbf{k}\mathbf{k}'}\sum_{\sigma\sigma'}\sum_{\alpha=\pm}\mathbf{V}(\mathbf{k})\,\mathbf{V}(\mathbf{k}')(-)\mathrm{Im}K_\alpha(\mathbf{k}',\mathbf{k},\omega+\mathrm{i}0^+), \quad (4.1.7)$$

$$\sigma''(\omega) = \frac{1}{\omega}\frac{1}{N_\mathrm{L}}\sum_{\mathbf{k}\mathbf{k}'}\sum_{\sigma\sigma'}\sum_{\alpha=\pm}\mathbf{V}(\mathbf{k})\,\mathbf{V}(\mathbf{k}')\Big(\,\mathrm{Re}K_\alpha(\mathbf{k}',\mathbf{k},\omega+\mathrm{i}0^+) - \mathrm{Re}K_\alpha(\mathbf{k}',\mathbf{k},0+\mathrm{i}0^+)\,\Big). \quad (4.1.8)$$

Now we consider the electronic Raman scattering in a system with two electronic bands separated by a certain energy gap $E_\mathrm{G}(T)$. There are two different types of contributions to the electronic Raman scattering, one due to the $\mathbf{A}^2$-term and the other due to the $(\mathbf{p}\cdot\mathbf{A})^2$-term. In the present study hereafter, we confine ourselves to discuss the latter contribution. The reason is as follows: In the Raman scattering measurements with high-T_c superconductors, [16) – 21)] one of the most unusual features is that the very weakly ω-dependent electronic Raman intensities extended up to several thousands of cm^{-1} have been observed. [19, 20, 21)] The electronic Raman signals are observable both for the crossed and the parallel polarization geometries, $\mathbf{e}_i\perp\mathbf{e}_f$ and $\mathbf{e}_i\|\mathbf{e}_f$, respectively, where $\mathbf{e}_i$ and $\mathbf{e}_f$ are the poralization vectors of the incident laser beam and the scattered one, respectivly. In order to discuss these phenomena, it is essential to include the contrbutions due to the $(\mathbf{p}\cdot\mathbf{A})^2$-term, because the contributions due to the $\mathbf{A}^2$-term are always proportional to $(\mathbf{e}_i\cdot\mathbf{e}_f)^2$.

Under the resonance condition, eq.(A.0.11), the electronic Raman scattering intensity per unit cell, $\mathrm{I}_{(pA)^2}(\omega)$, is given by

$$\mathrm{I}_{(pA)^2}(\omega) = \Big(1+f_\mathrm{B}(\omega)\Big)\,\chi''_{(pA)^2}(\omega+\mathrm{i}0^+), \quad (4.1.9)$$

with

$$\chi''_{(pA)^2}(\omega+\mathrm{i}0^+) \equiv \frac{1}{c^4}\frac{\mathrm{k}_f}{\mathrm{k}_i}\frac{1}{\pi}\frac{1}{N_\mathrm{L}}\sum_{\mathbf{k}\mathbf{k}'}\sum_{\sigma\sigma'}\sum_{\alpha=\pm}\mathrm{U}(\mathbf{k})\,\mathrm{U}(\mathbf{k}')(-)\mathrm{Im}K_\alpha(\mathbf{k}',\mathbf{k},\omega+\mathrm{i}0^+), \quad (4.1.10)$$

$$\mathrm{U}(\mathbf{k}) \equiv (\frac{1}{E_{\mathrm{g}}(T)+\hbar\omega_f}+\frac{1}{E_{\mathrm{g}}(T)-\hbar\omega_i})(\mathbf{e}_i\cdot\frac{e}{\hbar}\nabla_{\mathbf{k}}t_{\mathbf{k}})(\mathbf{e}_f\cdot\frac{e}{\hbar}\nabla_{\mathbf{k}}t_{\mathbf{k}}), \quad (4.1.11)$$

where the incident photon with frequency ω_i, wave vector $\mathbf{k}_i$ and polarization vector $\mathbf{e}_i$ is scattered into the state specified by the corresponding parameters, ω_f, $\mathbf{k}_f$ and $\mathbf{e}_f$, $f_{\mathrm{B}}(\omega)\equiv(\mathrm{e}^{\beta\omega}-1)^{-1}$ is the Bose distribution function, $E_{\mathrm{g}}(T)$ is the optical band gap, and $K_\alpha(\mathbf{k}',\mathbf{k},\omega{+}\mathrm{i}0^+)$ is calculated from eqs.(4.1.5) and (4.1.6). The derivation of eq.(4.1.9) is given in Appendix A. Eqs.(4.1.7) and (4.1.10) confirm the relation, eq.(A.0.29), to hold.

4.2 $1/N$-expansion and LTA

Now we obtain explicit forms of the transport coefficients including terms of the leading order in the $1/N$-expansion. The vertex corrections of this order for $K_\alpha(\mathbf{k}',\mathbf{k},\mathrm{i}\omega_n)$ are local and the summations over $\mathbf{k}$ and $\mathbf{k}'$ in the corresponding terms appearing in eqs.(4.1.7), (4.1.8) and (4.1.10) are decoupled as shown in Fig.8. Then, because of the factors, $\mathbf{V}(\mathbf{k})$ and $\mathbf{V}(\mathbf{k}')$, in eqs.(4.1.7) and (4.1.8) the vertex corrections always vanish for the conductivity. However, for the electronic Raman scattering intensity, because of the factors, $\mathrm{U}(\mathbf{k})$ and $\mathrm{U}(\mathbf{k}')$, in eq.(4.1.10) the vertex corrections vanish for the crossed polarization geometries $\mathbf{e}_i\perp\mathbf{e}_f$, while they do not vanish for the parallel polarization geometries $\mathbf{e}_i\|\mathbf{e}_f$. This is because the parity of the pseudo-current vertex in eq.(4.1.11) is different from that of the current vertex in eq.(4.1.4).

Thus, we obtain

$$K_\alpha(\mathbf{k}',\mathbf{k},\mathrm{i}\omega_n) \simeq K_\alpha^{(0)}(\mathbf{k},\mathrm{i}\omega_n)\,\delta_{\mathbf{k},\mathbf{k}'}\delta_{\sigma,\sigma'}, \quad (4.2.1)$$

with

$$K_+^{(0)}(\mathbf{k},\mathrm{i}\omega_n)=T\sum_{\mathrm{i}\epsilon_n}\Big(\,G_d(\mathbf{k},\mathrm{i}\omega_n)G_p(\mathbf{k},\mathrm{i}\omega_n{+}\mathrm{i}\epsilon_n)+G_{pd}(\mathbf{k},\mathrm{i}\omega_n)G_{pd}(\mathbf{k},\mathrm{i}\omega_n{+}\mathrm{i}\epsilon_n)\,\Big), \quad (4.2.2)$$

$$K_-^{(0)}(\mathbf{k},\mathrm{i}\omega_n)=T\sum_{\mathrm{i}\epsilon_n}\Big(\,G_p(\mathbf{k},\mathrm{i}\omega_n)G_d(\mathbf{k},\mathrm{i}\omega_n{+}\mathrm{i}\epsilon_n)+G_{dp}(\mathbf{k},\mathrm{i}\omega_n)G_{dp}(\mathbf{k},\mathrm{i}\omega_n{+}\mathrm{i}\epsilon_n)\,\Big), \quad (4.2.3)$$

where G_p and G_d are given in eqs.(2.0.10) and (2.0.51), respectively, and G_{pd} and G_{dp} are defined as

$$G_{dp}(\mathbf{k},\mathrm{i}\epsilon_n) \equiv \sqrt{W(\mathbf{k})}\,P(\mathrm{i}\epsilon_n)\,G_p(\mathbf{k},\mathrm{i}\epsilon_n), \quad (4.2.4)$$

$$G_{pd}(\mathbf{k},\mathrm{i}\epsilon_n) \equiv \sqrt{W(\mathbf{k})}\,G_p(\mathbf{k},\mathrm{i}\epsilon_n)\,P(\mathrm{i}\epsilon_n). \quad (4.2.5)$$

Diagrammatic expression for eqs.(4.2.2), (4.2.3), (4.2.4) and (4.2.5) is shown in Fig.9.

Inserting eq.(4.2.1) into eqs.(4.1.7) and (4.1.8) and eq.(4.1.10) with the crossed polarization geometries $\mathbf{e}_i \perp \mathbf{e}_f$ yields

$$\sigma^{'}(\omega) \simeq \frac{1}{\omega}\frac{1}{N_{\mathrm{L}}}\sum_{\mathbf{k}}\sum_{\sigma}\mathbf{V}(\mathbf{k})\,\mathbf{V}(\mathbf{k})\,(-)\mathrm{Im}K^{(0)}(\mathbf{k},\omega{+}\mathrm{i}0^{+}), \tag{4.2.6}$$

$$\sigma^{''}(\omega) \simeq \frac{1}{\omega}\frac{1}{N_{\mathrm{L}}}\sum_{\mathbf{k}}\sum_{\sigma}\mathbf{V}(\mathbf{k})\,\mathbf{V}(\mathbf{k})\left(\,\mathrm{Re}K^{(0)}(\mathbf{k},\omega{+}\mathrm{i}0^{+}) - \mathrm{Re}K^{(0)}(\mathbf{k},0{+}\mathrm{i}0^{+})\,\right), \tag{4.2.7}$$

$$\mathrm{I}^{\perp}_{(pA)^2}(\omega) \simeq \left(1 + f_{\mathrm{B}}(\omega)\right)\chi^{''\perp}_{(pA)^2}(\omega{+}\mathrm{i}0^{+}), \tag{4.2.8}$$

with

$$\chi^{''\perp}_{(pA)^2}(\omega{+}\mathrm{i}0^{+}) \equiv \frac{1}{c^4}\frac{\mathrm{k}_f}{\mathrm{k}_i}\frac{1}{\pi}\frac{1}{N_{\mathrm{L}}}\sum_{\mathbf{k}}\sum_{\sigma}\mathrm{U}(\mathbf{k})\,\mathrm{U}(\mathbf{k})\,(-)\mathrm{Im}K^{(0)}(\mathbf{k},\omega{+}\mathrm{i}0^{+}), \tag{4.2.9}$$

where $K^{(0)}(\mathbf{k},\omega{+}\mathrm{i}0^{+})$ is explicitly given by

$$K^{(0)}(\mathbf{k},\omega{+}\mathrm{i}0^{+}) \equiv \sum_{\alpha=\pm}K^{(0)}_{\alpha}(\mathbf{k},\omega{+}\mathrm{i}0^{+}) \tag{4.2.10}$$

$$\begin{aligned}
&= \frac{(-)}{2\pi\mathrm{i}}\int_{-\infty}^{+\infty}\mathrm{d}x\,f(x) \\
&\times \Big[\;\; 2\mathrm{i}\mathrm{Im}G_p(\mathbf{k},x{+}\mathrm{i}0^{+})\Big(\,G_d(\mathbf{k},x{+}\omega{+}\mathrm{i}0^{+}) + G_d(\mathbf{k},x{-}\omega{-}\mathrm{i}0^{+})\,\Big) \\
&\quad +2\mathrm{i}\mathrm{Im}G_d(\mathbf{k},x{+}\mathrm{i}0^{+})\Big(\,G_p(\mathbf{k},x{+}\omega{+}\mathrm{i}0^{+}) + G_p(\mathbf{k},x{-}\omega{-}\mathrm{i}0^{+})\,\Big) \\
&\quad +4\mathrm{i}\mathrm{Im}G_{dp}(\mathbf{k},x{+}\mathrm{i}0^{+})\Big(\,G_{dp}(\mathbf{k},x{+}\omega{+}\mathrm{i}0^{+}) + G_{dp}(\mathbf{k},x{-}\omega{-}\mathrm{i}0^{+})\,\Big)\;\Big].
\end{aligned} \tag{4.2.11}$$

Eqs.(4.2.6) and (4.2.9) confirm the relation, eq.(A.0.29), to hold in the leading order in the $1/N$-expansion as it should.

Next we derive formulae for calculating the transport coefficients in LTA with the simplified model given by eq.(3.1.1), which leads to

$$t_{\mathbf{k}} = \sqrt{W(\mathbf{k})} = 2t_{pd}a\sqrt{(k_x^2 + k_y^2)/2\pi}. \tag{4.2.12}$$

Substituting eq.(4.2.12) into eqs.(4.1.4) and (4.1.11), and then the results into eqs.(4.2.6), (4.2.7) and (4.2.9), we obtain

$$\sigma^{'}(\omega) \simeq (\frac{ea}{\hbar})^2\frac{1}{\omega}\frac{1}{N_{\mathrm{L}}}\sum_{\mathbf{k}}\sum_{\sigma}(\frac{1}{2\sqrt{\pi}})^2(-)\mathrm{Im}K^{(0)}(\mathbf{k},\omega{+}\mathrm{i}0^{+}), \tag{4.2.13}$$

$$\sigma''(\omega) \simeq (\frac{ea}{\hbar})^2 \frac{1}{\omega} \frac{1}{N_{\rm L}} \sum_{\mathbf{k}} \sum_{\sigma} (\frac{1}{2\sqrt{\pi}})^2 \Big(\, {\rm Re}K^{(0)}(\mathbf{k}, \omega{+}{\rm i}0^+) - {\rm Re}K^{(0)}(\mathbf{k}, 0{+}{\rm i}0^+) \, \Big), \quad (4.2.14)$$

$$\begin{aligned} \chi''^{\perp}_{(pA)^2}(\omega{+}{\rm i}0^+) \;&\simeq\; (\frac{ea}{\hbar})^4 \frac{1}{c^4} \frac{{\rm k}_f}{{\rm k}_i} \frac{1}{\pi} \qquad (4.2.15) \\ &\times\; \frac{1}{N_{\rm L}} \sum_{\mathbf{k}} \sum_{\sigma} (\frac{1}{E_{\rm g}(T){+}\hbar\omega_f} + \frac{1}{E_{\rm g}(T){-}\hbar\omega_i})^2 (\frac{1}{8\pi})^2 (-){\rm Im}K^{(0)}(\mathbf{k}, \omega{+}{\rm i}0^+). \end{aligned}$$

If we neglect the vertex corrections of the leading order in the $1/N$-expansion, the electronic Raman scattering response function for the parallel polarization geometries is given by

$$\chi''^{\parallel}_{(pA)^2}(\omega) \;=\; \Big(3 + \frac{8}{\pi} \sin 2\theta\Big) \; \chi''^{\perp}_{(pA)^2}(\omega). \quad (4.2.16)$$

where θ is the angle between $\mathbf{e}_i$ and the $\hat{\mathbf{x}}$.

In above, $K^{(0)}(\mathbf{k}, \omega{+}{\rm i}0^+)$ is given by eq.(4.2.11), where the integrations are evaluated numerically. Using eqs.(2.0.31) and (3.1.1), we rewrite a $\mathbf{k}$-summation as

$$\frac{1}{N_{\rm L}} \sum_{\mathbf{k}} F(\; W(\mathbf{k}) \;) \;=\; \int_0^{W_0} {\rm d}W \; R_0(W) \; F(W). \quad (4.2.17)$$

Using eq.(2.0.28) and changing the integration variable from $W(\mathbf{k})$ to $E_{-}(\mathbf{k})$, we further rewrite the $\mathbf{k}$-summation as

$$\frac{1}{N_{\rm L}} \sum_{\mathbf{k}} F(\; E_{-}(\mathbf{k}) \;) \;=\; \int_{E_{-}^{bot}}^{\omega_0(T)} {\rm d}\epsilon \; \rho^T_{\sigma}(\epsilon) \; F(\epsilon), \quad (4.2.18)$$

with

$$\rho^T_{\sigma}(\epsilon) \;\equiv\; \frac{1}{N_{\rm L}} \sum_{\mathbf{k}} \delta\Big(\epsilon{-}E_{-}(\mathbf{k})\Big) \;=\; \frac{2\epsilon - \epsilon_p - \omega_0(T)}{\epsilon - \omega_0(T)} \; \rho^T_{p\sigma}(\epsilon), \quad (4.2.19)$$

where $\rho^T_{p\sigma}(\epsilon)$ is given by eq.(3.2.7). For the numerical calculations hereafter, we employ the units so that $2t_{pd} = \hbar = c = e = a = 1$.

4.3 Optical conductivity

At $T = 0$, we can calculate $\sigma(\omega)$ analytically as shown in Appendix B. But, at finite temperatures, we must rely upon the entirely numerical calculations. The numerical results for the real part of the optical conductivity, $\sigma'(\omega)$, as functions of ω at $T = 0.010$, 0.015 and 0.025 for $\delta = 0.1$ are shown in Fig.10(a). We find that $\sigma'(\omega)$ is separated into two

parts, the intraband component $\sigma'_{\rm intra}(\omega)$ and the interband one $\sigma'_{\rm inter}(\omega)$. At $T = 0$, $\sigma'(\omega)$ is given by

$$\sigma'(\omega) \;=\; \frac{n_{\rm opt}}{m_{\rm b}}\pi\,\delta(\omega) \;+\; \sigma'_{\rm inter}(\omega), \tag{4.3.1}$$

with the optical carrier concentration $n_{\rm opt}$ and the band mass $m_{\rm b}$. At $T > 0$, the gap structure in $\sigma'_{\rm inter}(\omega)$ is smeared by the finite-T effects and $\sigma'_{\rm intra}(\omega)$ shows a Drude-like tail with a width increasing with T. The finite width is due to the scattering of the quasi-particles by the continuum $C^{\rm LTA}(\omega)$ in the slave-boson spectra, which increases with T as shown in Fig.4(a). The numerical results for $\sigma'(\omega)$ for $\delta = 0.1, 0.2, 0.3$ and 0.4 at $T = 0.025$ are shown in Fig.10(b). The intraband component at a fixed T becomes steeper monotonically as δ increases and the interband component becomes broader with increasing δ. Since the energy scale is such that $2t_{pd} = 1$ while a real value of t_{pd} is of $O(1\mathrm{eV})$, it is concluded that no clear mid-IR contribution is observed in Fig.10. Much clearer contributions may be expected from the terms of higher orders in the $1/N$-expansion and/or the finite-T effects at $T \gtrsim T_0$.

In order to examine the Drude-like components which represent the dynamical properties of the *ingap states*, $\sigma'_{\rm intra}(\omega)$ is plotted in enlarged scales in Fig.11. The clear Drude tail is observed in the inset of Fig.11 plotted on a log-log scale. The numerical results for $\sigma'_{\rm intra}(\omega)$ for $\delta = 0.1, 0.2, 0.3$ and 0.4 as functions of ω/ω_0 at $T \sim T_0$ are shown in Fig.11(b). These results show that, correspondingly to the scaling natures in the single-particle properties as seen in Fig.4(c), both of the ω- and the T-dependences of the dynamical properties are also scaled rather well by ω_0 or T_0, as far as the low energy behaviors are concerned. The numerical results for $\sigma''_{\rm intra}(\omega)$ are shown in Fig.12. In the primitive Drude model the optical conductivity is given by

$$\sigma_{\rm D}(\omega) \;=\; \frac{n_{\rm opt}}{m_{\rm b}}\,\frac{1}{\tau^{-1} - {\rm i}\omega} \;\equiv\; \sigma'_{\rm D}(\omega) \;+\; {\rm i}\sigma''_{\rm D}(\omega), \tag{4.3.2}$$

which leads to the relations,

$$\sigma''_{\rm D}(\omega) = \omega\tau\;\sigma'_{\rm D}(\omega), \qquad \sigma''_{\rm D}(\omega) \le \sigma'_{\rm D}(\tau^{-1}) = \frac{1}{2}\;\sigma'_{\rm D}(0), \tag{4.3.3}$$

where τ^{-1} is called the half-width. The results shown in Figs.11(a) and 12 are consistent with eq.(4.3.3). We note that the half-width of the Drude-like component is not of

$O(-2\mathrm{Im}\Sigma(\mathbf{k}, E_{-}(\mathbf{k})+\mathrm{i}0^{+}))$ given in Fig.5 but rather of $O(\tau_{\mathrm{ingap}}(\mathbf{k})^{-1})$ given in Fig.6. The reflectivity $R(\omega)$ is given by

$$R(\omega) \;=\; \left| \frac{N(\omega)-1}{N(\omega)+1} \right|^{2}, \tag{4.3.4}$$

where the complex refractive index $N(\omega)$ is related to the dielectric constant $\epsilon(\omega)$ and the conductivity $\sigma(\omega)$ through the relations as

$$\epsilon(\omega) \;=\; 1+\mathrm{i}\,\frac{4\pi}{\omega}\,\sigma(\omega) \;=\; N(\omega)^{2}. \tag{4.3.5}$$

The results for $R(\omega)$ are shown in Fig.13 with the absorptivity $A(\omega) = 1 - R(\omega)$ shown in the inset. We find that $R(\omega)$ obeys the Hagen-Rubens relation in the primitive Drude model,

$$R_{\mathrm{D}}(\omega) \;\simeq\; 1-\sqrt{2\omega/\pi\sigma_{\mathrm{D}}^{'}(0)}, \qquad \text{for } \omega \ll \tau^{-1}. \tag{4.3.6}$$

Since $\tau_{\mathrm{ingap}}(\mathbf{k})^{-1} \ll \sigma_{\mathrm{intra}}^{'}(0)$, $R(\omega)$ is almost equal to unity. Thus, the optical conductivity $\sigma_{\mathrm{intra}}(\omega)$ in the ingap states shows Drude-like behavior, although the ingap states themselves are due to the strong correlation effects indeed.

The integrated spectral weight of $\sigma_{\mathrm{intra}}^{'}(\omega)$ is called the Drude weight, W_{D}, i.e.,

$$W_{\mathrm{D}} \equiv \int_{0}^{W_{\mathrm{B}}(T)} \mathrm{d}\omega\; \sigma_{\mathrm{intra}}^{'}(\omega) \equiv \frac{\pi}{2}\frac{n_{\mathrm{opt}}}{m_{\mathrm{b}}} \equiv \frac{\omega_{\mathrm{p}}^{2}}{8}, \tag{4.3.7}$$

with the band width $W_{\mathrm{B}}(T) = E_{-}^{top}(=\omega_0(T)) - E_{-}^{bot}$ and the plasma frequency ω_{p}. The δ-dependence of the Drude weight, W_{D}, at $T = 0$ is shown in Fig.14 together with the integrated specral weights of other components of $\sigma(\omega)$, $W_{\mathrm{inter}}^{'}$ for $\sigma_{\mathrm{inter}}^{'}(\omega)$ and $W_{\mathrm{inter}}^{''}$ for $\sigma_{\mathrm{inter}}^{''}(\omega)$. We note that $W_{\mathrm{D}} \propto \delta$ [54, 55, 56] at $\delta \lesssim 0.1$, which means $n_{\mathrm{opt}} \to 0$ or $m_{\mathrm{b}} \to \infty$ as $\delta \to 0$. The single-particle properties [51] seem to favor the latter, $m_{\mathrm{b}} \to \infty$. In any case, these are very specific features to the ingap states which emerge due to the strong correlation effects. The more details about the specral weights of $\sigma(\omega)$ are studied in Appendix B. The numerical results for the T-dependence of the Drude weight for $\delta = 0.1, 0.2, 0.3$ and 0.4 at $T \lesssim 2T_0$ are shown in Fig.15. We note that the scaling nature breaks down at $T \gtrsim T_0$. We also note that for higher doping concentrations the T-dependence of the Drude weight becomes weaker, in other words, the plasma frequency is almost T-independent. Compared with the results in Fig.10, we find that ω_{p} is larger than $W_{\mathrm{B}}(T)$ and the band gap, $E_{\mathrm{G}}(T) = E_{+}^{bot}(=\epsilon_p) - E_{-}^{top}(=\omega_0(T))$, at finite temperatures.

Finally, T-dependences of the resistivity $\rho(T) = [\sigma'_{\rm intra}(0)]^{-1}$ for $\delta = 0.1, 0.2, 0.3$ and 0.4 at $T \lesssim 2T_0$ are shown in Fig.16. These results show that both of the ω- and the T-dependences of the single-particle properties are scaled rather well by ω_0 or T_0. Compared the results shown in Fig.16 with those in Fig.7, we find that the T-dependence of $\rho(T)$ is very similar to that of the p-hole scattering rate, although the latter do not reproduce the results of SCE correctly due to the poorness of LTA at $T \gtrsim T_0$ unfortunately. Therefore, we expect that, if we could take the results of SCE for the p-hole scattering rate proportional to $(T - T_0)$ at $T \gtrsim T_0$ to calculate $\rho(T)$, we should obtain $\rho(T) \propto (T - T_0)$ as has been observed in the experiments.

4.4 Electronic Raman scattering

We assume that the incident laser frequency $\omega_i = 1.0$ is comparable to the optical band gap $E_{\rm g}(T) = E_+^{bot}(=\epsilon_p)$ for the numerical calculations of eq.(4.2.15), though the numerical values of ϵ_p obtained in the present model are 0.506, 0.495 and 0.473 for $\delta = 0.1$ at $T =$ 0.010, 0.015 and 0.025, respectively.

The numerical results for the imaginary part of the electronic Raman scattering response function $\chi''^{\perp}_{(pA)^2}(\omega{+}{\rm i}0^+)$ defined by eq.(4.2.9) are shown in Fig.17. Comparing the results in Fig.17 with those in Fig.11(a) confirms eq.(A.0.29) to hold. The ω-dependence of $\chi''^{\perp}_{(pA)^2}(\omega{+}{\rm i}0^+)$ is essentially due to that in eq.(4.2.11), because ${\rm k}_f/{\rm k}_{\rm i} = \omega_f/\omega_{\rm i} \simeq 1$ for the frequency shift $\omega \equiv \omega_{\rm i} - \omega_f$ which is of interest. Note that $\omega = 0.01$ corresponds roughly to $100cm^{-1}$. As shown in the inset of Fig.17, the gradient in $\chi''^{\perp}_{(pA)^2}(\omega{+}{\rm i}0^+)$ at $\omega \simeq 0$ becomes steeper with decreasing T, as expected from the relations, $\chi''^{\perp}_{(pA)^2}(\omega{+}{\rm i}0^+) \propto \omega\sigma'_{\rm intra}(\omega) \simeq \omega\sigma'_{\rm intra}(0)$ at $\omega \simeq 0$, and the results for $\sigma'_{\rm intra}(0)$ given in Fig.11(a).

The numerical results for the scattering intensity ${\rm I}^{\perp}_{(pA)^2}(\omega)$ are shown in Fig.18. At low frequency shifts, $\omega \ll T$, we obtain $1 + f_{\rm B}(\omega) \simeq T/\omega$ and hence ${\rm I}^{\perp}_{(pA)^2}(\omega) \simeq T\sigma'_{\rm intra}(\omega)$. This relation is confirmed to hold by comparing the results given in the inset of Fig.18 with those in the inset of Fig.11(a). At frequencies where the Drude-like tail is observed in $\sigma'_{\rm intra}(\omega)$, we obtain ${\rm I}^{\perp}_{(pA)^2}(\omega) \simeq \omega^{-1}$, which is contradiction to the weakly ω-dependent electronic Raman intensity observed in the experiments. In order to explain such experiments we

need to include the terms of higher orders in the $1/N$-expansion and/or the finite-T effects at $T \gtrsim T_0$.

4.5 Generalized Drude analyses (GDA)

To clarify dynamical propertites of the ingap states, we analyze the results for $\sigma_{\rm intra}(\omega)$ with the generalized Drude formula, which is obtained by replacing τ^{-1} and $m_{\rm b}$ in eq.(4.3.2) by the ω-dependent counterparts, $\tau^{*}_{\rm opt}(\omega)^{-1}$ and $m_{\rm opt}(\omega)$, as [8) – 15) 53) 57) – 60)]

$$\sigma_{\rm intra}(\omega) = \frac{n_{\rm opt}}{m_{\rm b}} \frac{1}{\frac{m_{\rm opt}(\omega)}{m_{\rm b}}} \frac{1}{\tau^{*}_{\rm opt}(\omega)^{-1} - {\rm i}\omega}. \tag{4.5.1}$$

Using the numerical results for $\sigma_{\rm intra}(\omega) = \sigma^{'}_{\rm intra}(\omega) + {\rm i}\sigma^{''}_{\rm intra}(\omega)$ and $W_{\rm D}$, we evaluate $\tau^{*}_{\rm opt}(\omega)^{-1}$ and $m_{\rm opt}(\omega)/m_{\rm b}$ through such relations as

$$\tau^{*}_{\rm opt}(\omega)^{-1} = \omega\ \sigma^{'}_{\rm intra}(\omega)\ /\ \sigma^{''}_{\rm intra}(\omega), \tag{4.5.2}$$

$$\frac{m_{\rm opt}(\omega)}{m_{\rm b}} = \frac{n_{\rm opt}}{m_{\rm b}} \frac{1}{\sigma^{'}_{\rm intra}(\omega)} \frac{\tau^{*}_{\rm opt}(\omega)}{1+\omega\tau^{*}_{\rm opt}(\omega)^{2}}. \tag{4.5.3}$$

The numerical results for the ω-dependence of $\tau^{*}_{\rm opt}(\omega)^{-1}$ at various values of T for $\delta = 0.1$ are shown in Fig.19. We note that the ω-dependences of $\tau^{*}_{\rm opt}(\omega)^{-1}$ are weak for ω where the Drude-like tail in $\sigma^{'}_{\rm intra}(\omega)$ is observed as shown in Fig.11(a). Those of $m_{\rm opt}(\omega)$ are shown in Fig.20. In the low frequency limit, eq.(4.5.3) reduces to

$$\frac{m_{\rm opt}(0)}{m_{\rm b}} = \frac{n_{\rm opt}}{m_{\rm b}} \frac{A}{\sigma^{'}_{\rm intra}(0)^{2}}, \quad \text{with } A \equiv \lim_{\omega\to 0+}\Big(\frac{\sigma^{''}_{\rm intra}(\omega)}{\omega}\Big). \tag{4.5.4}$$

The T-dependences of $m_{\rm opt}(0)$ for $\delta = 0.1, 0.2, 0.3$ and 0.4 at $T \lesssim 2T_0$ are shown in Fig.21. The results show that the T-dependences are scaled rather well by ω_0 or T_0. We derive $m_{\rm opt}(0) = m_{\rm b}$ at $T = 0$ in Appendix B. We note that the optical mass $m_{\rm opt}(\omega)$ is of the same order as the band mass $m_{\rm b}$ deduced from the Drude tail irrespective of ω and δ.

Now, a question is why we only observe such optical masses as of $O(m_{\rm b})$ in a strongly correlated system like the d-p model. In fact, it shows significant contrast to the cases in the dense Kondo systems where the heavy electrons have been actually observed at low frequencies in the optical measurements. [58, 59)] The answer for the question is that the energy-dependence of $[2\tau_{\rm ingap}({\bf k})]^{-1}$ plays an essential role to detemine the ω-dependence

of $m_{\rm opt}(\omega)$, especially the enhancement at low frequencies, and the results shown in Fig.6 are only to yield the weak ω-dependence.

In order to prove this statement, we introduce a model for the quasi-particle scattering rate given by

$$[\ 2\tau_{\rm ingap}({\bf k})\ ]^{-1} = p(E_-({\bf k})-E_-^{bot})\ \theta(E_-({\bf k})-E_-^{bot})\ \theta(\omega_0-E_-({\bf k}))\ +\ \frac{1}{2\tau}, \qquad (4.5.5)$$

as illustrated in Fig.22, which is a simplified version of those shown in Fig.6. We then study effects of the coefficient p of the energy-linear term in $[2\tau_{\rm ingap}({\bf k})]^{-1}$ on the ω-dependences of $\tau^*_{\rm opt}(\omega)^{-1}$ and $m_{\rm opt}(\omega)/m_{\rm b}$. The numerical results for $\sigma^{'}(\omega)$, $\sigma^{''}(\omega)$, and $R(\omega)$ calculated at $T=0$ by using this model are shown in Figs.23, 24, and 25, respectively. We observe some remarkable deviation from the simple Drude behavior, eq.(4.3.3), for the ω-dependence of $\sigma^{''}(\omega)$ and $R(\omega)$ shown in Figs.24 and 25 to occur when p is larger than a certain critical value $p_{\rm c}$, i.e., the position and the height of the peak in $\sigma^{''}(\omega)$ are not monotonic functions of p, which result in $R(\omega)$ correspondingly.

The numerical results for $\tau^*_{\rm opt}(\omega)^{-1}$ and $m_{\rm opt}(\omega)/m_{\rm b}$ calculated by using eqs.(4.5.2) and (4.5.3) are shown in Figs.26 and 27, respectively. We note that the ω-dependence of $m_{\rm opt}(\omega)/m_{\rm b}$, particularly the enhancement at low frequencies, becomes significant when $p \gtrsim p_{\rm c}$, which means that larger p leads to larger mass enhancement. The mass enhancements as functions of p for various values of $(2\tau)^{-1}$ are plotted in Fig.28. We note that the mass enhancement at low frequencies critically depends also upon values of $(2\tau)^{-1}$. These analyses yield $10/(2\tau W_{\rm B})$ as a rough estimation of $p_{\rm c}$. Thus we may conclude that the energy-dependence of $[2\tau_{\rm ingap}({\rm k})]^{-1}$ shown in Fig.6 belongs to the cases with $p \lesssim p_{\rm c}$ and results in the weak ω-dependences of $\tau^*_{\rm opt}(\omega)^{-1}$ and $m_{\rm opt}(\omega)/m_{\rm b}$.

Finally, we make a few comments on the generalized Drude analyses (GDA). There seems to exist some confusions regarding how to determine the optical scattering rate in the theoretical and the experimental studies. The confusions are originated from the exsistence of the two different types of the optical scattering rates, the one, $\tau^*_{\rm opt}(\omega)^{-1}$, defined in eq.(4.5.1) and the other, $\tau_{\rm opt}(\omega)^{-1}$, given by the real part of the complex scattering rate,

$$\tau(\omega)^{-1} \ =\ \tau_{\rm opt}(\omega)^{-1}\ +\ {\rm i}\tau^{''}_{\rm opt}(\omega)^{-1}, \qquad (4.5.6)$$

where each component is related to $\tau^{*}_{\rm opt}(\omega)^{-1}$ and/or $m_{\rm opt}(\omega)/m_{\rm b}$ through the relations as

$$\tau_{\rm opt}(\omega)^{-1} \equiv \tau^{*}_{\rm opt}(\omega)^{-1}\frac{m_{\rm opt}(\omega)}{m_{\rm b}}, \qquad \tau^{''}_{\rm opt}(\omega)^{-1} \equiv -\omega\left(\frac{m_{\rm opt}(\omega)}{m_{\rm b}} - 1\right). \tag{4.5.7}$$

We plot in Fig.29 the numerical results for $\tau_{\rm opt}(\omega)^{-1}$ calculated from eq.(4.5.7) by using the results for $\tau^{*}_{\rm opt}(\omega)^{-1}$ and $m_{\rm opt}(\omega)/m_{\rm b}$ shown in Figs.26 and 27, respectively. Comparing these results with those for $\tau^{*}_{\rm opt}(\omega)^{-1}$ shown in Fig.26, it is clear to see that they are quite different from each other, espcially when $p \gtrsim p_{\rm c}$, and both have no direct relation to the model scattering rate shown in Fig.22, on which both of the optical scattering rates are based. Thus we strongly emphasize that it is quite dangerous to link the information on either of the optical scattering rates directly to that of the quasi-particle scattering rate as has been often done and that the two types of the optical scattering rates can be entirely different from each other.

Chapter 5

Summary and Discussion

We have developed an approximation procedure to determine the single-particle properties at $T \lesssim T_0$ in the d-p model by including terms of the leading order in the $1/N$-expansion and then calculated the transport coefficients such as the optical conductivity $\sigma(\omega)$ and the electronic Raman scattering intensity $I(\omega)$ using those results. The coherence temperature T_0 is known to be of $0.2\omega_0$, where ω_0 is a half of the band width of the *ingap states* at $T = 0$ and is proportional to the doped hole concentration δ at $\delta \lesssim 0.1$.

The model described in the hole-picture includes as the fundamental parameters the Cu $3d_{x^2-y^2}$-level ϵ_d, the O $2p_\sigma$-level ϵ_p, the transfer integral between the adjacent Cu and O sites, t_{pd}, and the infinite intraatomic Coulomb repulsion at the Cu sites, $U = \infty$. In order to include the $U = \infty$ effects properly, we have introduced the auxiliary bosons and used the Feynman diagram technique with imposing the strict local constraints which guarantee the equivalence between the original infinite-U model and the modified version in the auxiliary boson representation.

The numerical results for the optical conductivity $\sigma(\omega)$ have told us that the *ingap states* contribute to the Drude-like components with the integrated intensity (the Drude weight $W_{\rm D}$), which is also proportional to δ at $\delta \lesssim 0.1$ and almost T-independent with the moderate values of δ, as has been observed in experiments. Both of the ω- and the T-dependences in $\sigma(\omega)$ are found to be scaled well by ω_0. The generalized Drude analyses (GDA) of $\sigma(\omega)$ show that the optical scattering rate $\tau^*_{\rm opt}(\omega)^{-1}$ and the optical mass $m_{\rm opt}(\omega)$ are only weakly ω-dependent in contradiction to the experimental observations and that

$m_{\rm opt}(\omega)$ is of the same order as the band mass $m_{\rm b}$ deduced from the Drude tail irrespective of δ, although the absolute magnitude of $m_{\rm b}$ can not be determined soley within the frame work of GDA. The numerical results for the electronic Raman scattering intensity also do not explain the anomalously broad peak extended up to several thousands of cm^{-1} observed in the experiments.

As for the origins of these discrepancies two possibilities come up to our minds. One is that the *ingap states* themselves do not have such anomalous optical properties at $T \lesssim T_0$. The other is that it is essential to include the terms of higher orders in the $1/N$-expansion, especially the terms including effects of the incoherent states around the edges of the ingap band and the coherent states around the atomic d-level ϵ_d.

GDA have also told us that the energy-dependence of the quasi-particle scattering rate plays a crucial role in determining the ω-dependence of the optical mass $m_{\rm opt}(\omega)$ and that there are no direct relations between the quasi-particle scattering rate and two types of the optical scattering rates, $\tau^{*}_{\rm opt}(\omega)^{-1}$ and $\tau_{\rm opt}(\omega)^{-1}$, which have been used rather often in confusion.

Appendix A

Electronic Raman scattring due to the intrasubband transition from the $(\mathbf{p}\cdot\mathbf{A})^2$-term

We consider a two-band electronic system which couples to a radiation field described by a vector potential $\mathbf{A}$. The hamiltonian in the Coulomb gauge where $div\mathbf{A} = 0$ is given by

$$H = \sum_i \Big(\frac{1}{2m_i}\big(\mathbf{p}_i - \frac{e}{c}\mathbf{A}(\mathbf{r}_i,t)\big)^2 + U(\mathbf{r}_i) \Big) \tag{A.0.1}$$

$$= H_0 + H_1 + \sum_i \frac{e^2}{2m_i c^2}\mathbf{A}(\mathbf{r}_i,t)^2, \tag{A.0.2}$$

with

$$H_0 = \sum_i \Big(\frac{1}{2m_i}\mathbf{p}_i^2 + U(\mathbf{r}_i) \Big) \tag{A.0.3}$$

$$= \sum_{\mathbf{k}}\sum_{\sigma}\sum_{\gamma=\pm} E_\gamma(\mathbf{k}) a^\dagger_{\mathbf{k}\sigma\gamma} a_{\mathbf{k}\sigma\gamma}, \tag{A.0.4}$$

$$H_1 = \sum_i -\frac{e}{m_i c}\mathbf{p}_i \cdot \mathbf{A}(\mathbf{r}_i,t) \tag{A.0.5}$$

$$= -\sqrt{\frac{2\pi\hbar}{cV}} \sum_{\gamma,\gamma'=\pm} \sum_{\mathbf{q}} \sum_{\lambda} \sqrt{\frac{1}{\mathrm{q}}} (\mathbf{e}_{\mathbf{q}\lambda}\cdot\mathbf{J}_{\mathbf{q},\gamma'\to\gamma})(b_{\mathbf{q}\lambda} + b^\dagger_{-\mathbf{q}\lambda}), \tag{A.0.6}$$

$$\mathbf{J}_{\mathbf{q},\gamma'\to\gamma} = \frac{e}{\hbar}\sum_{\mathbf{k}}\sum_{\sigma}\Big(\nabla_{\mathbf{k}'} E_{\gamma'}(\mathbf{k}')\big|_{\mathbf{k}'=\mathbf{k}+\mathbf{q}/2} \Big)\, a^\dagger_{\mathbf{k}+\mathbf{q}\sigma\gamma} a_{\mathbf{k}\sigma\gamma'}. \tag{A.0.7}$$

The i-th electron with charge $e<0$ and mass m_i itinerates under a certain periodic potential $U(\mathbf{r}_i)$. Then N_L electrons form a Bloch band $E_\gamma(\mathbf{k})$. The operator $a^\dagger_{\mathbf{k}\sigma\gamma}$ creates an electron

with wave vector $\mathbf{k}$, spin σ and the band index γ. The operator $b_{\mathbf{q}\lambda}$ annihilates a photon specified by the polarization vetor $\mathbf{e}_{\mathbf{q}\lambda}$ with wave vector $\mathbf{q}$ and mode λ and by the frequency $\omega_{\mathbf{q}} = c\mathrm{q}$ with light velocity c.

Since the Raman scattering is a two-photon process, one need to evaluate the S-matrix including the 2nd power of $\mathbf{A}$. The contribution from the $(\mathbf{p}\cdot\mathbf{A})^2$-term is given by

$$\hat{S}_1^{(2)} = (-\frac{\mathrm{i}}{\hbar})^2 \int_{-\infty}^{+\infty} \mathrm{dt}_1 H_1(\mathrm{t}_1) \int_{-\infty}^{\mathrm{t}_1} \mathrm{dt}_2 H_1(\mathrm{t}_2), \qquad \text{(A.0.8)}$$

where $\hat{O}(\mathrm{t}) \equiv \mathrm{e}^{\mathrm{i}H_0\mathrm{t}/\hbar}\ \hat{O}\ \mathrm{e}^{-\mathrm{i}H_0\mathrm{t}/\hbar}$. The initial and the final states in the scattering process, $|i\rangle$ and $|f\rangle$, are given by the product of the eigen states of the electronic system and the radiation field:

$$|\,i\rangle = |\,i_{\mathrm{e}}\rangle\, b^{\dagger}_{\mathbf{k}_i\lambda_i}\,|0\rangle\,, \qquad |f\rangle = |\,f_{\mathrm{e}}\rangle\, b^{\dagger}_{\mathbf{k}_f\lambda_f}\,|0\rangle\,, \qquad \text{(A.0.9)}$$

with the radiation vacuum state $|0\rangle$. In the Raman scattering experiments we observe the energy shift, $\hbar\omega = \hbar\omega_i - \hbar\omega_f$, and the momentum transfer, $\hbar\mathbf{q} = \hbar\mathbf{k}_i - \hbar\mathbf{k}_f$, in the system with the absorbed and the emitted photon frequency, ω_i and ω_f, respectively.

Here we show that the contribution to the electronic Raman scattering intensity from eq.(A.0.6) or (A.0.8) is proportional to $\omega\sigma^{'}(\omega)$ with the real part of the optical conductivity $\sigma^{'}(\omega)$ irrespective of the polarization geometries when the resonance condition is satisfied. The matrix element of eq.(A.0.8) is written in terms of the electronic interband and intraband transition processes obeying energy conservation law, $E_f - E_i = \hbar\omega$, with the energy E_i and E_f of the states $|\,i_{\mathrm{e}}\rangle$ and $|\,f_{\mathrm{e}}\rangle$, respectively, as follows:

$$\begin{aligned}
\langle f|\,\hat{S}_1^{(2)}\,|\,i\rangle \;=\; & \frac{\mathrm{i}}{\hbar c\mathrm{V}}(2\pi\hbar)^2 \sum_{\gamma,\gamma^{'}=\pm}\sum_{\delta,\delta^{'}=\pm} \sqrt{\frac{1}{\mathrm{k}_i\mathrm{k}_f}}\ \delta\left(E_f - E_i - \hbar\omega\right) \\
\times\ \Big(\ & \langle f_{\mathrm{e}}|\,(\mathbf{e}_{\mathbf{k}_i\lambda_i}\cdot\mathbf{J}_{\mathbf{k}_i,\gamma^{'}\to\gamma})\frac{1}{H_0 - E_i + \hbar\omega_f}(\mathbf{e}_{\mathbf{k}_f\lambda_f}\cdot\mathbf{J}_{-\mathbf{k}_f,\delta^{'}\to\delta})\,|\,i_{\mathrm{e}}\rangle \\
& + \\
& \langle f_{\mathrm{e}}|\,(\mathbf{e}_{\mathbf{k}_f\lambda_f}\cdot\mathbf{J}_{-\mathbf{k}_f,\gamma^{'}\to\gamma})\frac{1}{H_0 - E_i - \hbar\omega_i}(\mathbf{e}_{\mathbf{k}_i\lambda_i}\cdot\mathbf{J}_{\mathbf{k}_i,\delta^{'}\to\delta})\,|\,i_{\mathrm{e}}\rangle\ \Big). \qquad \text{(A.0.10)}
\end{aligned}$$

Here we assume that the chemical potential $\mu(T)$ lies in the band $E_+(\mathbf{k})$ and that the width of each band $\mathrm{W_B}(T)$ is narrower than the band gap $E_{\mathrm{G}}(T)$, and consider the resonant Raman scattering for low energy shifts at low temperatures,

$$T << W_{\mathrm{B}}(T) < E_{\mathrm{G}}(T), \qquad \hbar\omega << \hbar\omega_i, \hbar\omega_f \sim E_{\mathrm{G}}(T). \qquad \text{(A.0.11)}$$

As for the electronic transition processes there are three different types to be considered. The first is the two successive intraband transition processes within the band $E_+(\mathbf{k})$ with photons absorbed and emitted giving a small factor, $1/\hbar\omega_f - 1/\hbar\omega_i = \hbar\omega/\hbar\omega_f\hbar\omega_i \ll 1$, because the wave number $k_i, k_f \ll 1/a$ with the lattice constant a. The second is the intraband transition process within the band $E_+(\mathbf{k})$ with a photon absorbed (emitted) followed by the interband transition process with a photon emitted (absorbed) giving finite contribution for $|\omega| \sim E_G(T)$ which is of no interest. The third is the two successive interband transition processes with photons absorbed and emitted as illustrated in Fig.30, i.e., the *intrasubband* transition [61] within the band $E_+(\mathbf{k})$ giving the dominant contribution to the matrix element, eq.(A.0.10).

Under the resonance condition, eq.(A.0.11), by defining the *pseudo-current* operators in the band $E_+(\mathbf{k})$ as

$$\mathbf{J}_{\mu,\mathbf{q}} = \sum_{\mathbf{k}}\sum_{\sigma} \mathrm{U}_{\mu,\mathbf{q}}(\mathbf{k}) a^{\dagger}_{\mathbf{k}+\mathbf{q}\sigma+} a_{\mathbf{k}\sigma+}, \quad (\mu = i, f) \quad , \tag{A.0.12}$$

$$\mathrm{U}_{f,\mathbf{q}}(\mathbf{k}) \equiv \frac{1}{E_g(T) + \hbar\omega_f}\Big(\mathbf{e}_i \cdot \frac{e}{\hbar}\nabla_{\mathbf{k}} E_+(\mathbf{k})\Big)\Big(\mathbf{e}_f \cdot \frac{e}{\hbar}\nabla_{\mathbf{k}'} E_+(\mathbf{k}')\Big|_{\mathbf{k}'=\mathbf{k}+\mathbf{q}}\Big) \tag{A.0.13}$$

$$\mathrm{U}_{i,\mathbf{q}}(\mathbf{k}) \equiv \frac{1}{E_g(T) - \hbar\omega_i}\Big(\mathbf{e}_f \cdot \frac{e}{\hbar}\nabla_{\mathbf{k}} E_+(\mathbf{k})\Big)\Big(\mathbf{e}_i \cdot \frac{e}{\hbar}\nabla_{\mathbf{k}'} E_+(\mathbf{k}')\Big|_{\mathbf{k}'=\mathbf{k}+\mathbf{q}}\Big), \tag{A.0.14}$$

with $\mathbf{e}_i \equiv \mathbf{e}_{\mathbf{k}_i\lambda_i}, \mathbf{e}_f \equiv \mathbf{e}_{\mathbf{k}_f\lambda_f}$, $\mathbf{q} = \mathbf{k}_i - \mathbf{k}_f$, and the optical band gap $E_g(T) = \mu(T) - E_-^{top}$ where E_-^{top} is the upper band edge of $E_-(\mathbf{k})$, we obtain

$$\langle f|\,\hat{S}_1^{(2)}\,|\,i\rangle \sim -\frac{\mathrm{i}}{\hbar c\mathrm{V}}(2\pi\hbar)^2\sqrt{\frac{1}{\mathrm{k}_i\mathrm{k}_f}}\ \langle f_e|\,\mathbf{J}_{f,\mathbf{q}} + \mathbf{J}_{i,\mathbf{q}}\,|\,i_e\rangle\,\delta\left(E_f - E_i - \hbar\omega\right). \tag{A.0.15}$$

Then the transition probability per unit time is

$$w_{i\to f} = \frac{(2\pi\hbar)^4}{(\hbar c\mathrm{V})^2}\frac{1}{\mathrm{k}_i\mathrm{k}_f}\ \Big|\ \langle f_e|\,\mathbf{J}_{f,\mathbf{q}} + \mathbf{J}_{i,\mathbf{q}}\,|\,i_e\rangle\ \Big|^2 \frac{1}{2\pi\hbar}\delta\left(E_f - E_i - \hbar\omega\right). \tag{A.0.16}$$

When the incident light is described by a plane wave, $\mathbf{e}_i(1/\sqrt{\mathrm{V}})\mathrm{e}^{\mathrm{i}\mathbf{k}_i\cdot\mathbf{r}}$, c/V photons per unit time go through the system. The density of states with energy between ω_f and $\omega_f + \mathrm{d}\omega$ and with wave vector between $\mathbf{k}_f$ and $\mathbf{k}_f + \mathrm{d}\Omega$ is $\mathrm{V}\mathrm{k}_f^2/(2\pi)^3 c$. Then using eq.(A.0.16) the number of the photons scattered into frequency interval $\mathrm{d}\omega$ and solid angle $\mathrm{d}\Omega$ per unit time per unit cell, i.e., the electronic Raman intensity, at finite temperature $T \equiv 1/\beta$ is given by

$$\mathrm{I}_{(pA)^2}(\omega) = \frac{1}{\mathrm{V}}\sum_{|f_e\rangle}\frac{\mathrm{V}\mathrm{k}_f^2}{(2\pi)^3 c}\frac{\mathrm{V}}{c}\sum_{|i_e\rangle}\mathrm{e}^{-\beta E_i}\ w_{i\to f} \tag{A.0.17}$$

$$= \frac{1}{\mathrm{V}}\frac{1}{c^4}\frac{\mathrm{k}_f}{\mathrm{k}_i}\frac{1}{2\pi}\int_{-\infty}^{+\infty}\mathrm{dt}\mathrm{e}^{\mathrm{i}\omega\mathrm{t}}\left\langle\ \left(\mathbf{J}^{\dagger}_{f,\mathbf{q}}(\mathrm{t})+\mathbf{J}^{\dagger}_{i,\mathbf{q}}(\mathrm{t})\right)\left(\mathbf{J}_{f,\mathbf{q}}(0)+\mathbf{J}_{i,\mathbf{q}}(0)\right)\ \right\rangle \tag{A.0.18}$$

$$= \left(1+f_{\mathrm{B}}(\omega)\right)\ \chi''_{(pA)^2}(\mathbf{q},\omega+\mathrm{i}0^{+}), \tag{A.0.19}$$

with the Bose distribution function $f_{\mathrm{B}}(\omega)\equiv(\mathrm{e}^{\beta\omega}-1)^{-1}$ and the electronic Raman scattering response function

$$\chi_{(pA)^2}(\mathbf{q},\omega)\equiv\frac{1}{c^4}\frac{\mathrm{k}_f}{\mathrm{k}_i}\frac{1}{\pi}\frac{1}{\mathrm{V}}\int_{-\infty}^{+\infty}\mathrm{dt}\mathrm{e}^{\mathrm{i}\omega\mathrm{t}}\mathrm{i}\theta(\mathrm{t})\left\langle\ \left[\left(\mathbf{J}^{\dagger}_{f,\mathbf{q}}(\mathrm{t})+\mathbf{J}^{\dagger}_{i,\mathbf{q}}(\mathrm{t})\right),\left(\mathbf{J}_{f,\mathbf{q}}(0)+\mathbf{J}_{i,\mathbf{q}}(0)\right)\right]_{-}\ \right\rangle. \tag{A.0.20}$$

Eq.(A.0.19) is nothing but the fluctuation-dissipation theorem.

Furthermore, the retarded function $\chi''_{(pA)^2}(\mathbf{q},\omega+\mathrm{i}0^{+})$ is given by the analytic continuation of the temperature Green's function,

$$\chi_{(pA)^2}(\mathbf{q},\mathrm{i}\omega_n) = \frac{1}{c^4}\frac{\mathrm{k}_f}{\mathrm{k}_i}\frac{1}{\pi}\frac{1}{\mathrm{V}}\int_0^{\beta}\mathrm{d}\tau\mathrm{e}^{\mathrm{i}\omega_n\tau}(-)\left\langle\mathrm{T}_{\tau}\left[\left(\mathbf{J}^{\dagger}_{f,\mathbf{q}}(\tau)+\mathbf{J}^{\dagger}_{i,\mathbf{q}}(\tau)\right)\left(\mathbf{J}_{f,\mathbf{q}}(0)+\mathbf{J}_{i,\mathbf{q}}(0)\right)\right]\right\rangle \tag{A.0.21}$$

$$= \frac{1}{c^4}\frac{\mathrm{k}_f}{\mathrm{k}_i}\frac{1}{\pi}\frac{1}{\mathrm{V}}\sum_{\mu,\nu=i,f}\sum_{\mathbf{k}\mathbf{k}'}\sum_{\sigma\sigma'}\mathrm{U}_{\mu,\mathbf{q}}(\mathbf{k})\,\mathrm{U}_{\nu,\mathbf{q}}(\mathbf{k}')K(\mathbf{q},\mathbf{k}',\mathbf{k},\mathrm{i}\omega_n), \tag{A.0.22}$$

with

$$K(\mathbf{q},\mathbf{k}',\mathbf{k},\mathrm{i}\omega_n)\equiv\int_0^{\beta}\mathrm{d}\tau\mathrm{e}^{\mathrm{i}\omega_n\tau}(-)\left\langle\mathrm{T}_{\tau}\left[a^{\dagger}_{\mathbf{k}'\sigma'+}(\tau)a_{\mathbf{k}'+\mathbf{q}\sigma'+}(\tau)a^{\dagger}_{\mathbf{k}+\mathbf{q}\sigma+}(0)a_{\mathbf{k}\sigma+}(0)\right]\right\rangle, \tag{A.0.23}$$

where $\hat{O}(\tau)\equiv\mathrm{e}^{(H_0-\mu\mathrm{N})\tau}\hat{O}\mathrm{e}^{-(H_0-\mu\mathrm{N})\tau}$ with the Matsubara frequency $\omega_n{=}2n\pi T$, which yields

$$\chi''_{(pA)^2}(\mathbf{q},\omega+\mathrm{i}0^{+}) = \frac{1}{c^4}\frac{\mathrm{k}_f}{\mathrm{k}_i}\frac{1}{\pi}\frac{1}{\mathrm{V}}\sum_{\mu,\nu=i,f}\sum_{\mathbf{k}\mathbf{k}'}\sum_{\sigma\sigma'}\mathrm{U}_{\mu,\mathbf{q}}(\mathbf{k})\,\mathrm{U}_{\nu,\mathbf{q}}(\mathbf{k}')(-)\mathrm{Im}K(\mathbf{q},\mathbf{k}',\mathbf{k},\omega+\mathrm{i}0^{+}). \tag{A.0.24}$$

On the other hand, the optical conductivity $\sigma(\mathbf{q},\omega)$ calculated for the band $E_{+}(\mathbf{k})$ is written in terms of the retarded current current response function $\chi_{JJ}(\mathbf{q},\omega+\mathrm{i}0^{+})$ as

$$\sigma(\mathbf{q},\omega) = -\frac{1}{\mathrm{i}\omega}\left(\ \chi_{JJ}(\mathbf{q},\omega+\mathrm{i}0^{+})-\chi_{JJ}(\mathbf{q},0+\mathrm{i}0^{+})\ \right). \tag{A.0.25}$$

The retarded function $\chi_{JJ}(\mathbf{q},\omega+\mathrm{i}0^{+})$ is given by the analytic continuation of the temperature Green's function,

$$\chi_{JJ}(\mathbf{q},\mathbf{k}',\mathbf{k},\mathrm{i}\omega_n) = \frac{1}{\mathrm{V}}\int_0^{\beta}\mathrm{d}\tau\mathrm{e}^{\mathrm{i}\omega_n\tau}(-)\left\langle\ \mathrm{T}_{\tau}\left[\mathbf{J}^{\dagger}_{\mathbf{q},+\to+}(\tau)\,\mathbf{J}_{\mathbf{q},+\to+}(0)\right]\ \right\rangle$$

$$= \frac{1}{\mathrm{V}}\sum_{\mathbf{k}\mathbf{k}'}\sum_{\sigma\sigma'}\mathbf{V}_{\mathbf{q}}(\mathbf{k})\,\mathbf{V}_{\mathbf{q}}(\mathbf{k}')K(\mathbf{q},\mathbf{k}',\mathbf{k},\mathrm{i}\omega_n), \tag{A.0.26}$$

with

$$\mathbf{V_q}(\mathbf{k}) \;=\; \frac{e}{\hbar}\,\nabla_{\mathbf{l}} E_{+}(\mathbf{l})|_{\mathbf{l}=\mathbf{k}+\mathbf{q}}\,. \tag{A.0.27}$$

Then the real part of the optical conductivity, eq.(A.0.25), yields

$$\sigma^{'}(\mathbf{q},\omega) \;=\; \frac{1}{\omega}\sum_{\mathbf{k}\mathbf{k}^{'}}\sum_{\sigma\sigma^{'}} \mathbf{V_q}(\mathbf{k})\,\mathbf{V_q}(\mathbf{k}^{'})(-)\mathrm{Im}K(\mathbf{q},\mathbf{k}^{'},\mathbf{k},\omega{+}\mathrm{i}0^{+}). \tag{A.0.28}$$

Combining eqs.(A.0.24), (A.0.28) and (A.0.11), we at last obtain the relation as

$$\chi^{''}_{(pA)^2}(\mathbf{q},\omega{+}\mathrm{i}0^{+}) \;\propto\; \omega\,\sigma^{'}(\mathbf{q},\omega). \tag{A.0.29}$$

Appendix B

The optical conductivity at T=0

Here we investigate the properties of the optical conductivity $\sigma(\mathbf{q}\to\mathbf{0},\omega) \equiv \sigma(\omega)$ at $T = 0$, where the quasi-particle scattering rate is equal to zero and the optical conductivity is separated into two parts, the intraband component and the interband one. We employ the units so that $2t_{pd} = \hbar = e = a = 1$ also in this appendix.

The interband component $K^{(0)}_{\rm inter}(\mathbf{k}, \omega{+}\mathrm{i}0^+)$ in eq.(4.2.11) is written as

$$\mathrm{Im}K^{(0)}_{\rm inter}(\mathbf{k}, \omega{+}\mathrm{i}0^+) = -\pi\theta\Big(-E_-(\mathbf{k})\Big)\, R_{\rm inter}(\mathbf{k})\, \delta\Big(\omega-(E_+(\mathbf{k})-E_-(\mathbf{k}))\Big), \quad \text{(B.0.1)}$$

$$\mathrm{Re}K^{(0)}_{\rm inter}(\mathbf{k}, \omega{+}\mathrm{i}0^+) = -\theta\Big(-E_-(\mathbf{k})\Big)\, R_{\rm inter}(\mathbf{k})\, \frac{1}{E_+(\mathbf{k})-E_-(\mathbf{k})-\omega}, \quad \text{(B.0.2)}$$

where

$$R_{\rm inter}(\mathbf{k}) = b\Big(A_-(\mathbf{k})^2{+}A_+(\mathbf{k})^2\Big) + \frac{2}{W(\mathbf{k})}(E_-(\mathbf{k})-\omega_0)(E_+(\mathbf{k})-\omega_0)A_+(\mathbf{k})A_-(\mathbf{k}), \quad \text{(B.0.3)}$$

$$= \frac{b(\epsilon_p-\omega_0)^2}{(\epsilon_p-\omega_0)^2 + 4bW(\mathbf{k})}. \quad \text{(B.0.4)}$$

In deriving eq.(B.0.4), we have used eqs.(2.0.27), (2.0.52) and the explicit form of eq.(4.2.4) or (4.2.5),

$$G_{dp}(\mathbf{k}, \mathrm{i}\omega_n) = \frac{1}{\sqrt{W(\mathbf{k})}} \sum_{\gamma=\pm} (E_\gamma(\mathbf{k})-\omega_0) \frac{1 - A_\gamma(\mathbf{k})}{\mathrm{i}\omega_n - E_\gamma(\mathbf{k})}, \quad \text{(B.0.5)}$$

together with the relation, $\sum_{\gamma=\pm} A_\gamma(\mathbf{k}) = 1$, from eq.(2.0.29). Then, from eqs.(4.2.13) and (4.2.14), we obtain

$$\sigma'_{\rm inter}(\omega) = \frac{(\epsilon_p-\omega_0)^2}{8}\frac{1}{\omega^2}, \quad \text{(B.0.6)}$$

$$\sigma''_{\rm inter}(\omega) \;=\; \frac{(\epsilon_p-\omega_0)^2}{8\pi}\Big(\;\frac{1}{\omega}(E_{\rm min}^{-1}-E_{\rm max}^{-1})\;+\;\frac{1}{\omega^2}\log\frac{E_{\rm max}(\omega-E_{\rm min})}{E_{\rm min}(E_{\rm max}-\omega)}\;\Big), \qquad \text{(B.0.7)}$$

which are finite for $E_{\rm min}\leq\omega\leq E_{\rm max}$ with $E_{\rm min}=E_+({\rm k_F})=\epsilon_p+\omega_0$ and $E_{\rm max}=E_+^{top}-E_-^{bot}=\sqrt{(\epsilon_p-\omega_0)^2+8b}$. The corresponding integrated intensities are given by

$$W'_{\rm inter}=\frac{(\epsilon_p-\omega_0)^2}{8}\,(E_{\rm min}^{-1}-E_{\rm max}^{-1}),\qquad W''_{\rm inter}=\frac{1}{\pi}\,W'_{\rm inter}\log\frac{E_{\rm max}}{E_{\rm min}}. \qquad \text{(B.0.8)}$$

Eqs.(B.0.6) and (B.0.7) obey the Kramers-Krönig relations as eqs.(B.0.1) and (B.0.2) do. The numerical plots of eqs.(B.0.6) and (B.0.7) for $\delta=0.1$ and 0.4 are shown in Fig.31.

Similarly, the intraband component $K^{(0)}_{\rm intra}({\bf k},\omega{+}{\rm i}0^+)$ in eq.(4.2.11) is also written as

$$\begin{aligned}
{\rm Im}K^{(0)}_{\rm intra}({\bf k},\omega{+}{\rm i}0^+) \;&=\; -\pi\lim_{\varepsilon\to0^+}R_{\rm intra}({\bf k})\int_{-\infty}^{+\infty}{\rm d}x\;\theta(-x) \qquad \text{(B.0.9)}\\
&\times\;\Delta(x{-}E_-({\bf k}))\Big(\;\Delta(x{+}\omega{-}E_-({\bf k}))-\Delta(x{-}\omega{-}E_-({\bf k}))\;\Big),\\
{\rm Re}K^{(0)}_{\rm intra}({\bf k},\omega{+}{\rm i}0^+) \;&=\; -\lim_{\varepsilon\to0^+}R_{\rm intra}({\bf k})\int_{-\infty}^{+\infty}{\rm d}x\;\theta(-x) \qquad \text{(B.0.10)}\\
&\times\;\Delta(x{-}E_-({\bf k}))\Big(\;{\rm P}(x{+}\omega{-}E_-({\bf k}))+{\rm P}(x{-}\omega{-}E_-({\bf k}))\;\Big),
\end{aligned}$$

with

$$\begin{aligned}
R_{\rm intra}({\bf k}) \;&=\; 2bA_-({\bf k})A_+({\bf k})+\frac{2}{W({\bf k})}(E_-({\bf k})-\omega_0)^2A_+({\bf k})^2 \qquad \text{(B.0.11)}\\
&=\; \frac{4b^2W({\bf k})}{(\epsilon_p-\omega_0)^2+4bW({\bf k})}, \qquad \text{(B.0.12)}\\
\Delta(u) \;&=\; \frac{1}{\pi}\,\frac{\varepsilon}{u^2+\varepsilon^2},\qquad {\rm P}(u)\;=\;\frac{u}{u^2+\varepsilon^2}. \qquad \text{(B.0.13)}
\end{aligned}$$

Then, from eqs.(4.2.13), (4.2.14) and (4.3.7), we obtain

$$\begin{aligned}
\sigma'_{\rm intra}(0) \;&=\; \lim_{\varepsilon\to0^+}\;\frac{1}{4}\frac{1}{N_{\rm L}}\sum_{\bf k}\sum_{\sigma}R_{\rm intra}({\bf k})\;\Delta(E_-({\bf k}))^2\;=\frac{1}{\pi}\,\frac{\epsilon_p\;\omega_0}{\epsilon_p+\omega_0}\;\lim_{\varepsilon\to0^+}\frac{1}{2\varepsilon}, \qquad \text{(B.0.14)}\\
\frac{n_{\rm opt}}{m_{\rm b}} \;&=\; \lim_{\varepsilon\to0^+}\frac{1}{4\pi}\frac{1}{N_{\rm L}}\sum_{\bf k}\sum_{\sigma}R_{\rm intra}({\bf k})\;\Delta(E_-({\bf k}))\;=\frac{1}{\pi}\,\frac{\epsilon_p\;\omega_0}{\epsilon_p+\omega_0}\;\equiv\;\frac{2}{\pi}W_{\rm D}, \qquad \text{(B.0.15)}\\
A \;&=\; \lim_{\varepsilon\to0^+}\frac{5\pi}{24}\frac{1}{N_{\rm L}}\sum_{\bf k}\sum_{\sigma}R_{\rm intra}({\bf k})\;\Delta(E_-({\bf k}))^3 \qquad \text{(B.0.16)}\\
&-\;\lim_{\varepsilon\to0^+}\frac{1}{8\pi}\frac{1}{N_{\rm L}}\sum_{\bf k}\sum_{\sigma}R_{\rm intra}({\bf k})\;\Delta(E_-({\bf k}))\;{\rm P}(E_-({\bf k}))^2=\frac{1}{\pi}\,\frac{\epsilon_p\;\omega_0}{\epsilon_p+\omega_0}\;\lim_{\varepsilon\to0^+}\Big(\frac{1}{2\varepsilon}\Big)^2.
\end{aligned}$$

In deriving the above, we have changed a k-summation into a u-integration using eq.(4.2.18) and used the following formulae applicable for a smooth function ${\rm F}(u)$,

$$\lim_{\varepsilon\to0^+}\int_{-\infty}^{+\infty}{\rm d}u{\rm F}(u)\Delta(u)^2\;=\;\frac{1}{2\pi}\lim_{\varepsilon\to0^+}\frac{1}{\varepsilon}\;{\rm F}(0), \qquad \text{(B.0.17)}$$

$$\lim_{\varepsilon\to 0^+}\int_{-\infty}^{+\infty} \mathrm{d}u \mathrm{F}(u)\Delta(u)^3 = \frac{3}{8\pi^2}\lim_{\varepsilon\to 0^+}\frac{1}{\varepsilon^2}\mathrm{F}(0), \tag{B.0.18}$$

$$\lim_{\varepsilon\to 0^+}\int_{-\infty}^{+\infty} \mathrm{d}u \mathrm{F}(u)\Delta(u)\mathrm{P}(u)^2 = \frac{1}{8}\lim_{\varepsilon\to 0^+}\frac{1}{\varepsilon^2}\mathrm{F}(0). \tag{B.0.19}$$

Inserting eqs.(B.0.14), (B.0.15) and (B.0.16) into eq.(4.5.4), we obtain

$$m_{\mathrm{opt}}(0) = m_{\mathrm{b}}, \tag{B.0.20}$$

which is irrespective of δ.

Finally, we note that effects of strong correlation are clearly seen in the three kinds of integrated intensities of the conductivity: the Drude weight W_{D} in eq.(B.0.15) and the interband weights, W'_{inter} and W''_{inter}, in eq.(B.0.8). Taking account of the relations, $n = n_p + n_d = 1+\delta = 2-\epsilon_p\omega_0/b$ and $\omega_0, b \propto \delta$ at $\delta << 1$, we find

$$W_{\mathrm{D}} \propto \delta, \qquad W'_{\mathrm{inter}} \propto \delta, \qquad W''_{\mathrm{inter}} \propto \delta^2.$$

These results remain to be valid also for the free 2D d-p model with the mixing weight given by eq.(3.1.1) where ω_0 and b are replaced by ϵ_d and 1, respectively. No singularity is found at n=1 for all of the integrated intensities.

Bibliography

[1] J. G. Bednorz and K. A. Müller: Z. Phys. **B64** (1986) 189.

[2] M. Gurvitch and A. T. Fiory: Phys. Rev. Lett. **59** (1987) 1337.

[3] S. Martin, A. T. Fiory, R. M. Fleming, L. F. Schneemeyer, and J. V. Waszczak: Phys. Rev. **B41** (1990) 846.

[4] T. A. Friedmann, H. W. Rabin, J. Giapintzakis, J. P. Rice, and D. M. Ginsberg: Phys. Rev. **B42** (1990) 6217.

[5] Y. Kubo, Y. Shimakawa, T. Manako, and H. Igarashi: Phys. Rev. **B43** (1991) 7875.

[6] H. Takagi, B. Batlogg, H. L. Kao, J. Kwo, R. J. Cava, J. J. Krajewski, and W. F. Peck, Jr.: Phys. Rev. Lett. **69** (1992) 2975.

[7] B. Koch, H. P. Geserich, and TH. Wolf: Solid State Commun. **71** (1989) 495.

[8] Z. Schlesinger, R. T. Collins, F. Holtzberg, C. Feild, S. H. Blanton, U. Welp, G. W. Crabtree, and Y. Fang: Phys. Rev. Lett. **65** (1990) 801.

[9] S. Uchida, T. Ido, H. Takagi, T. Arima, Y. Tokura, and S. Tajima: Phys. Rev. **B43** (1991) 7942.

[10] L. D. Rotter, Z. Schlesinger, R. T. Collins, F. Holtzberg, C. Feild, U. W. Welp, G. W. Crabtree, J. Z. Liu, Y. Fang, K. G. Vandervoort, and S. Fleshler: Phys. Rev. Lett. **67** (1991) 2741.

[11] I. Terasaki, S. Takebayashi, I. Tsukada, A. Maeda, and K. Uchinokura: Physica **C185-189** (1991) 1017.

[12] G. Jehl, T. Zetterer, H. H. Otto, J. Schützmann, S. Shulga, and K. F. Renk: Europhys. Lett. **17** (1992) 255.

[13] S. L. Cooper, A. L. Kotz, M. A. Karlow, M. V. Klein, W. C. Lee, J. Giapintzakis, and D. M. Ginsberg: Phys. Rev. **B45** (1992) 2549.

[14] L. D. Rotter, Z. Schlesinger, R. T. Collins, F. Holtzberg, C. Feild, U. W. Welp, G. W. Crabtree, Y. Fang, K. G. Vandervoort, S. Fleshler, and J. Z. Liu: Chin. J. Phys. **30** (1992) 271.

[15] F. Gao, D. B. Romero, D. B. Tanner, J. Talvacchio, and M. G. Forrester: Phys. Rev. **B47** (1993) 1036.

[16] A. Yamanaka, T. Kimura, F. Minami, K. Inoue, and S. Takekawa: Jpn. J. Appl. Phys. **27** (1988) L1902.

[17] F. Slakey, S. L. Cooper, M. V. Klein, J. P. Rice, and D. M. Ginsberg: Phys. Rev. **B39** (1989) 2781.

[18] M. C. Krantz, H. J. Rosen, J. Y. T. Wei, and D. E. Morris: Phys. Rev. **B40** (1989) 2635.

[19] T. Staufer, R. Hackl, and P. Müleer: Solid State Commun. **75** (1990) 975.

[20] S. Sugai, T. Ido, H. Takagi, S. Uchida, M. Sato, and S. Shamoto: Solid State Commun. **76** (1990) 365.

[21] D. Reznik, A. Kotz, S. L. Cooper, M. V. Klein, W. C. Lee, and D. M. Ginsberg: Physica **C185-189** (1991) 1029.

[22] T. Nishikawa, J. Takeda, and M. Sato: J. Phys. Soc. Jpn. **62** (1993) 2568.

[23] J. Takeda, T. Nishikawa, and M. Sato: J. Phys. Soc. Jpn. **62** (1993) 2571.

[24] B. Batlogg: Phys. Today **44** (1991) 44.

[25] P. B. Allen: Comments Cond. Mat. Phys. **15** (1992) 327.

[26] P. W. Anderson: Science **235** (1987) 1196.

[27] C. M. Varma, P. B. Littlewood, S. Schmitt-Rink, E. Abrahams, and A. E. Ruckenstein: Phys. Rev. Lett. **63** (1989) 1996.

[28] C. M. Varma: Int. J. Mod. Phys. **B3** (1989) 2083.

[29] P. B. Littlewood and C. M. Varma: J. Appl. Phys. **69** (1991) 4979.

[30] G. Kotliar, E. Abrahams, A. E. Ruckenstein, C. M. Varma, P. B. Littlewood, and S. Schmitt-Rink: Europhys. Lett. **15** (1991) 655.

[31] T. Moriya, Y. Takahashi, and K. Ueda: J. Phys. Soc. Jpn. **59** (1990) 2905.

[32] T. Moriya and Y. Takahashi: J. Phys. Soc. Jpn. **60** (1991) 776.

[33] K. Miyake and O. Narikiyo: J. Phys. Soc. Jpn. **63** (1994) 2042.

[34] K. Miyake and O. Narikiyo: J. Phys. Soc. Jpn. **63** (1994) 3821.

[35] T. Tanamoto, K. Kuboki, and H. Fukuyama: J. Phys. Soc. Jpn. **60** (1991) 3072.

[36] T. Tanamoto, H. Kohno, and H. Fukuyama: J. Phys. Soc. Jpn. **61** (1992) 1886.

[37] T. Tanamoto, H. Kohno, and H. Fukuyama: J. Phys. Soc. Jpn. **62** (1993) 717.

[38] T. Tanamoto, H. Kohno, and H. Fukuyama: J. Phys. Soc. Jpn. **62** (1993) 1455.

[39] T. Tanamoto, H. Kohno, and H. Fukuyama: J. Phys. Soc. Jpn. **63** (1994) 2739.

[40] P. Coleman: Phys. Rev. **B29** (1984) 3035.

[41] H. Jichu, T. Matsuura, and Y. Kuroda: J. Phys. Soc. Jpn. **58** (1989) 4280.

[42] H. Jichu, T. Matsuura, and Y. Kuroda: J. Phys. Soc. Jpn. **59** (1990) 2820.

[43] T. Matsuura, K. Miura, Y. Ōno, D. Hirashima, and Y. Kuroda: Progr. Theor. Phys. Supplement **106** (1991) 51.

[44] D. S. Hirashima, Y. Ōno, K. Miura, T. Matsuura, and H. Jichu: J. Phys. Soc. Jpn. **60** (1991) 2269.

[45] D. S. Hirashima, Y. Ōno, T. Matsuura, and Y. Kuroda: J. Phys. Soc. Jpn. **60** (1991) 1864.

[46] D. S. Hirashima, Y. Ōno, T. Matsuura, and Y. Kuroda: J. Phys. Soc. Jpn. **61** (1992) 649.

[47] B. Jin and Y. Kuroda: J. Phys. Soc. Jpn. **57** (1988) 1687.

[48] Y. Ōno, T. Matsuura, and Y. Kuroda: Physica **C159** (1989) 878.

[49] Y. Ōno, T. Matsuura, and Y. Kuroda: J. Phys. Soc. Jpn. **60** (1991) 3475.

[50] Y. Ōno, T. Matsuura, and Y. Kuroda: J. Phys. Soc. Jpn. **63** (1994) 1406.

[51] Y. Ōno, T. Matsuura, and Y. Kuroda: submitted to J. Phys. Soc. Jpn.

[52] Explicit forms of the $O(1/N)$-corrections are given in the forth-coming paper: Y. Ōno, T. Matsuura, and Y. Kuroda, preprint.

[53] I. Sawada, Y. Ōno, T. Matsuura, and Y. Kuroda: Physica **C235-240** (1994) 2293. Note that the definition of $2\tau_{\rm ingap}(\omega)^{-1}$ in this reference is $-{\rm Im}\Sigma(\mathbf{k}, E_-(\mathbf{k})+{\rm i}0^+)$, eq.(3.3.8) with $\omega = E_-(\mathbf{k})$.

[54] I. Sadakata and E. Hanamura: J. Phys. Soc. Jpn. **34** (1973) 882.

[55] D. Baeriswyl, J. Carmelo, and A. Luther: Phys. Rev. **B33** (1986) 7247.

[56] A. J. Millis and S. N. Coppersmith: Phys. Rev. **B42** (1990) 10807.

[57] P. B. Allen: Phys. Rev. **B3** (1971) 305.

[58] B. C. Webb, A. J. Sievers, and T. Mihalisin: Phys. Rev. Lett. **57** (1986) 1951.

[59] P. E. Sulewski, A. J. Sievers, M. B. Maple, M. S. Torikachvili, J. L. Smith, and Z. Fisk: Phys. Rev. **B38** (1988) 5338.

[60] G. A. Thomas, J. Orenstein, D. H. Rapkine, M. Capizzi, A. J. Millis, R. N. Bhatt, L. F. Schneemeyer, and J. V. Waszczak: Phys. Rev. Lett. **61** (1988) 1313.

[61] G. Abstreiter, M. Cardona, and A. Pinczuk: in *Light Scattering in Solids* IV, ed. M. Cardona and G. Güntherodt (Springer, Berlin, 1984) p27.

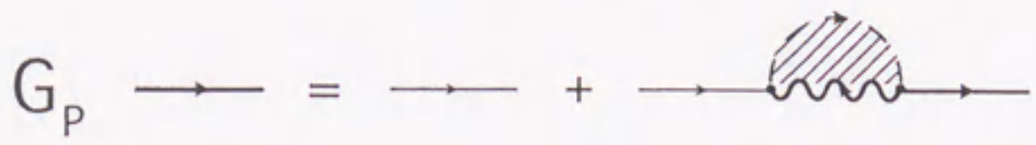

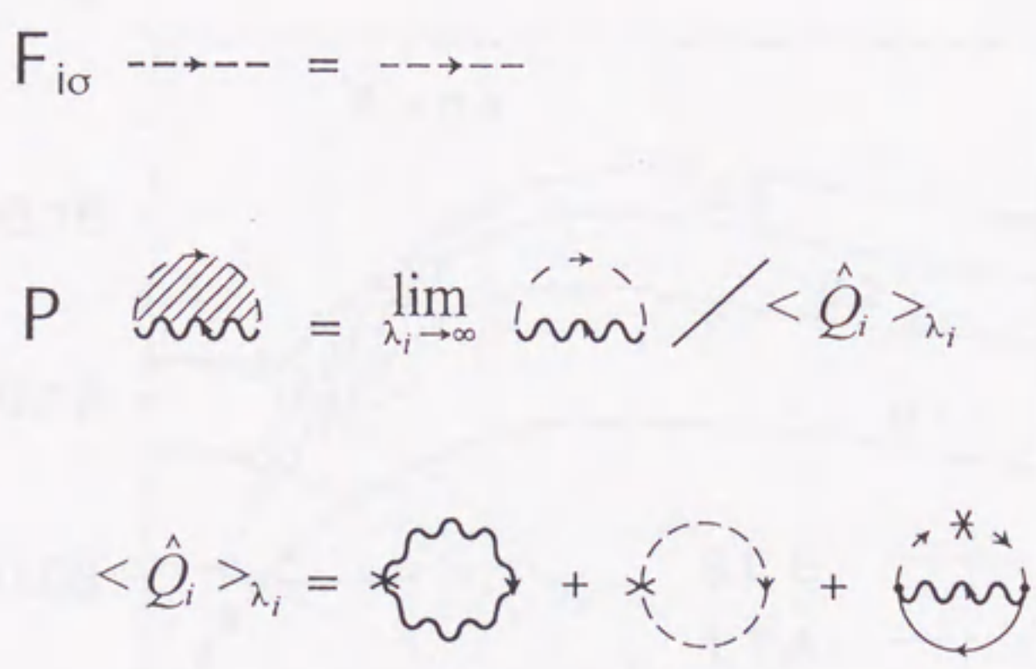

Fig.1 Diagrammatic descriptions of the SCE, (2.0.10)-(2.0.18).

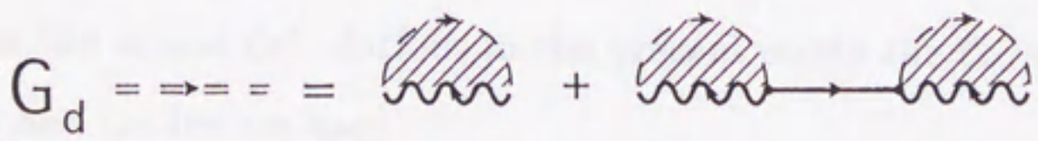

Fig.2 Diagrammatic description of the d-hole Green's function, eq.(2.0.51).

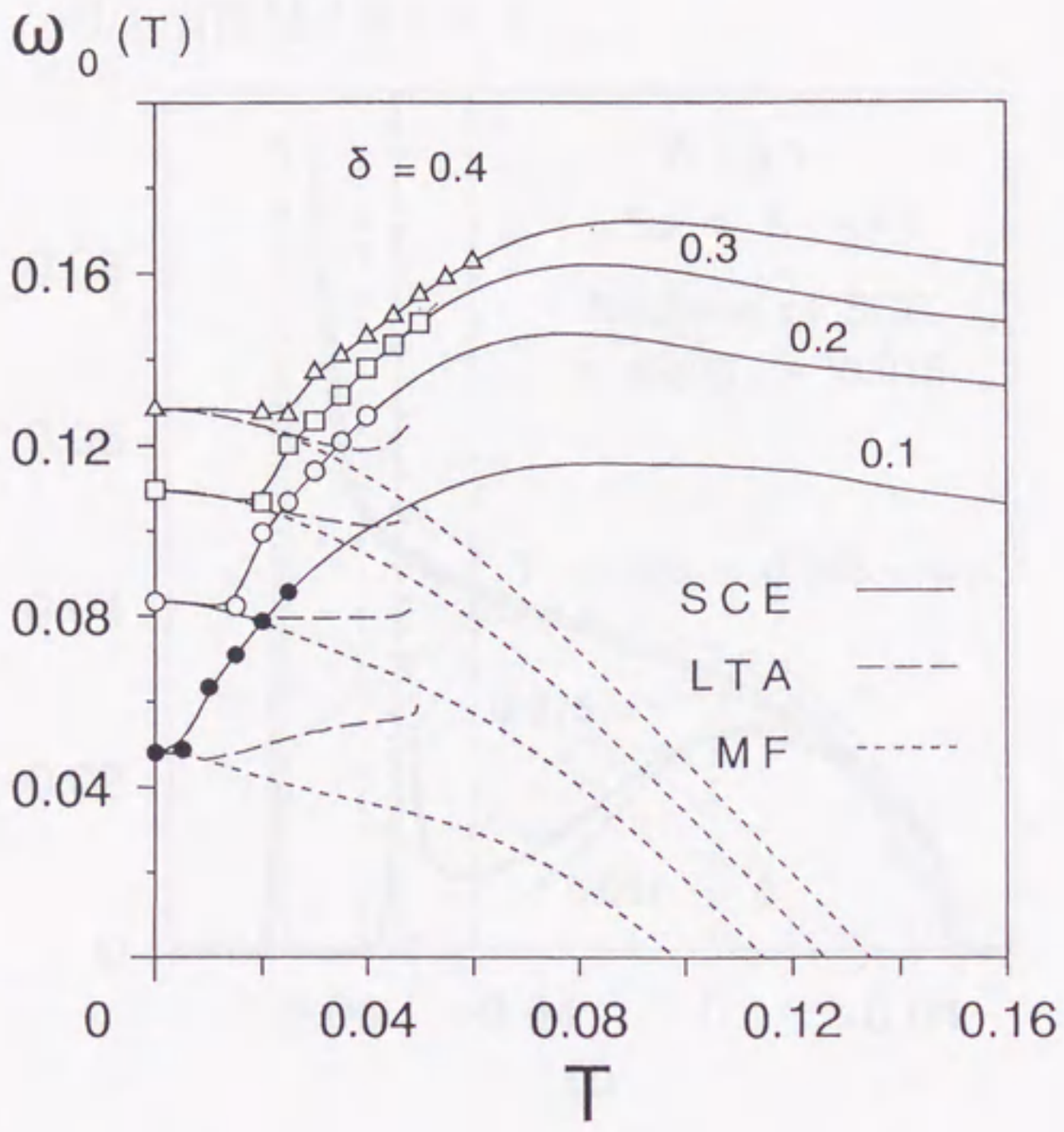

Fig.3 T-dependence of ω_0 for $\delta = 0.1, 0.2, 0.3$, and 0.4. The solutions of SCE are indicated by the solid line, those of LTA by the dashed line, and those of MF by the dotted line. For the actual calculations in the present study the data indicated by triangles, squares and circles are used.

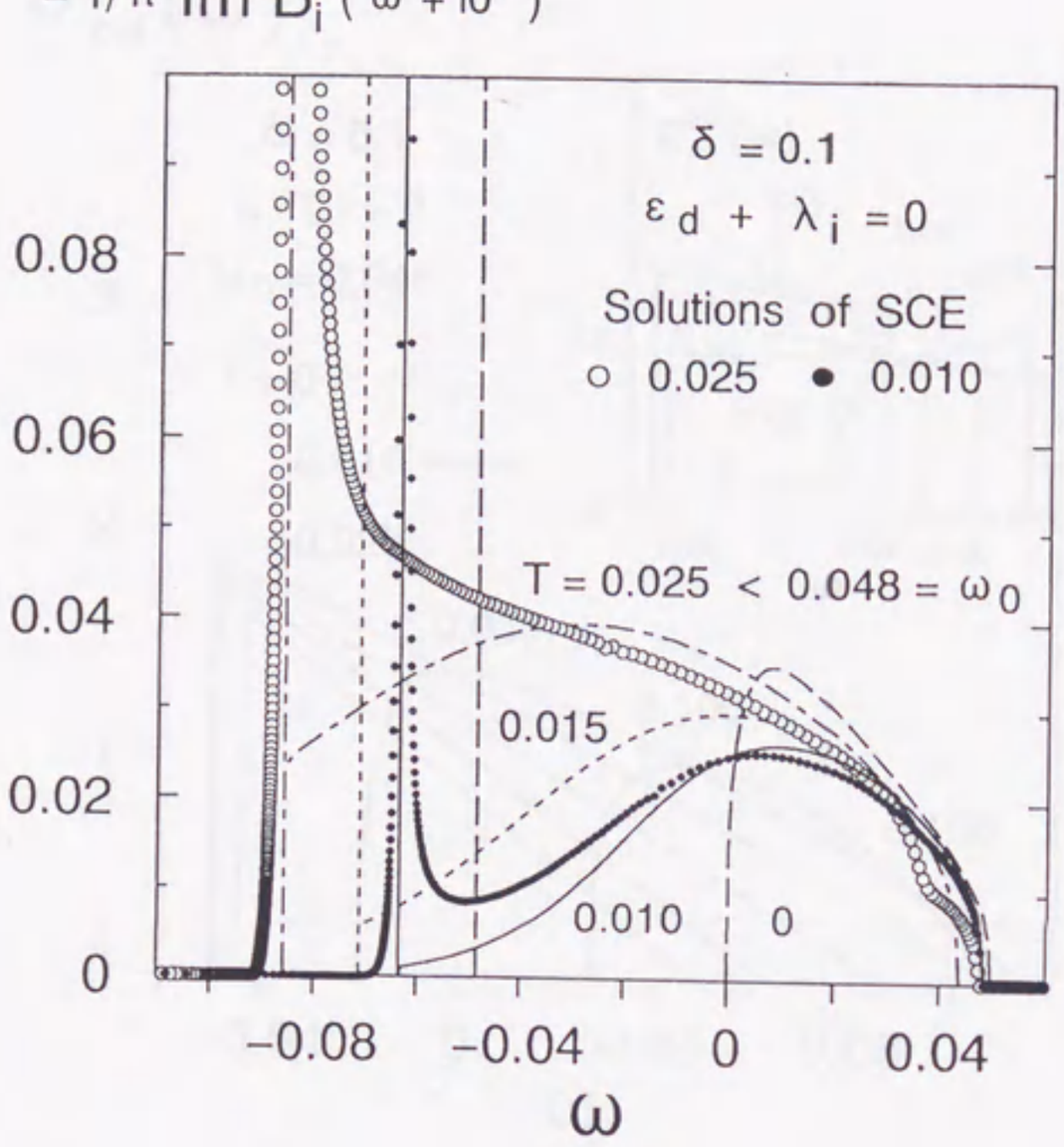

Fig.4 (a) ω-dependence of Im $B_i(\omega+i0^+)$ with $\lambda_i + \epsilon_d = 0$ for $\delta = 0.1$ at T =0.0, 0.010, 0.015 and 0.025 compared with the solutions of SCE.

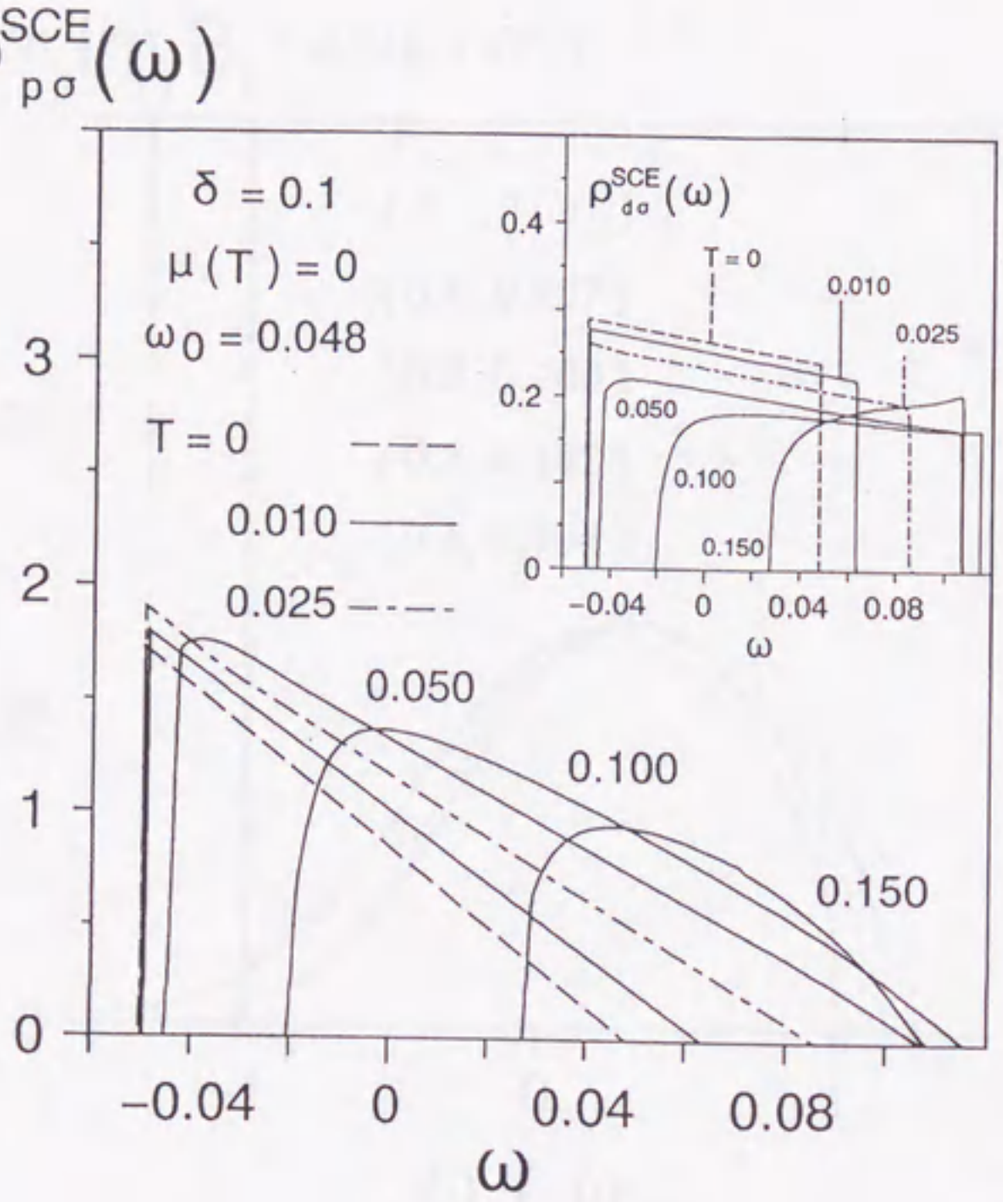

Fig.4 (b) The density of states per spin for the p-holes calculated from eq.(2.0.21) with the solutions of SCE at various values of T. The corresponding results for the itinerant component of the d-holes from eq.(2.0.51) are shown in the inset. Note that these results are well approximated to eqs.(3.2.7) and (3.2.8) even at $T \lesssim 2T_0$.

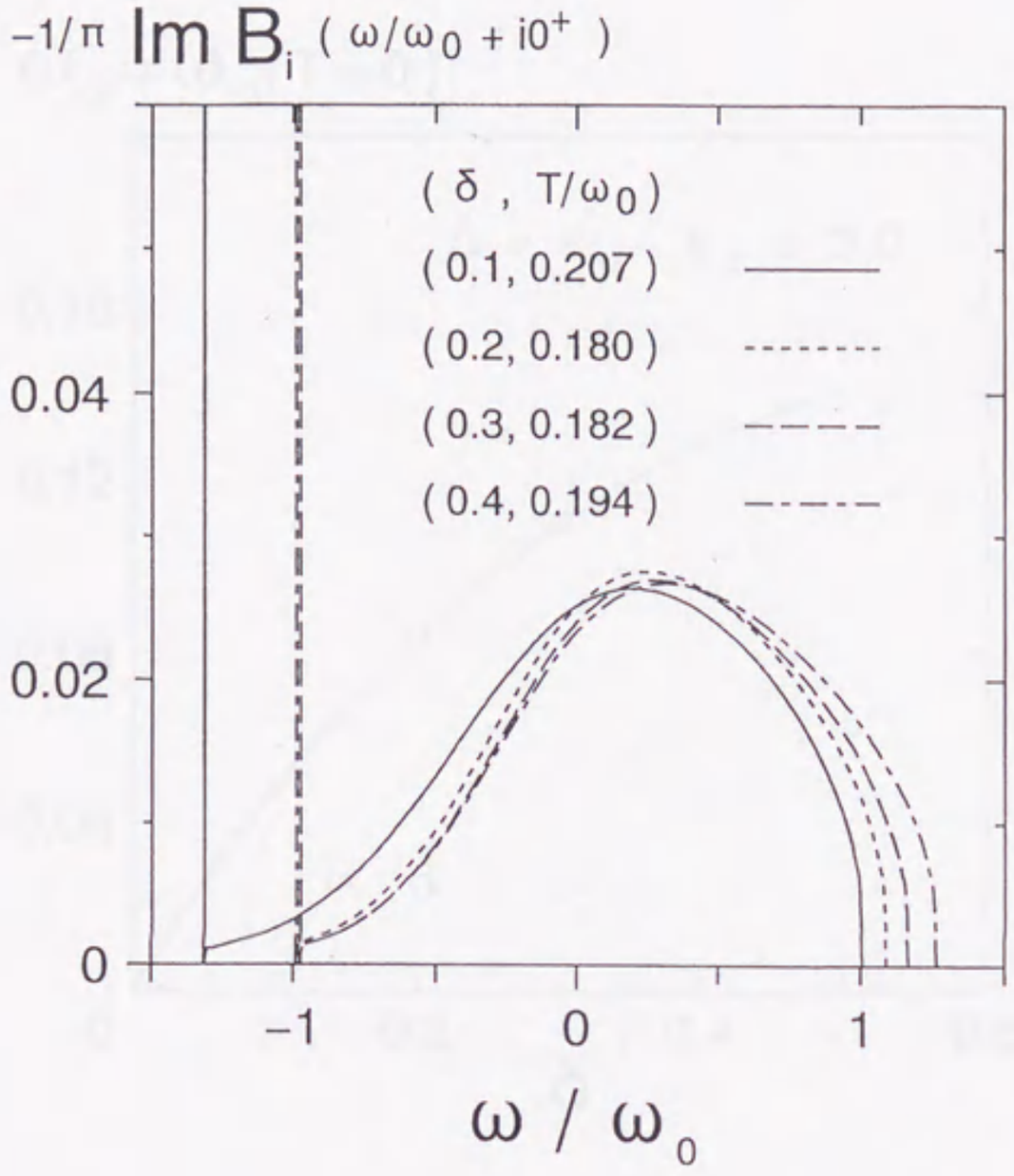

Fig.4 (c) ω-dependence of Im $B_i(\omega+i0^+)$ with $\lambda_i + \epsilon_d = 0$ for $\delta = 0.1, 0.2, 0.3$, and 0.4 as functions of ω/ω_0 at $T \sim T_0$.

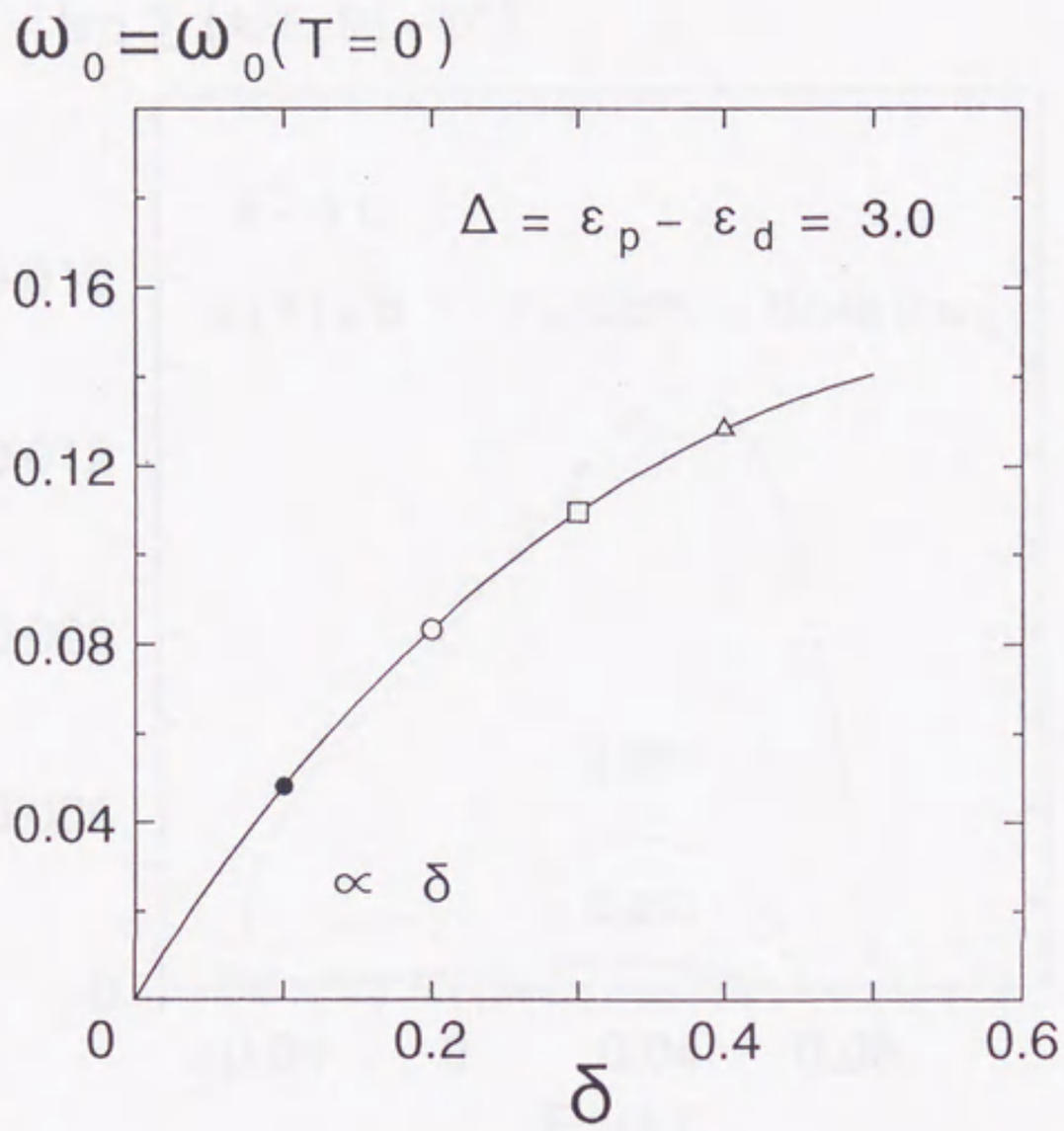

Fig.4 (d) ω_0 as a function of δ. The marked points are for comparison with those in Fig.3.

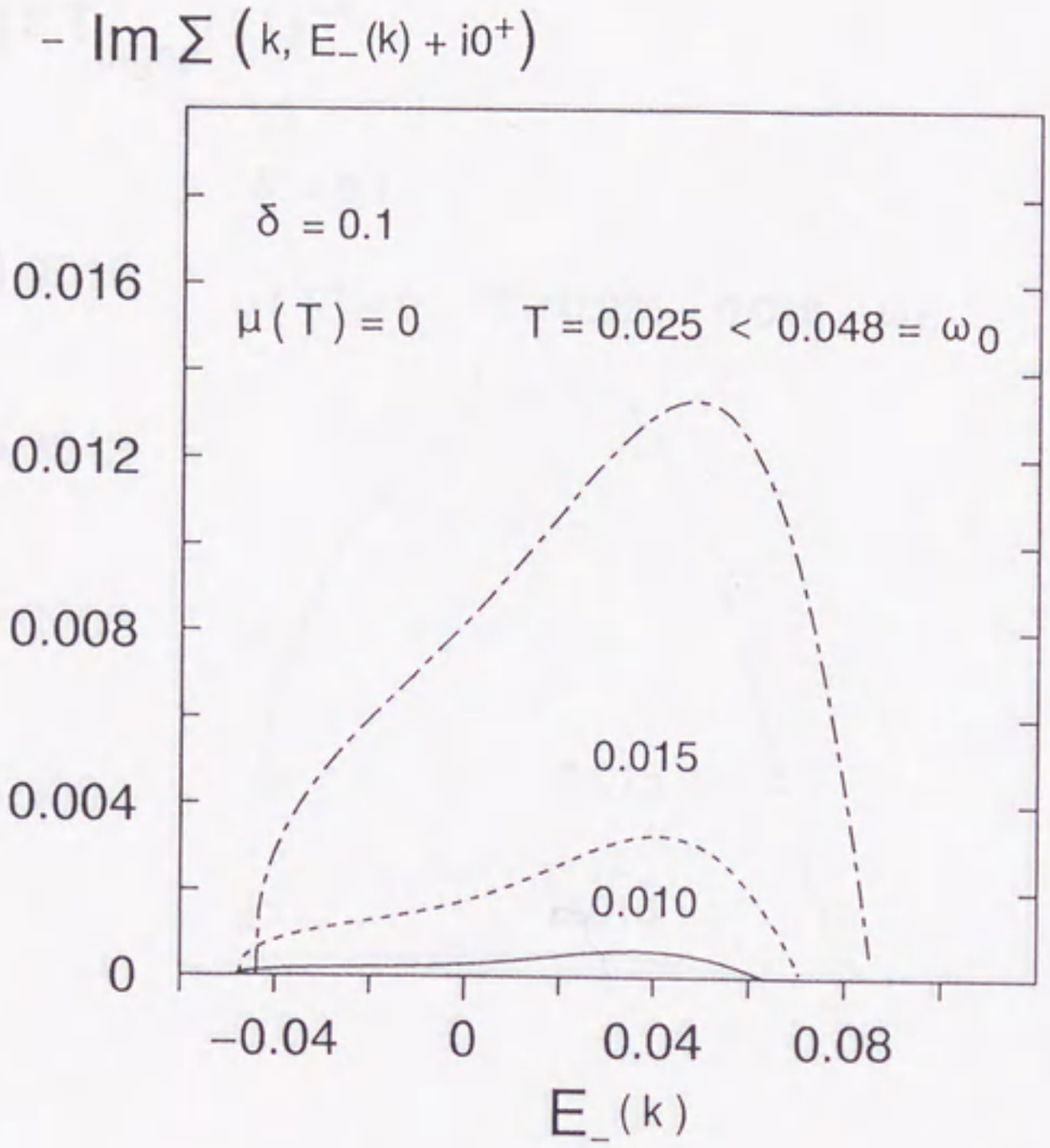

Fig.5 The p-hole scattering rate as a function of the energy with $\mu(T) = 0$ at various values of T for $\delta = 0.1$.

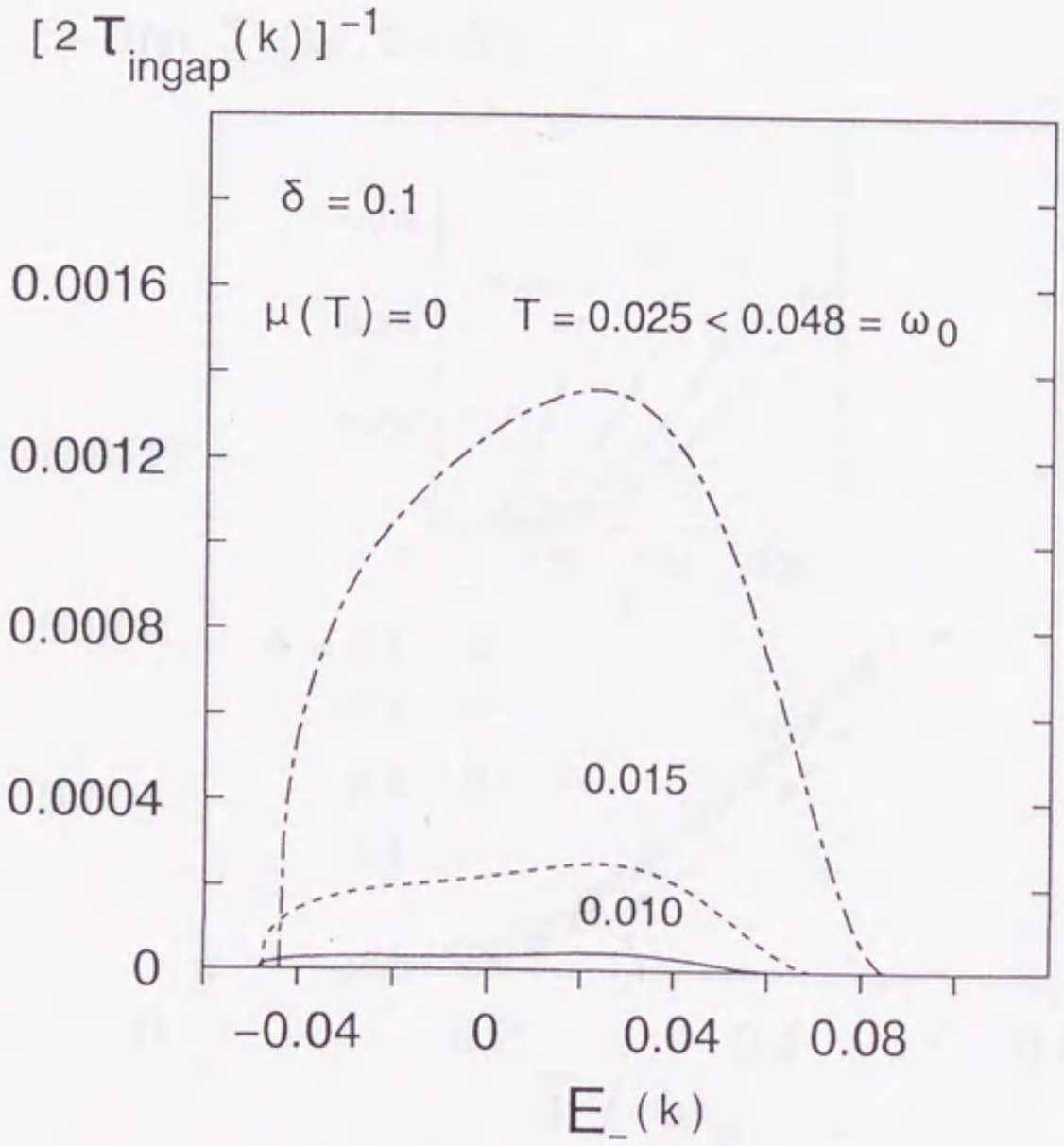

Fig.6 The quasi-particle scattering rate defined by eq.(3.3.9) as a function of the energy with $\mu(T) = 0$ at various values of T for $\delta = 0.1$.

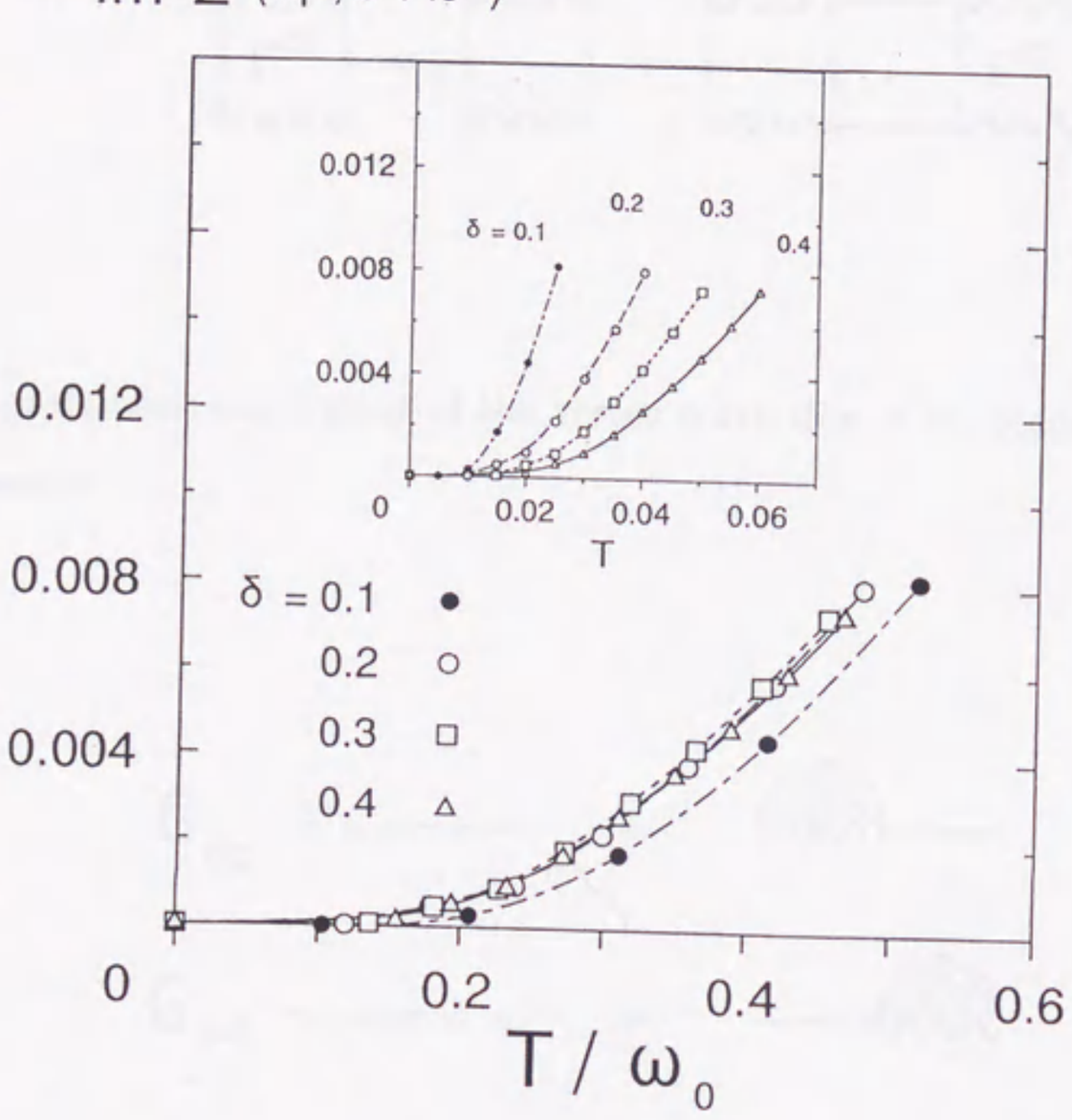

Fig.7 T-dependence of the p-hole scattering rate with the energy $\mu(T)$ for $\delta = 0.1, 0.2, 0.3,$ and 0.4 at $T \lesssim 2T_0$.

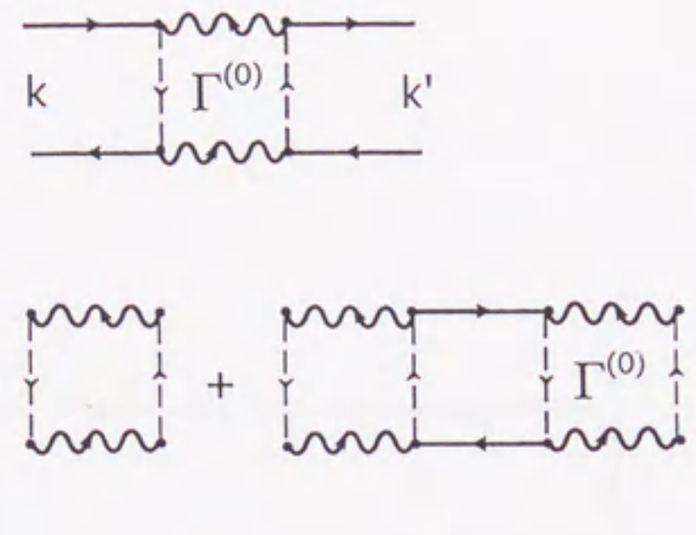

Fig.8 Diagrammatic description of the vertex correction of the leading order in the $1/N$-expansion.

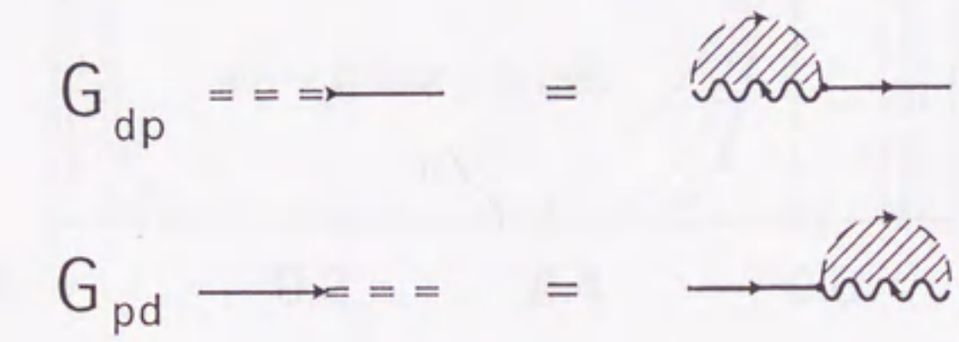

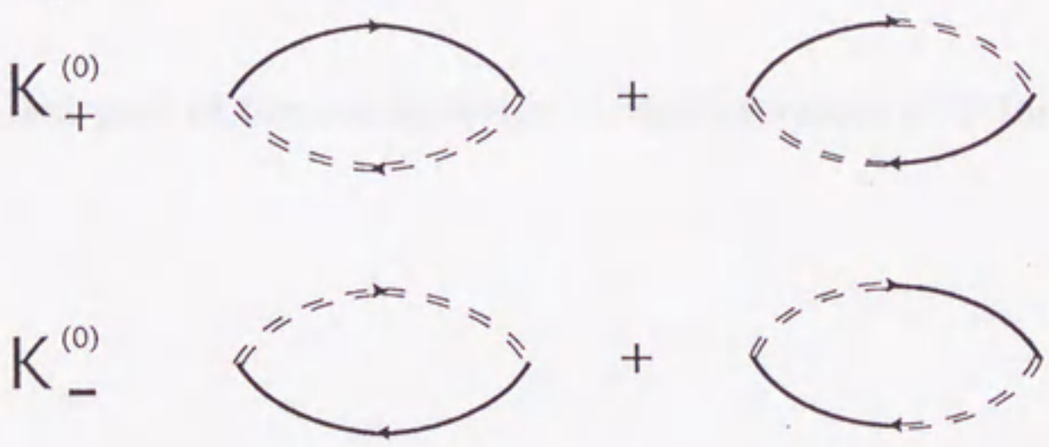

Fig.9 Diagrammatic descriptions of the Green's functions defined in eqs.(4.2.2), (4.2.3), (4.2.4) and (4.2.5).

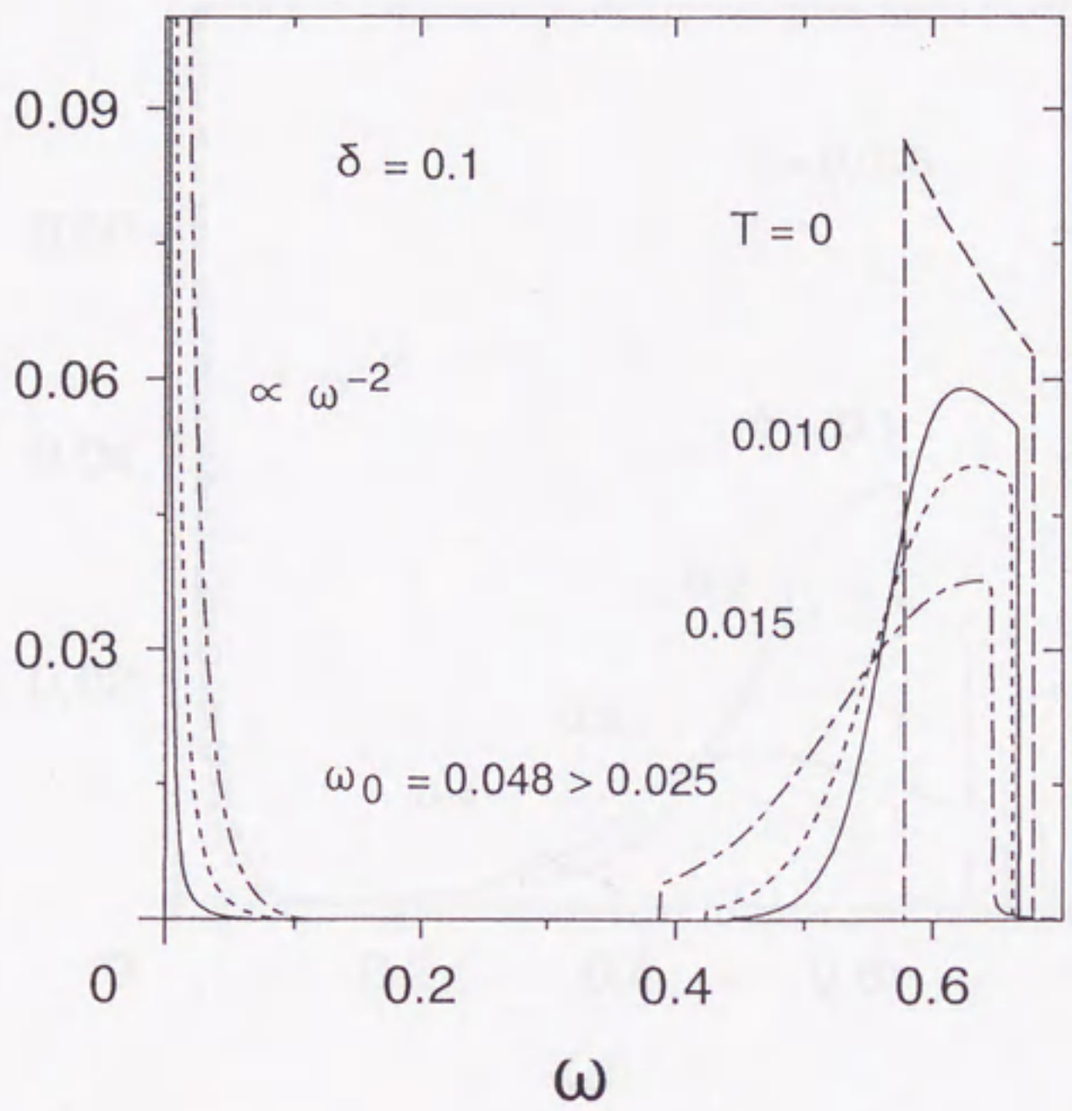

Fig.10 (a) The real part of the conductivity at various values of T for $\delta = 0.1$.

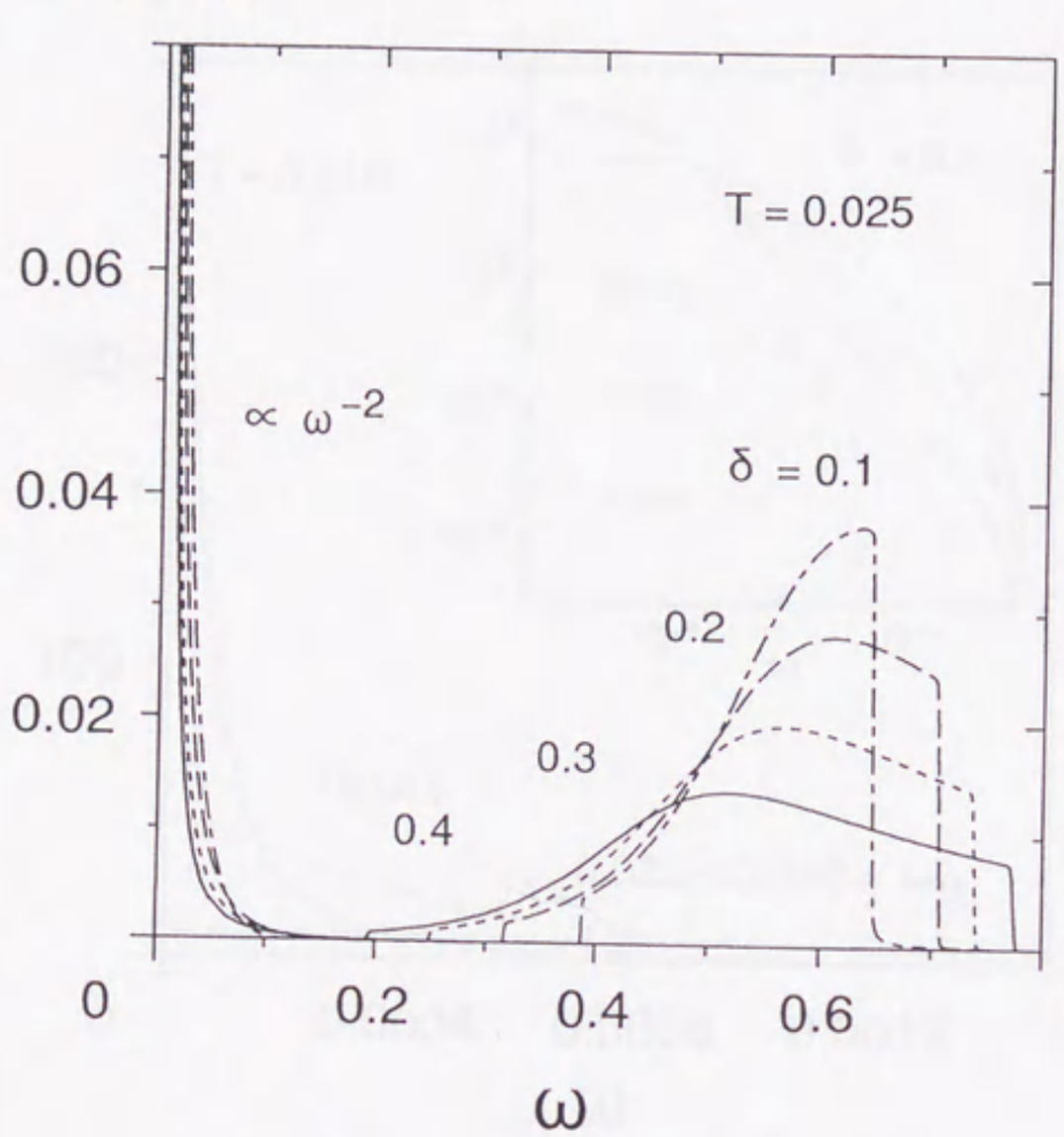

Fig.10 (b) The real part of the conductivity for various values of δ at $T = 0.025$.

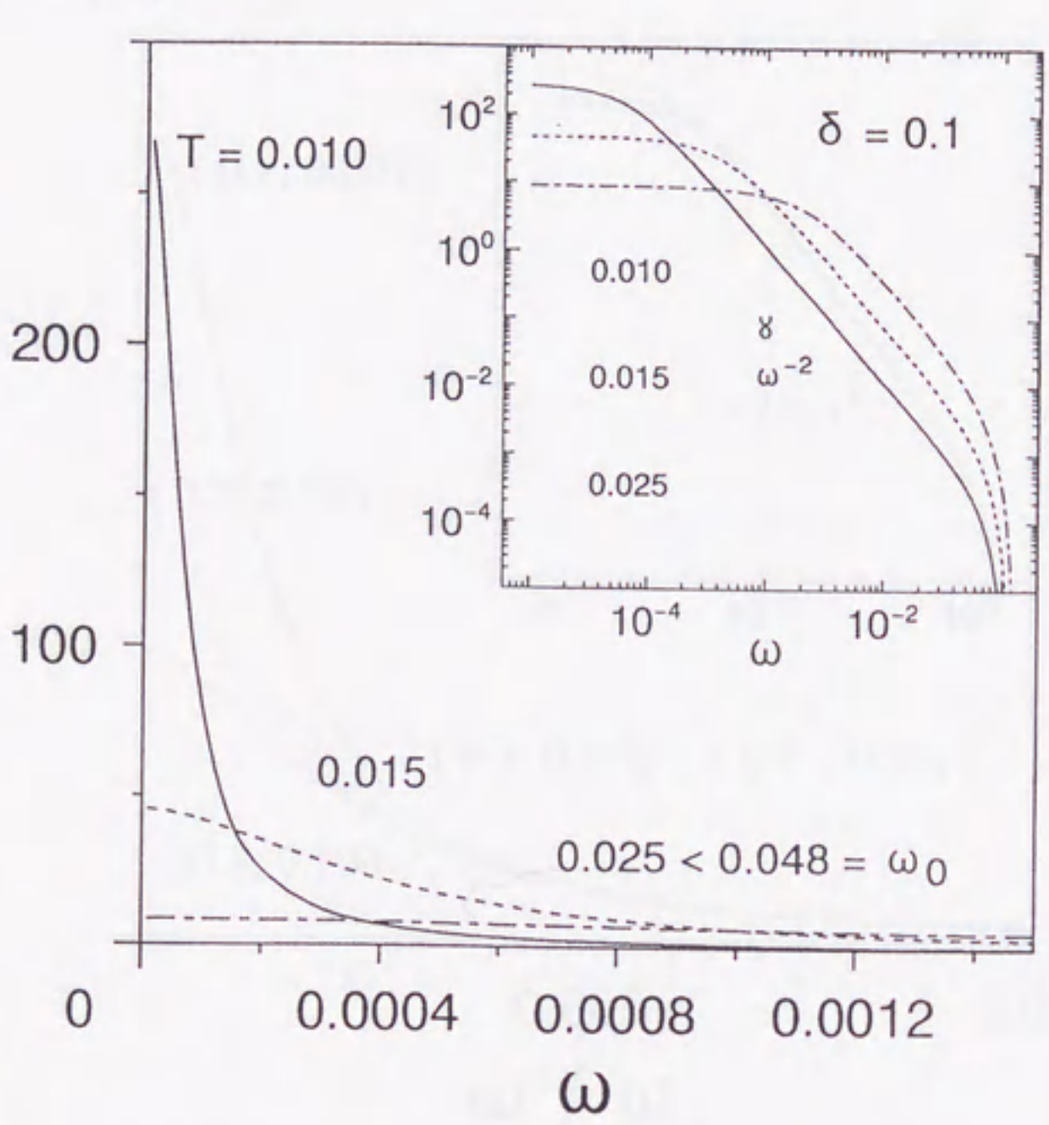

Fig.11 (a) The real part of the intraband component of the conductivity at various values of T for $\delta = 0.1$.

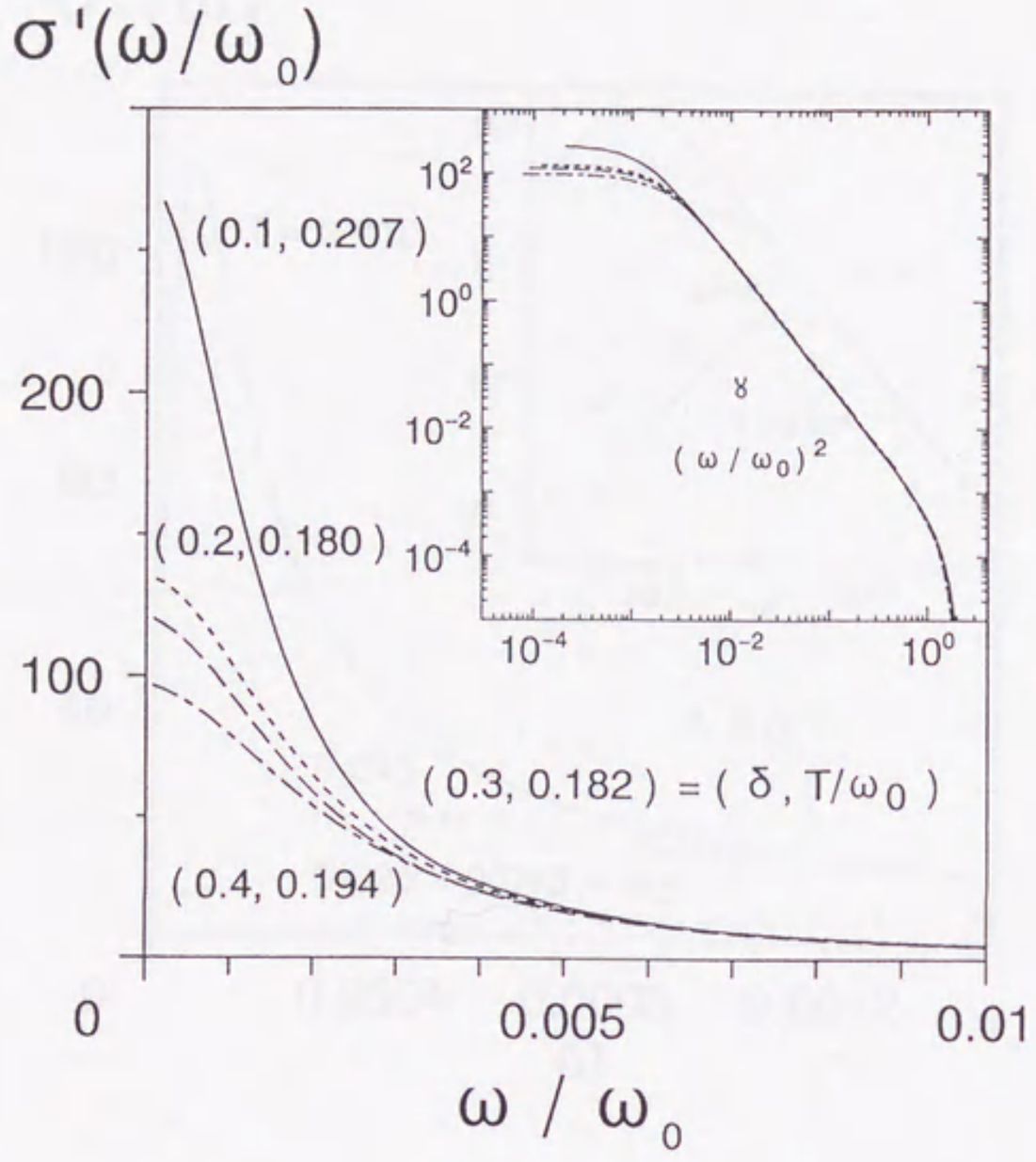

Fig.11 (b) The real part of the intraband component of the conductivity for various values of δ at $T \sim T_0$.

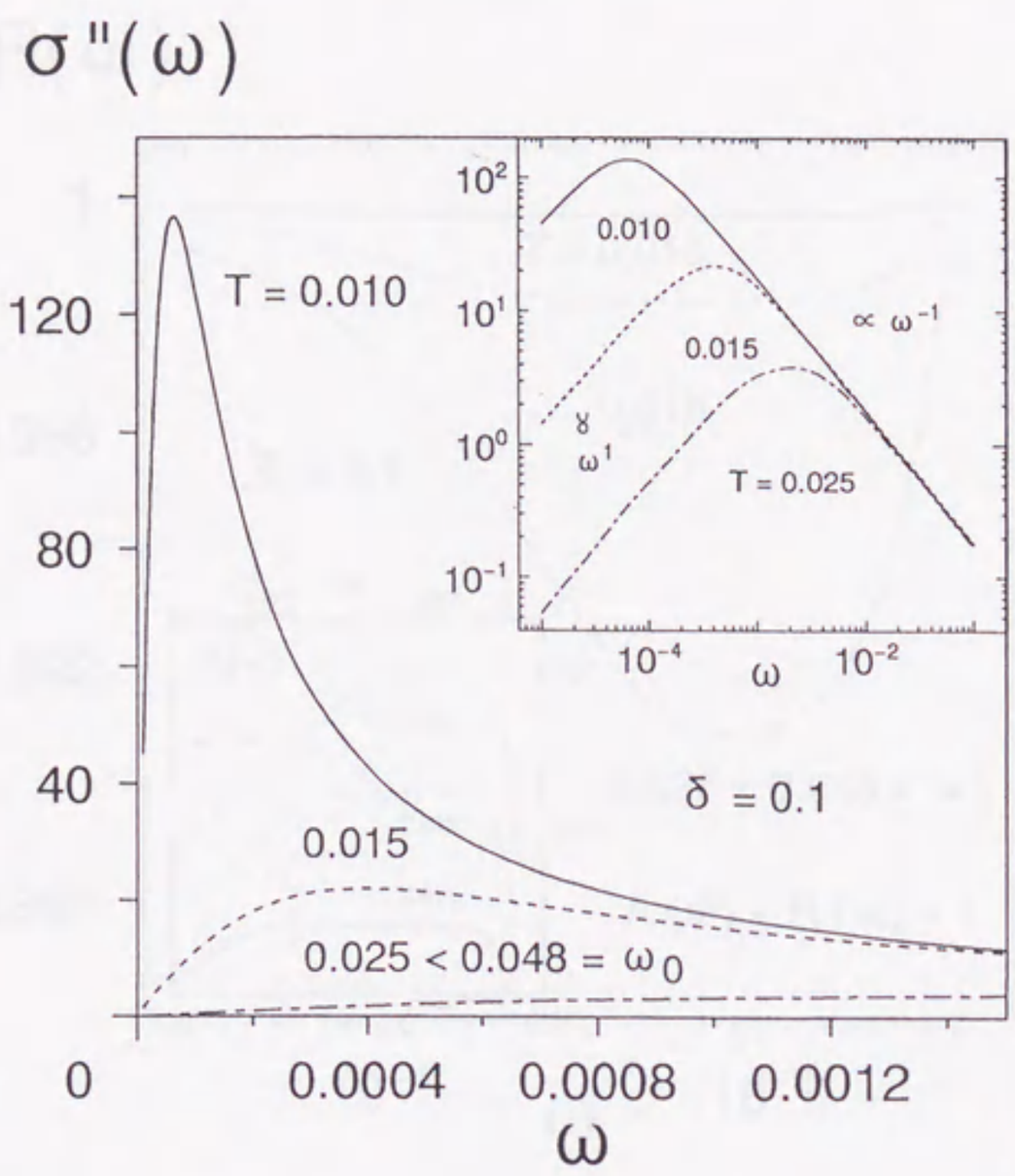

Fig.12 The imaginary part of the intraband component of the conductivity at various values of T for $\delta = 0.1$.

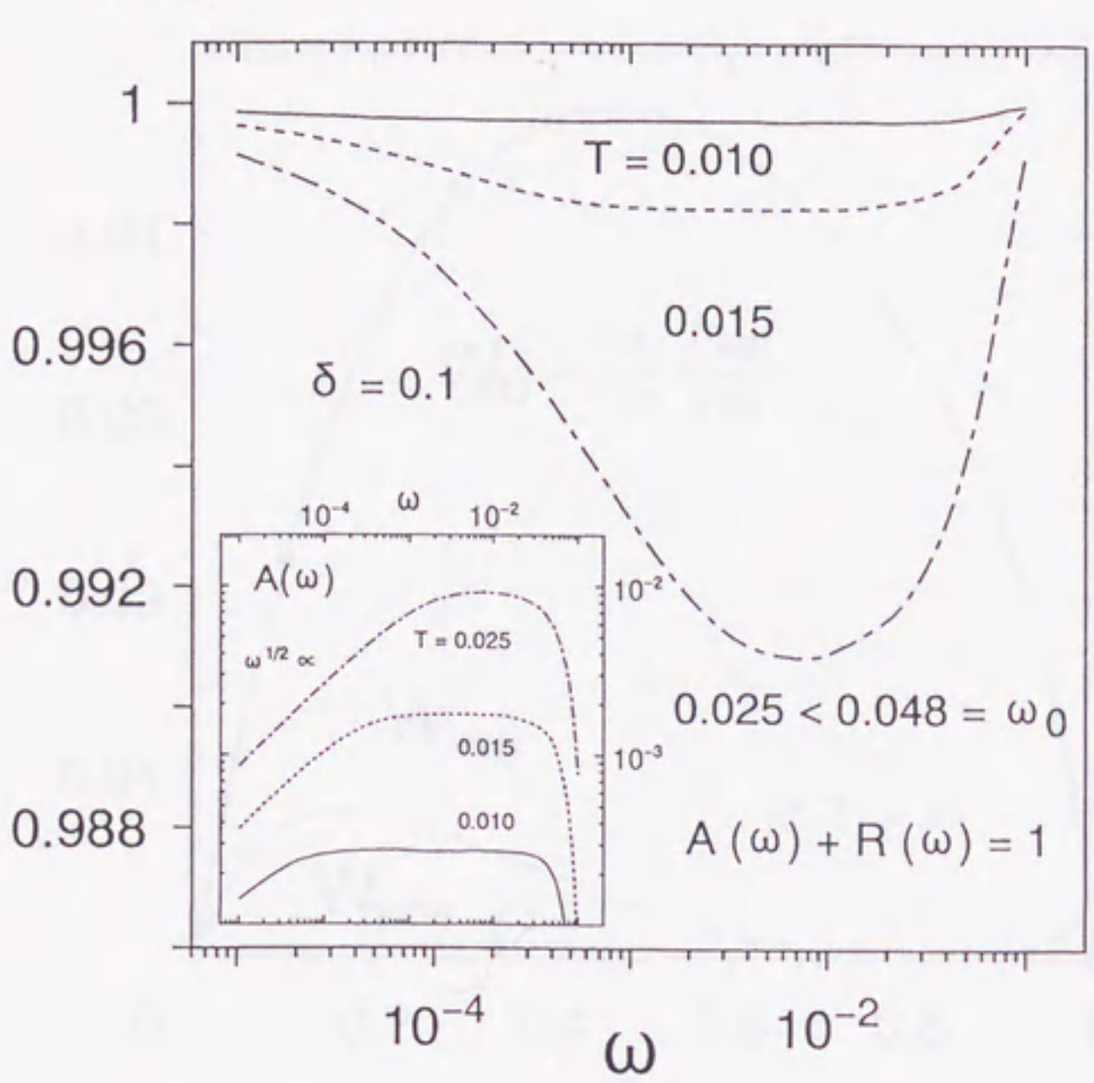

Fig.13 The intraband component of the reflectivity together with the absorptivity shown in the inset at various values of T for $\delta = 0.1$.

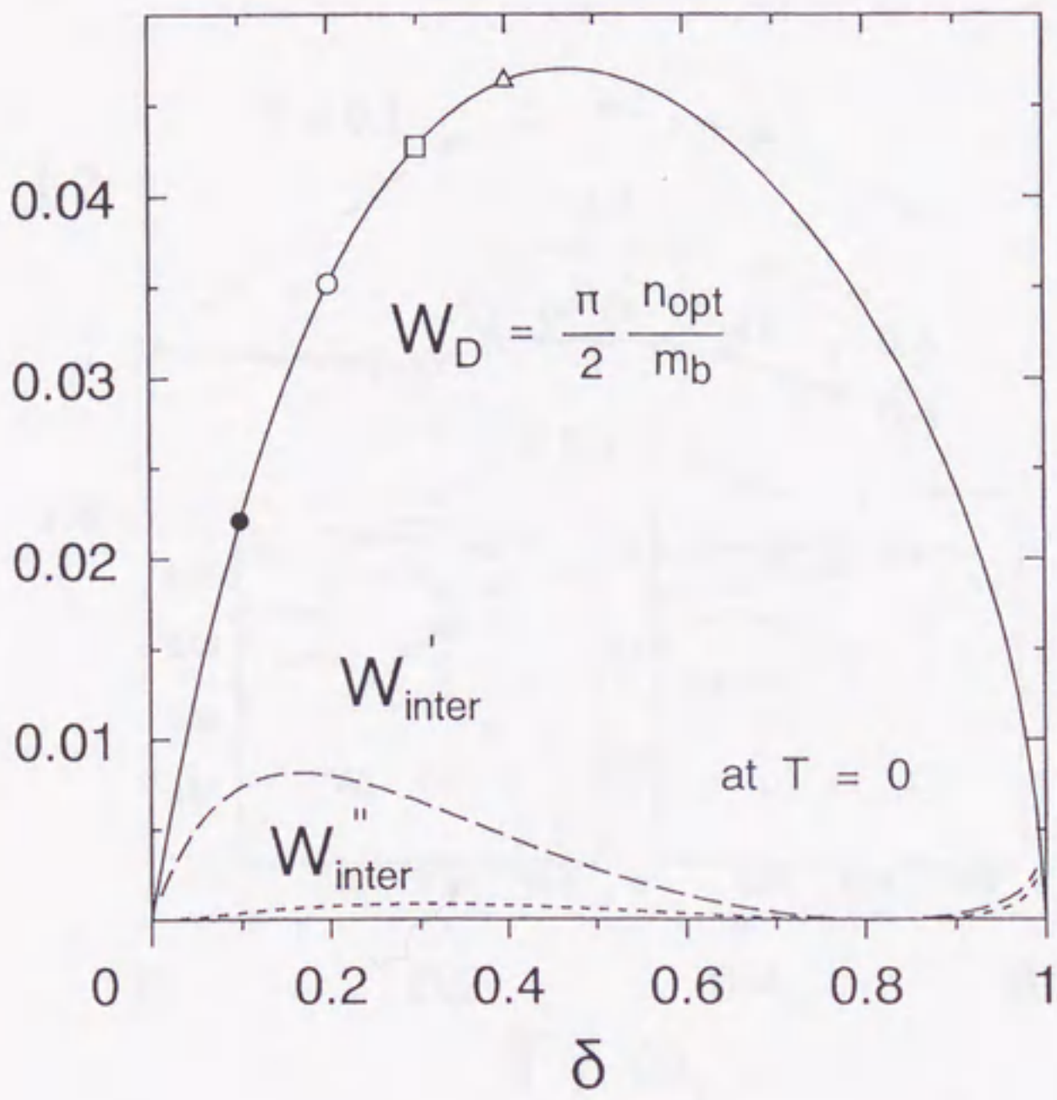

Fig.14 Spectral weights of the conductivity at $T = 0$ as functions of δ. The marked points are for comparison with those in Fig.15. The weights of the interband component vanish at $\delta \simeq 0.8$ due to the the wave-function renormalization factors, $R_{\rm inter}$, while they increase again at $\delta \gtrsim 0.8$ due to the crossing of the bands $E_\gamma(\mathbf{k})$ with $\gamma = \pm$.

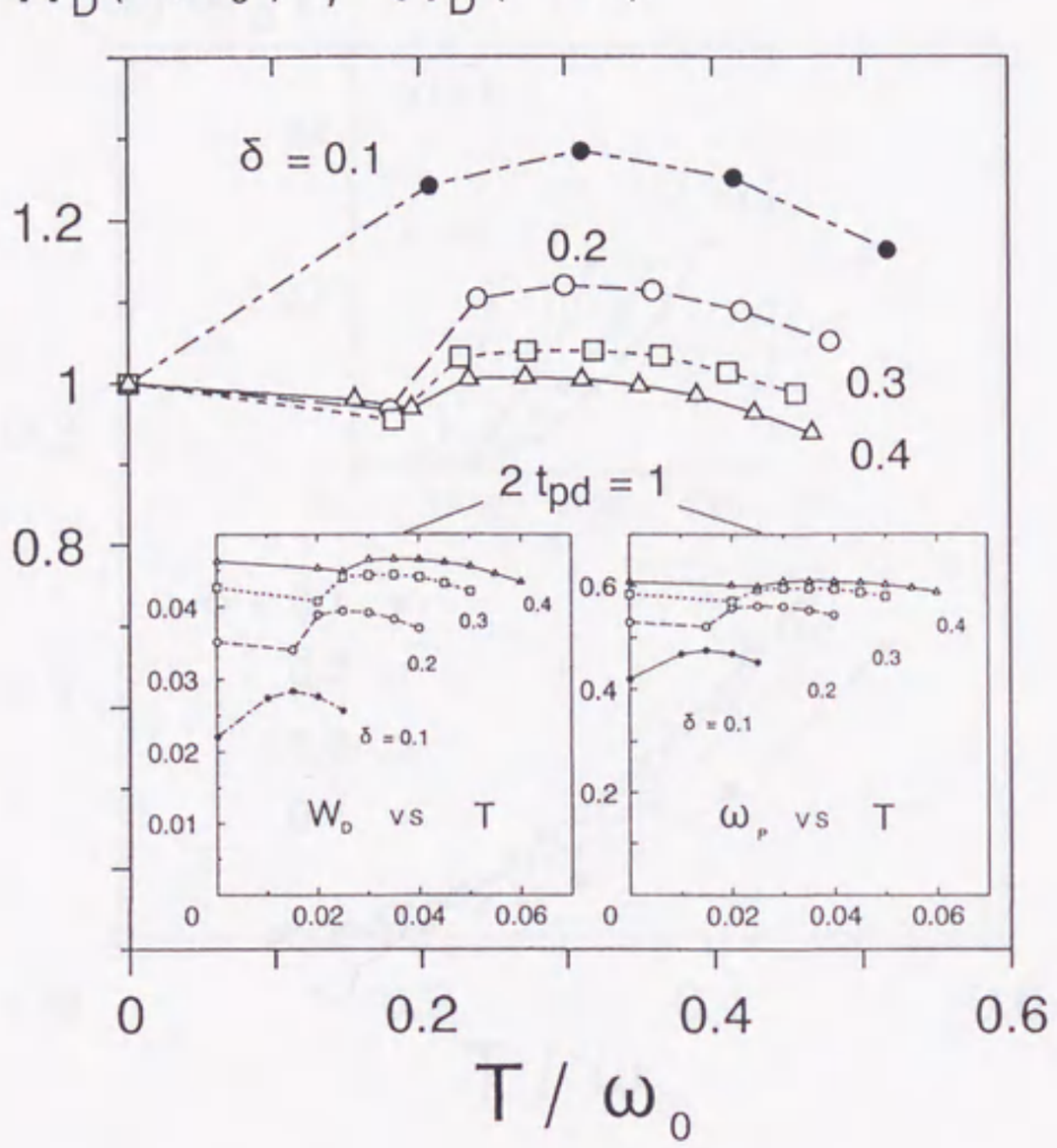

Fig.15 T-dependence of Drude weight for $\delta = 0.1, 0.2, 0.3$, and 0.4 at $T \lesssim 2T_0$. T-dependence of plasma frequency derived from Drude weight is shown in the inset.

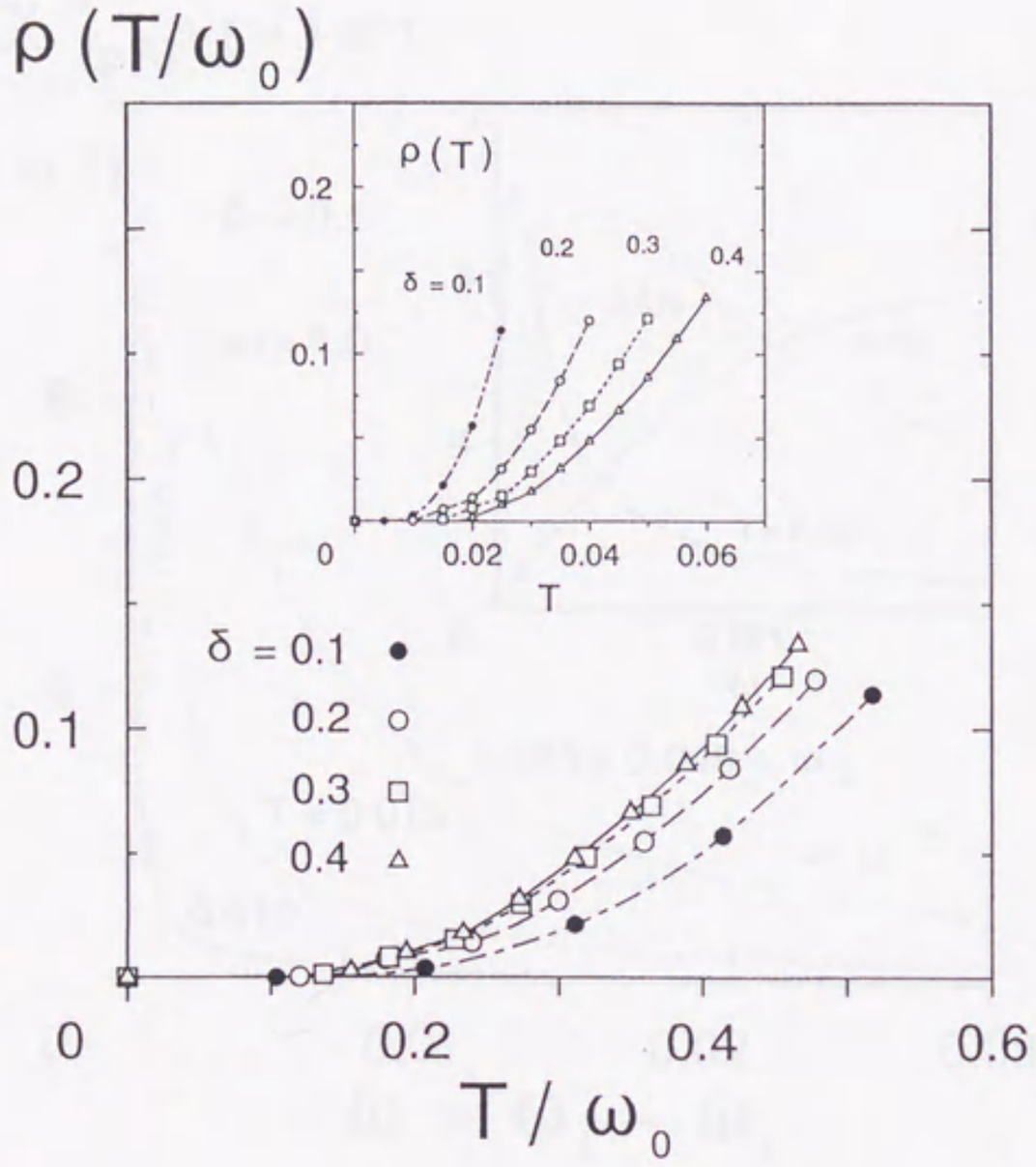

Fig.16 T-dependence of the resistivity for $\delta = 0.1, 0.2, 0.3$, and 0.4 at $T \lesssim 2T_0$.

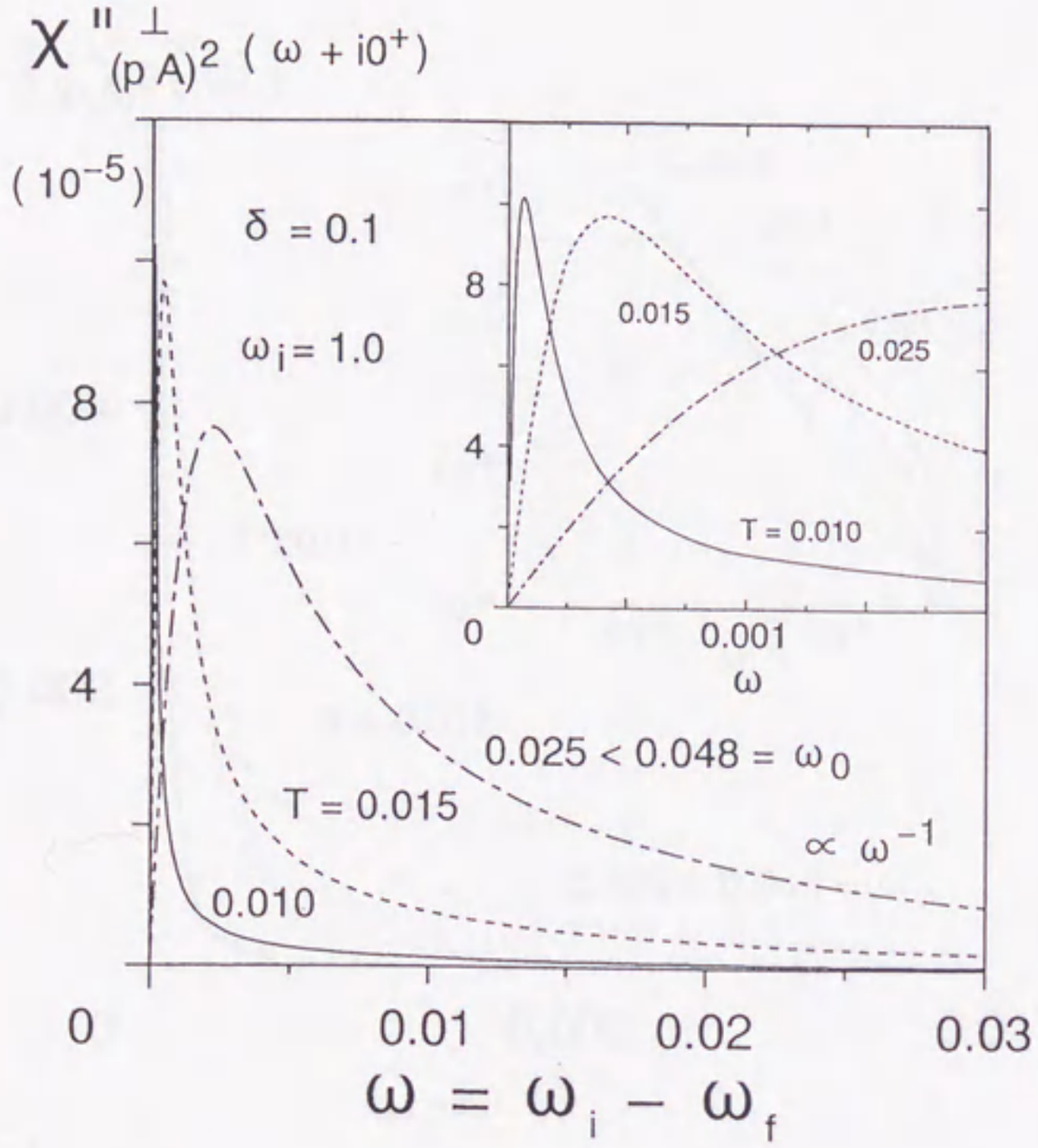

Fig.17 The imaginary part of the electronic Raman scattering response function defined in eq.(4.2.15) for the crossed polarization geometries as a function of the frequency shift at various values of T for $\delta = 0.1$.

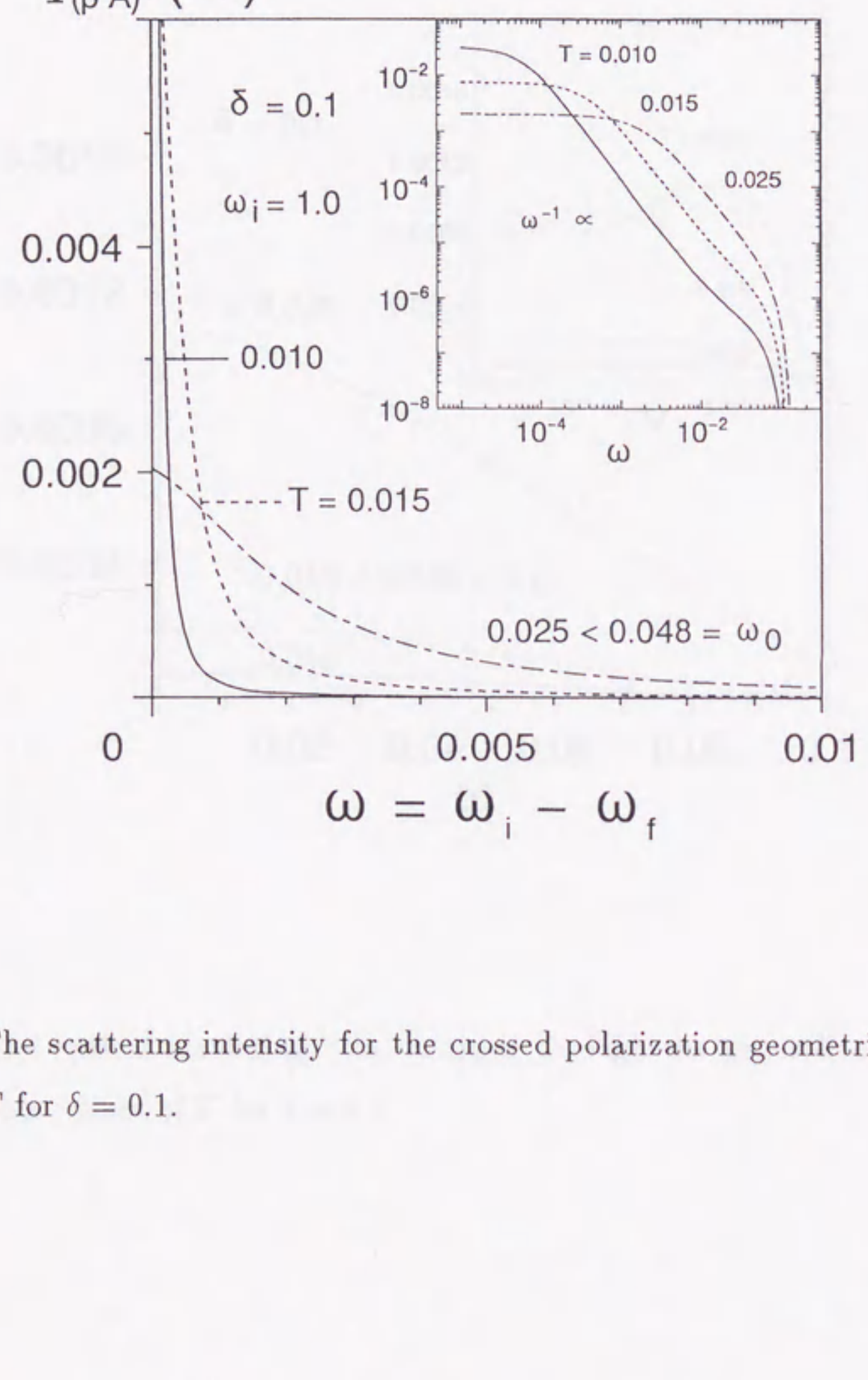

Fig.18 The scattering intensity for the crossed polarization geometries at various values of T for $\delta = 0.1$.

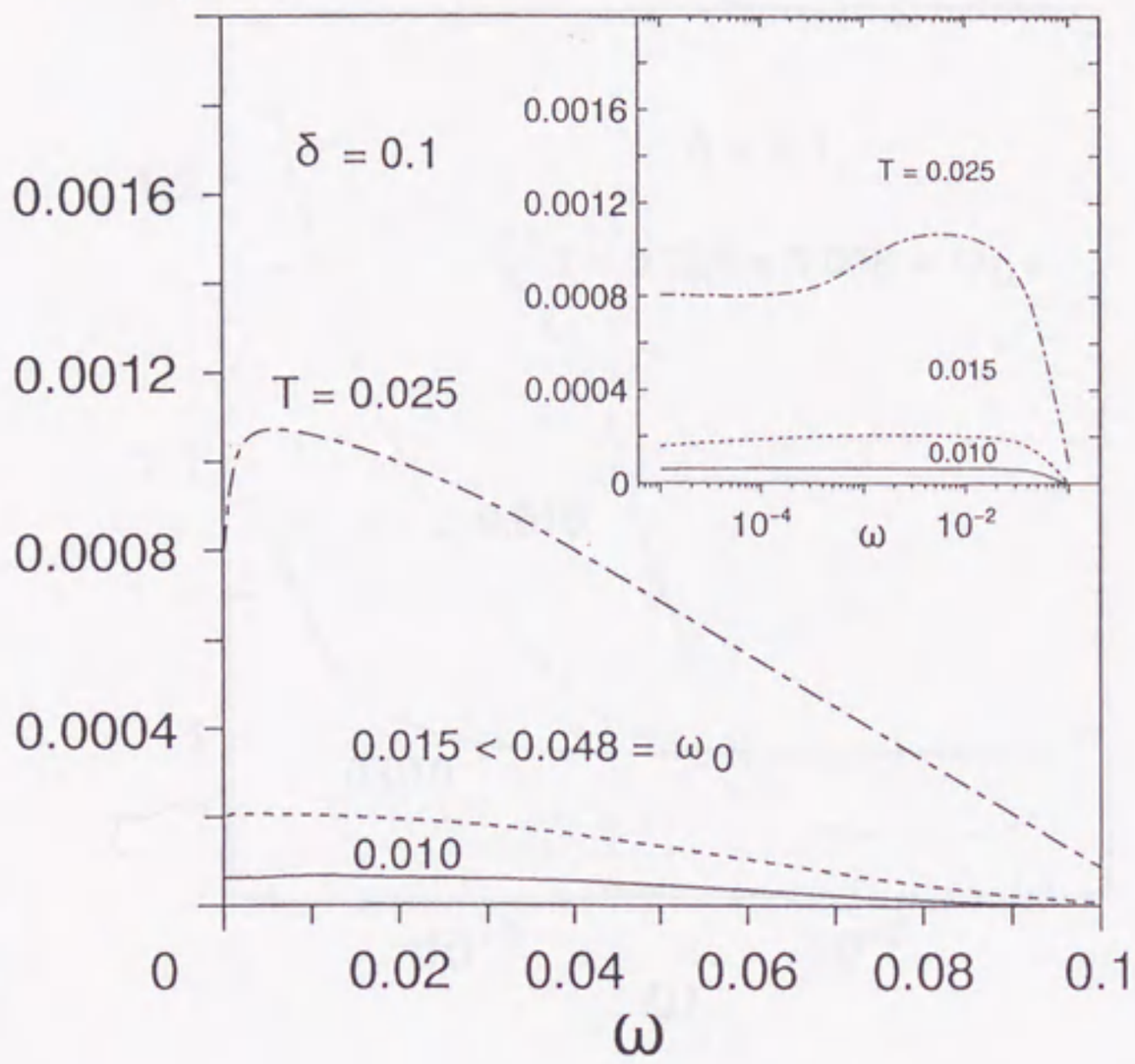

Fig.19 The optical scattering rate obtained through the generalized Drude analysis at various values of T for $\delta = 0.1$.

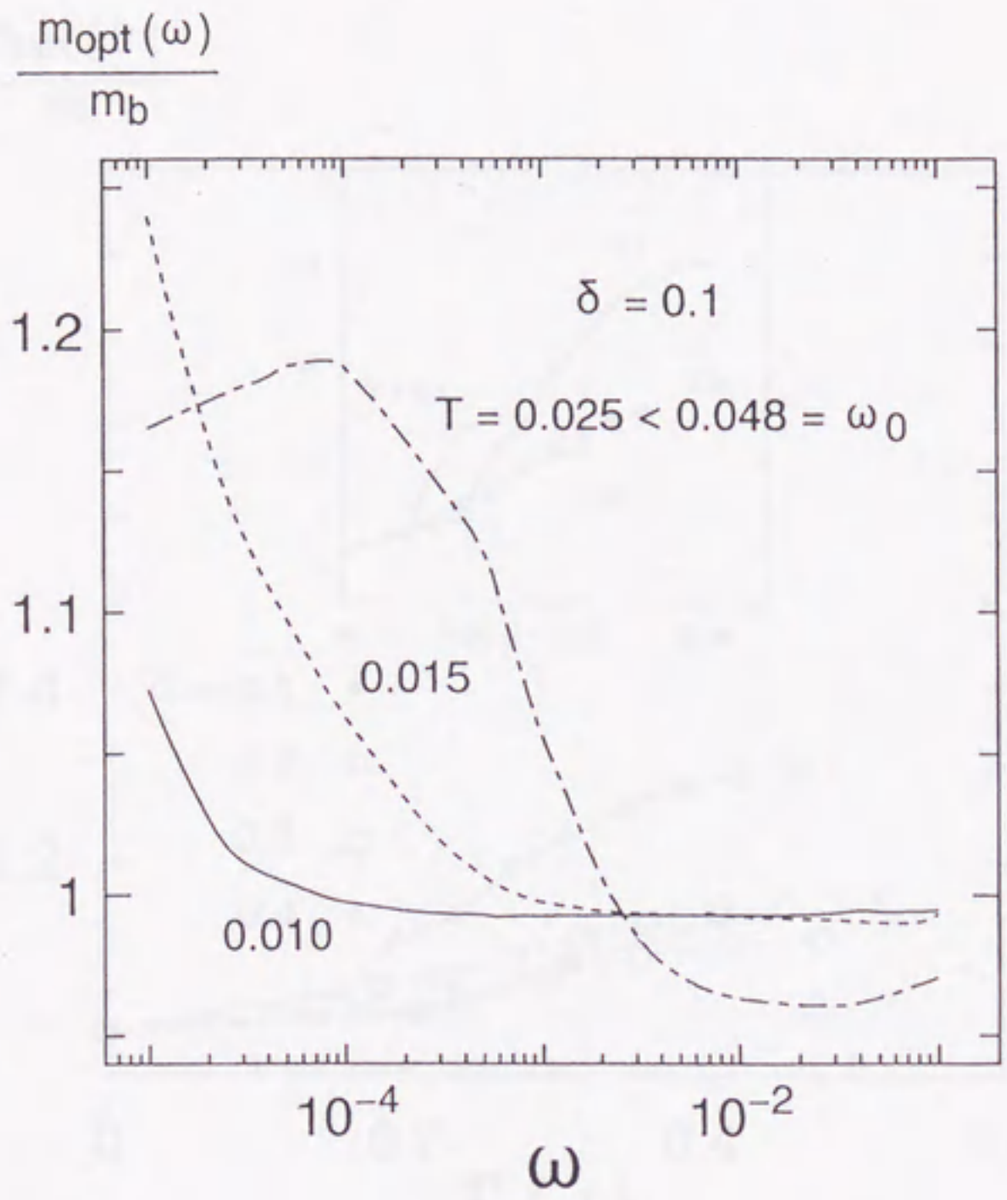

Fig.20 The optical mass obtained through the generalized Drude analysis at various values of T for $\delta = 0.1$.

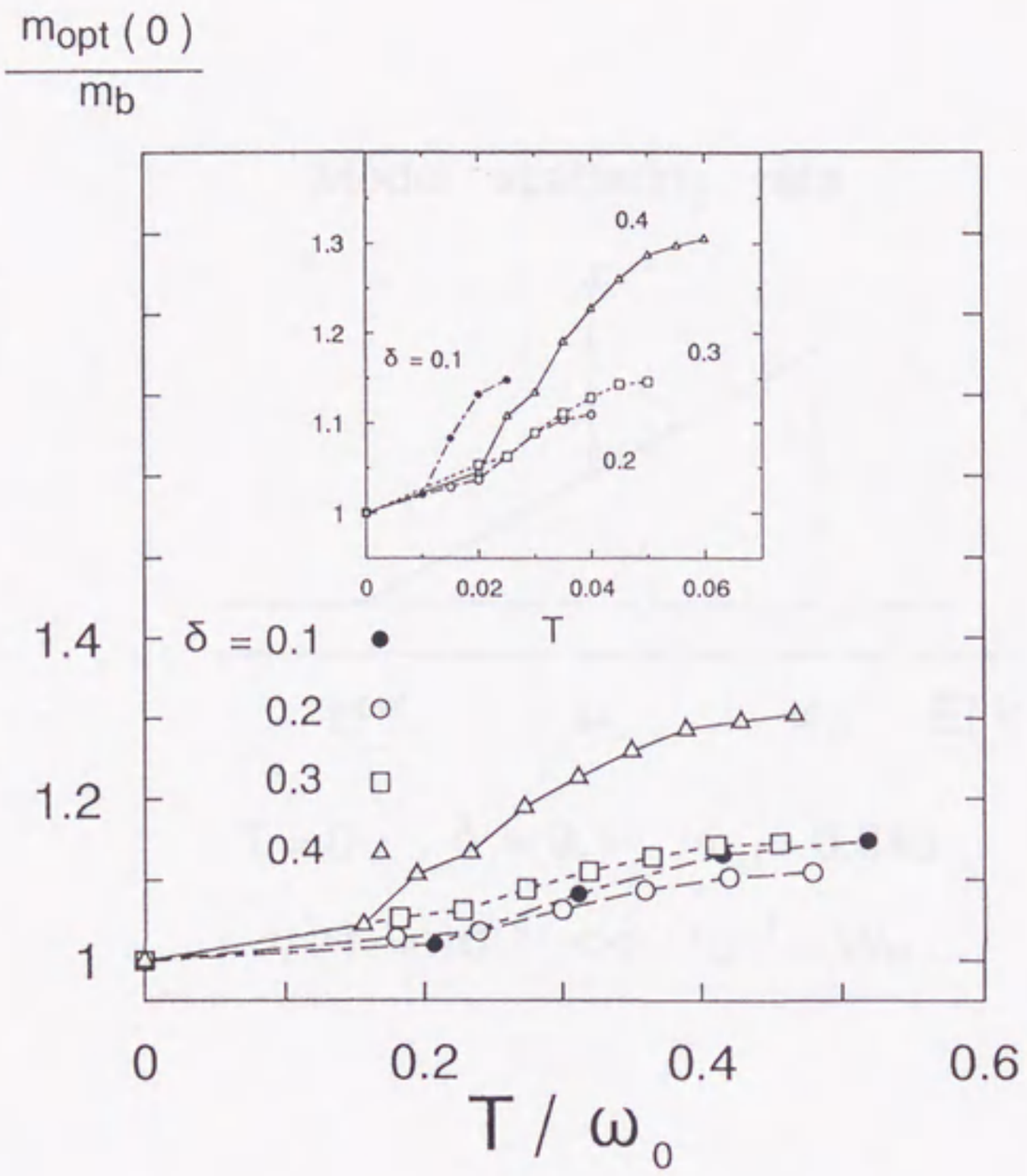

Fig.21 T-dependence of the optical mass in the low frequency limit for $\delta = 0.1, 0.2, 0.3,$ and 0.4 at $T \lesssim 2T_0$.

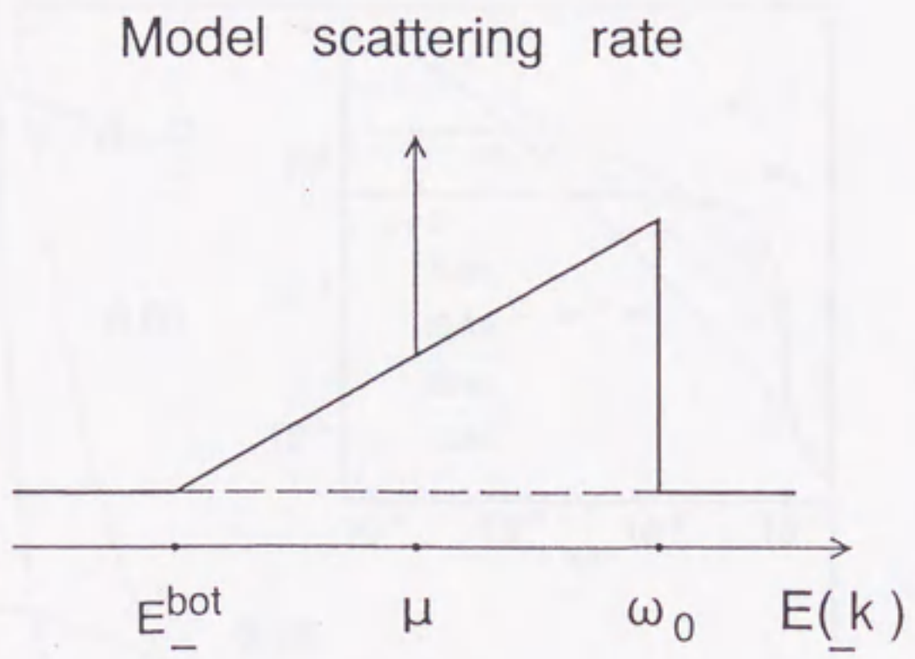

Fig.22 A model for the quasi-particle scattering rate together with a set of parameters taken for investigating the origin of the ω-dependence of the optical mass $m_{\rm opt}(\omega)$.

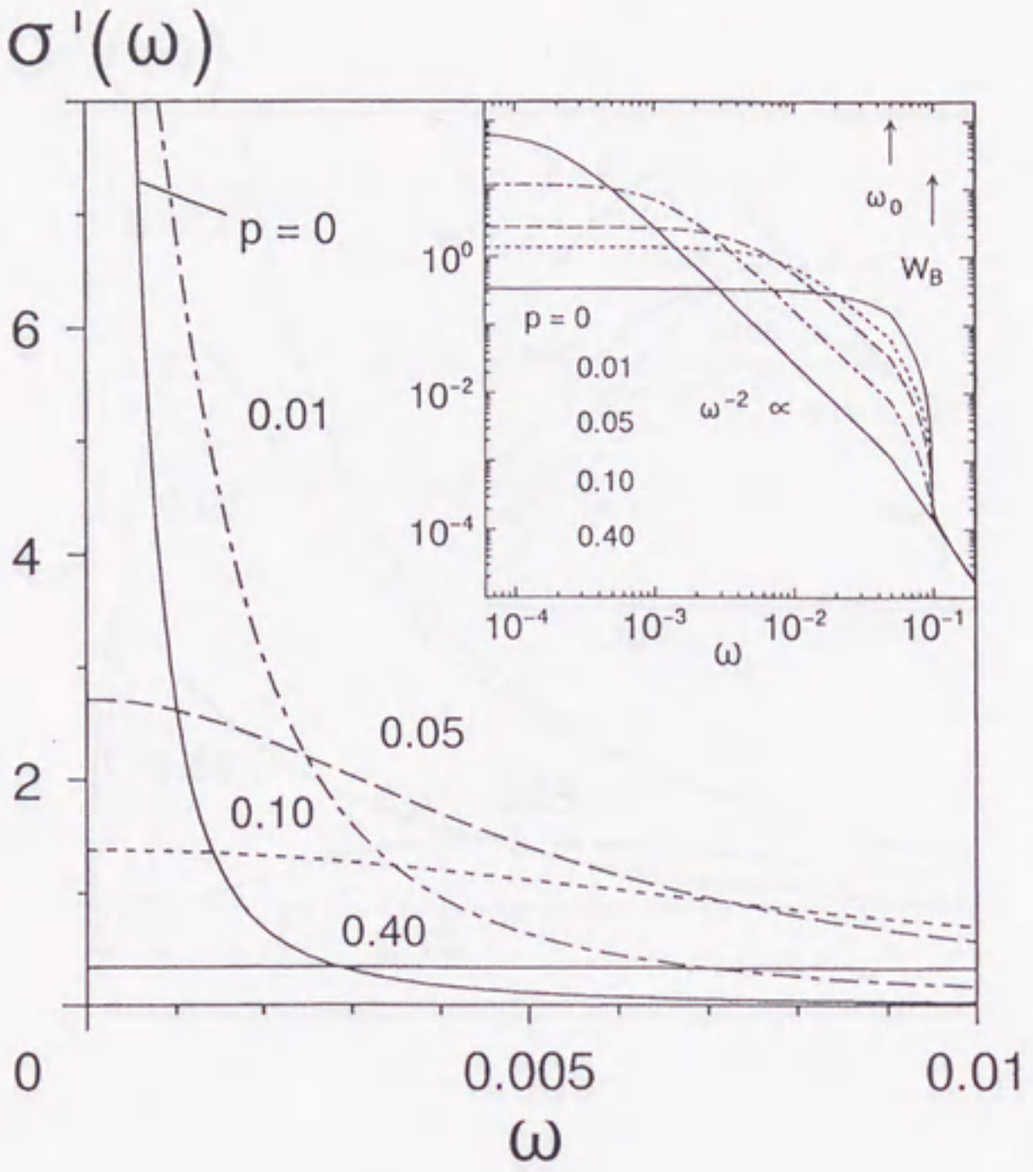

Fig.23 p-dependence of the real part of the conductivity. The cusps at $\omega = \omega_0$ seen in the inset are due to the Fermi edge at $T = 0$.

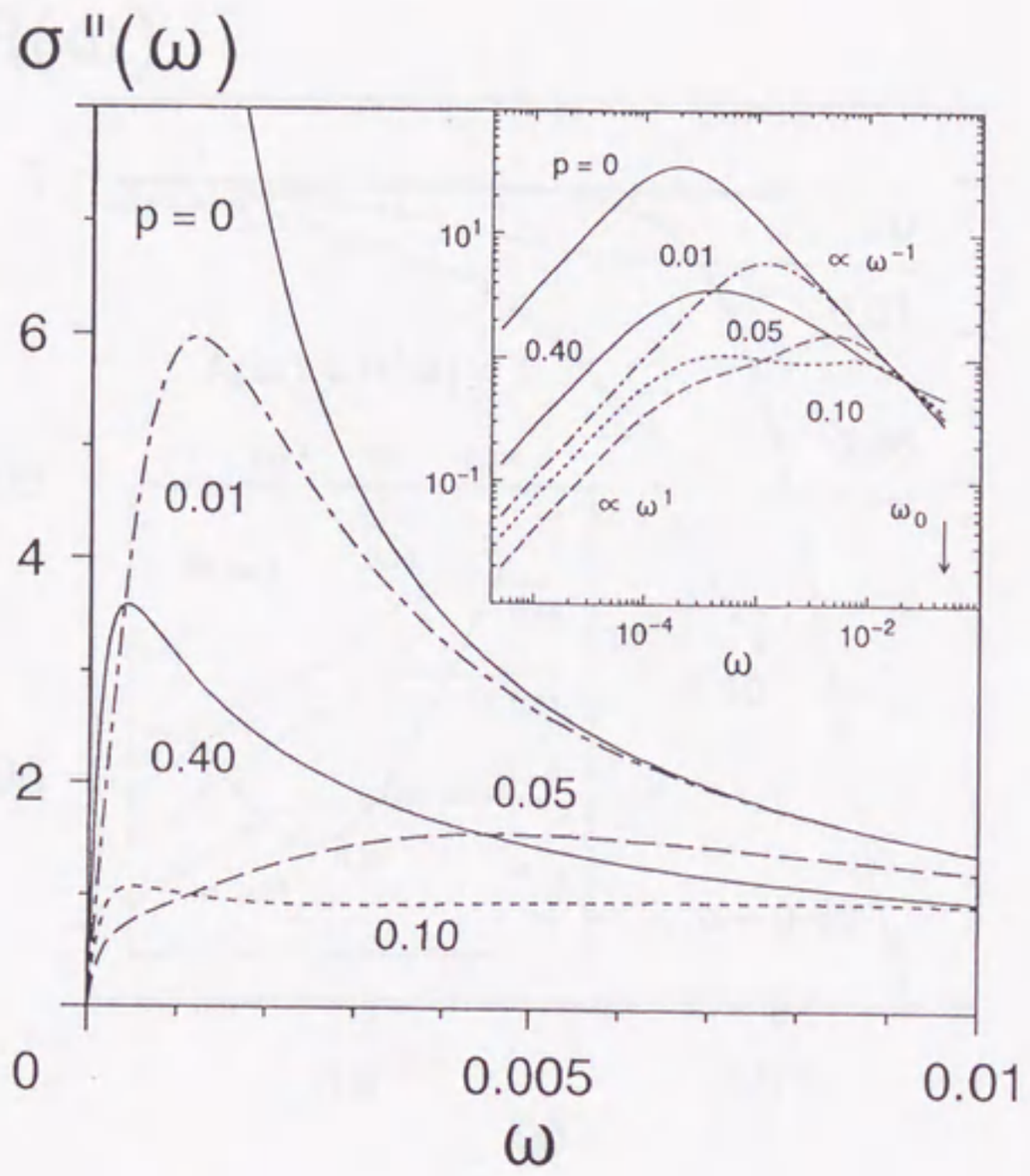

Fig.24 p-dependence of the imaginary part of the conductivity. Note that the non-monotonic shift of the position and the height of the peak with increasing p.

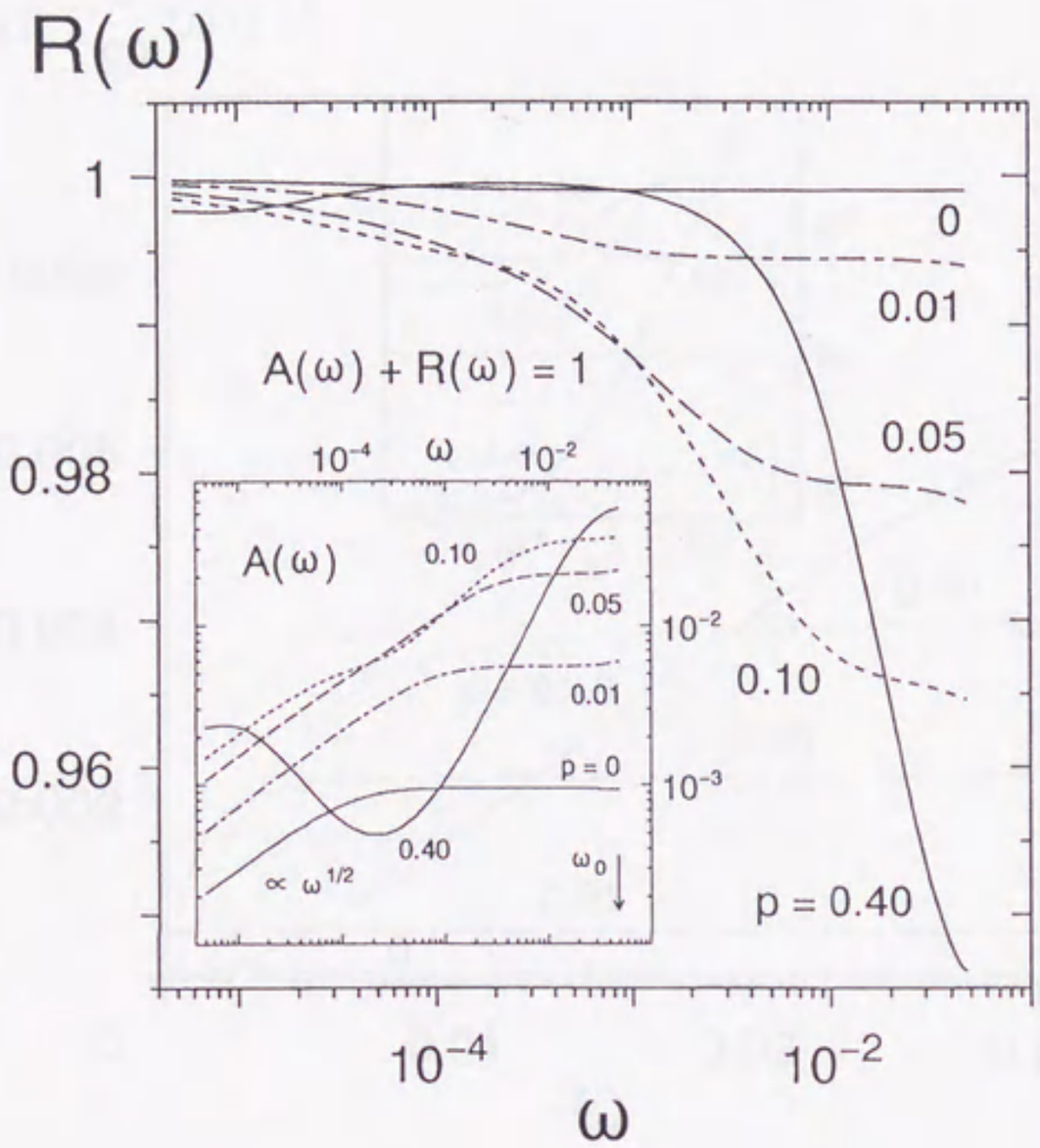

Fig.25 p-dependence of the reflectivity together with the absorptivity shown in the inset.
Note that the non-monotonic behaviors of the curves corresponding those in Fig.24.

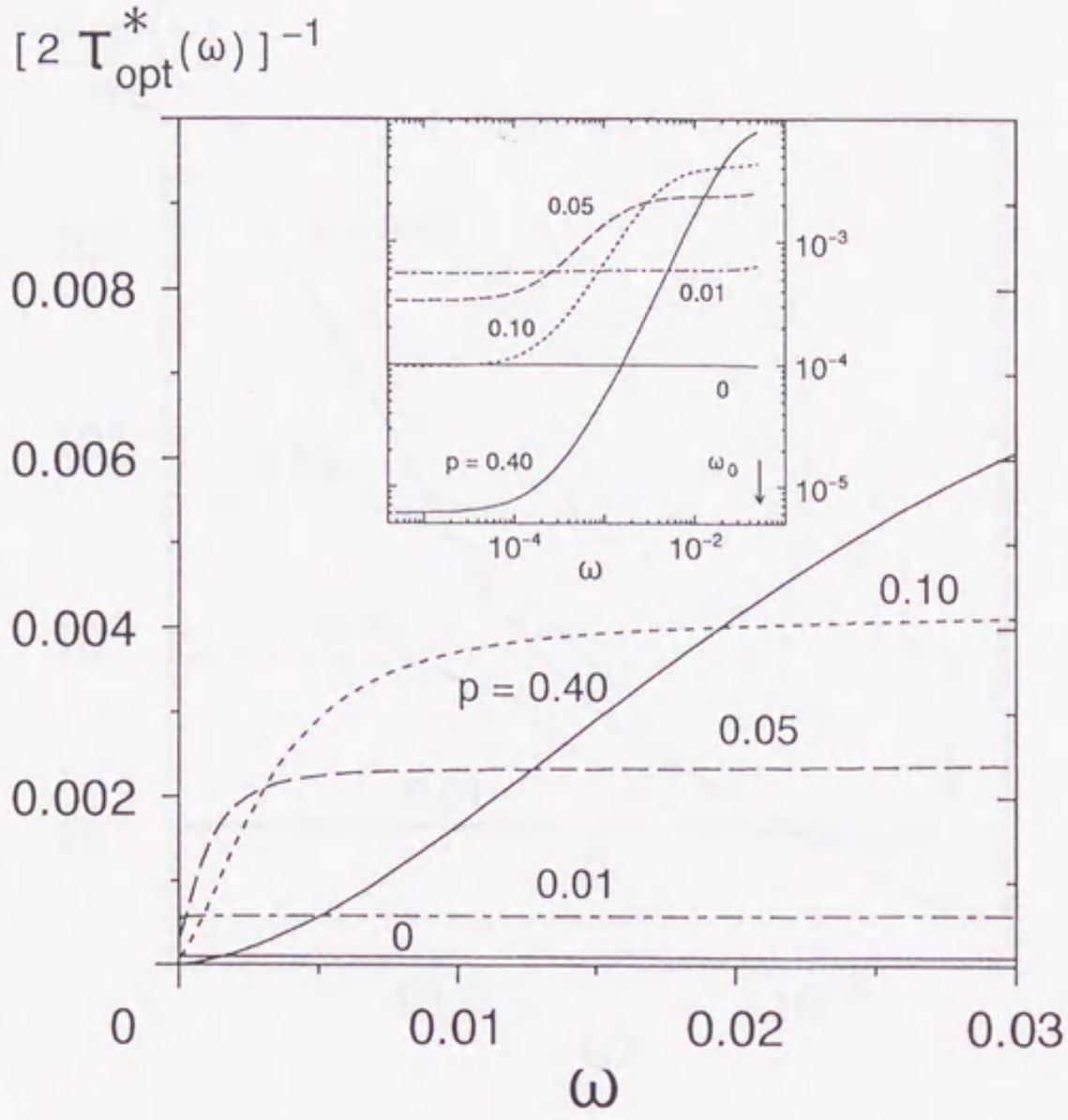

Fig.26 p-dependence of the optical scattering rate obtained through the generalized Drude analysis. The ω-dependence becomes significant at $p > 0.01 \simeq p_c$.

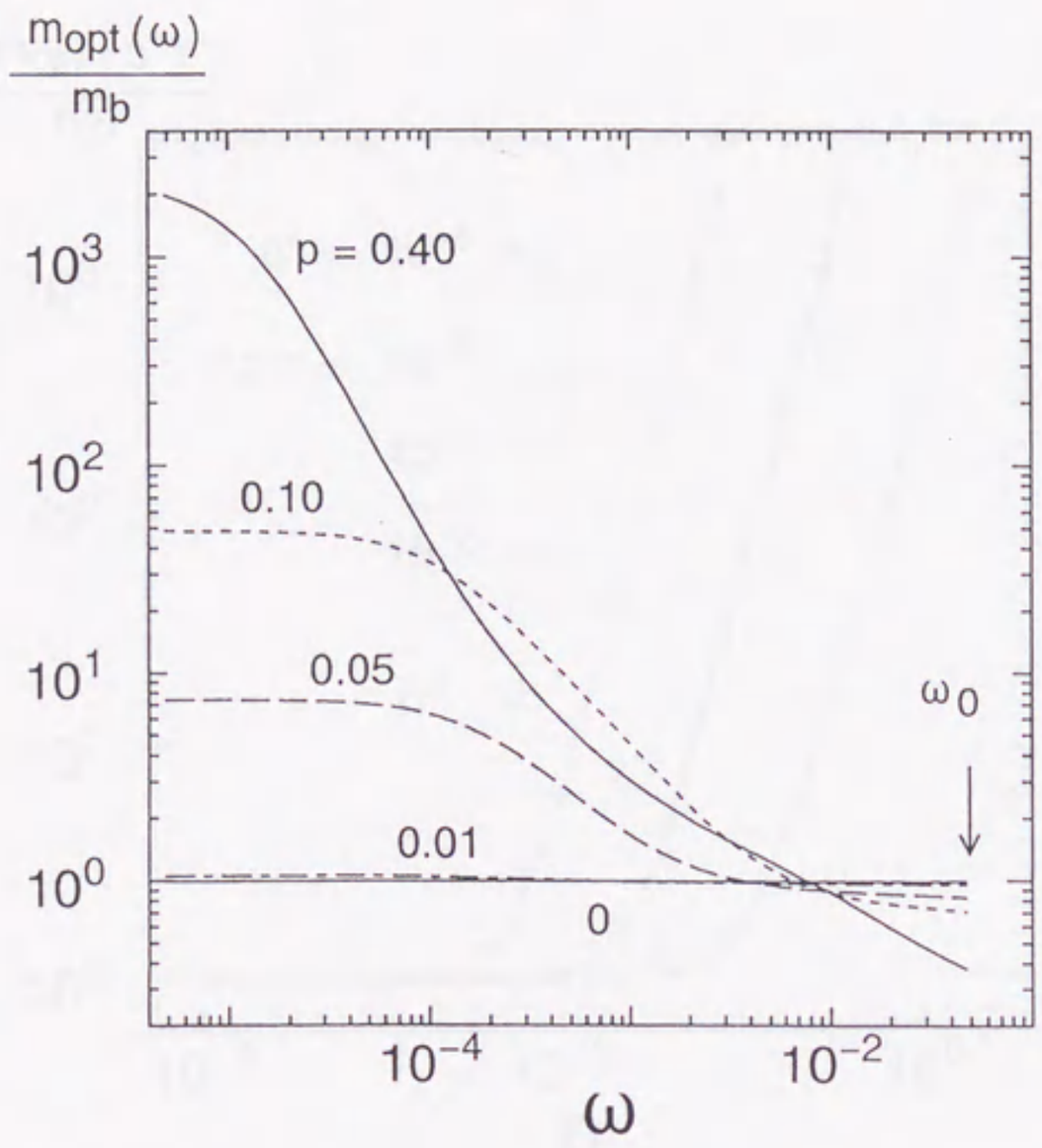

Fig.27 p-dependence of the optical mass obtained through the generalized Drude analysis. Note that the optical mass at low frequencies is significantly enhanced at $p > 0.01 \simeq p_c$.

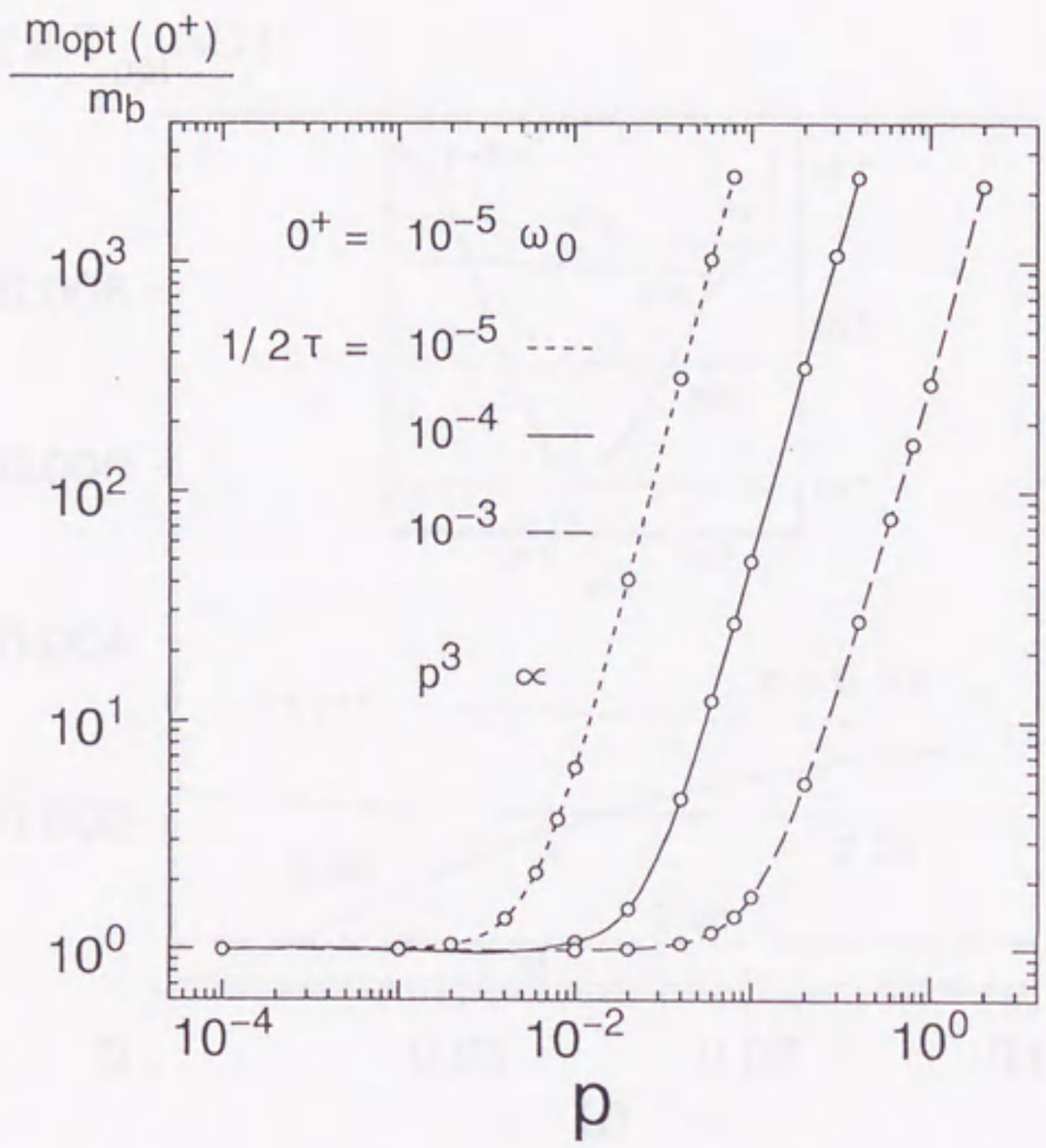

Fig.28 $(2\tau)^{-1}$-dependence of the optical mass at lowest frequencies. We find that the optical mass is proportional to p^3.

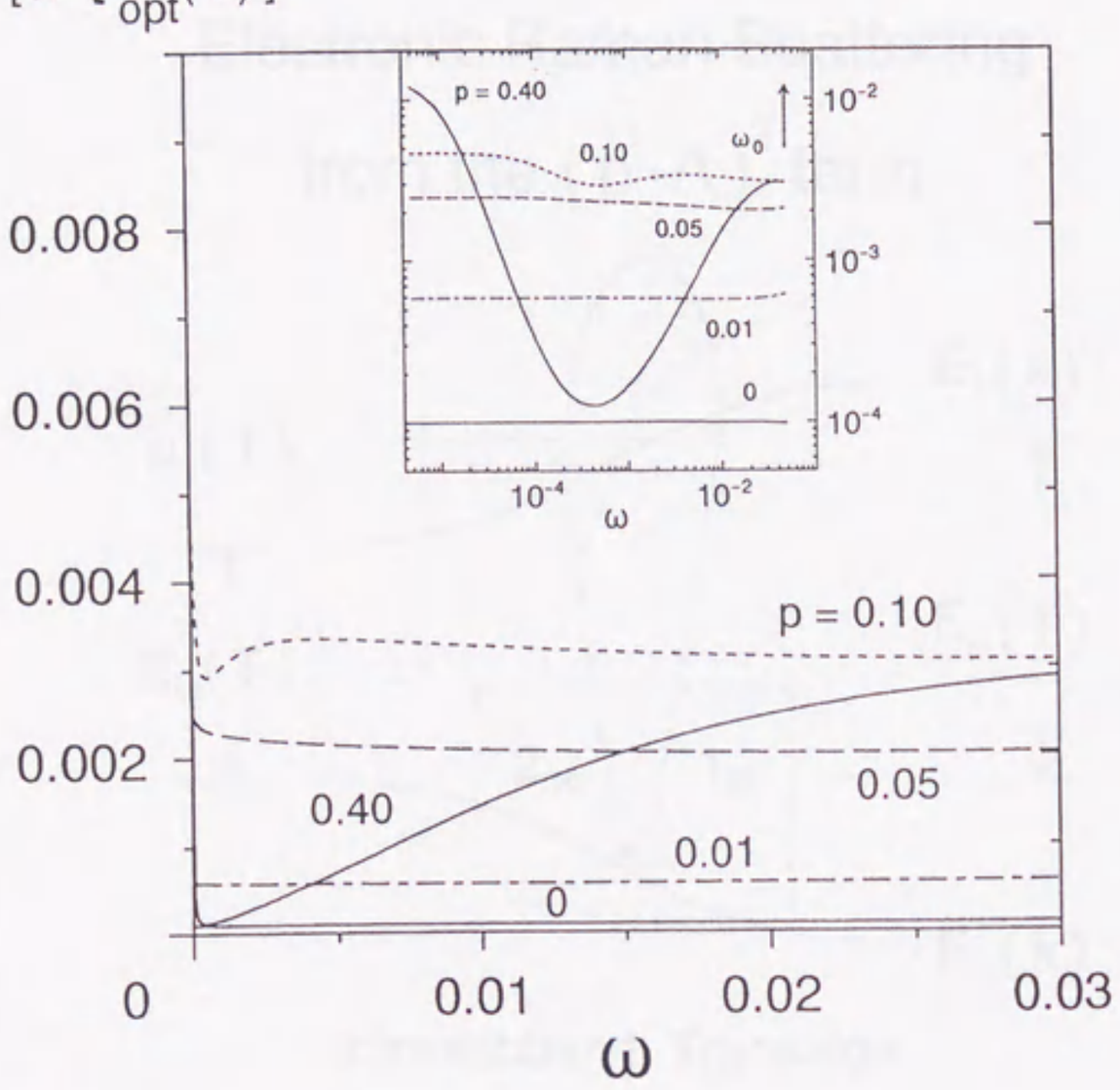

Fig.29 p-dependence of the optical scattering rate determined by eq.(4.5.7).

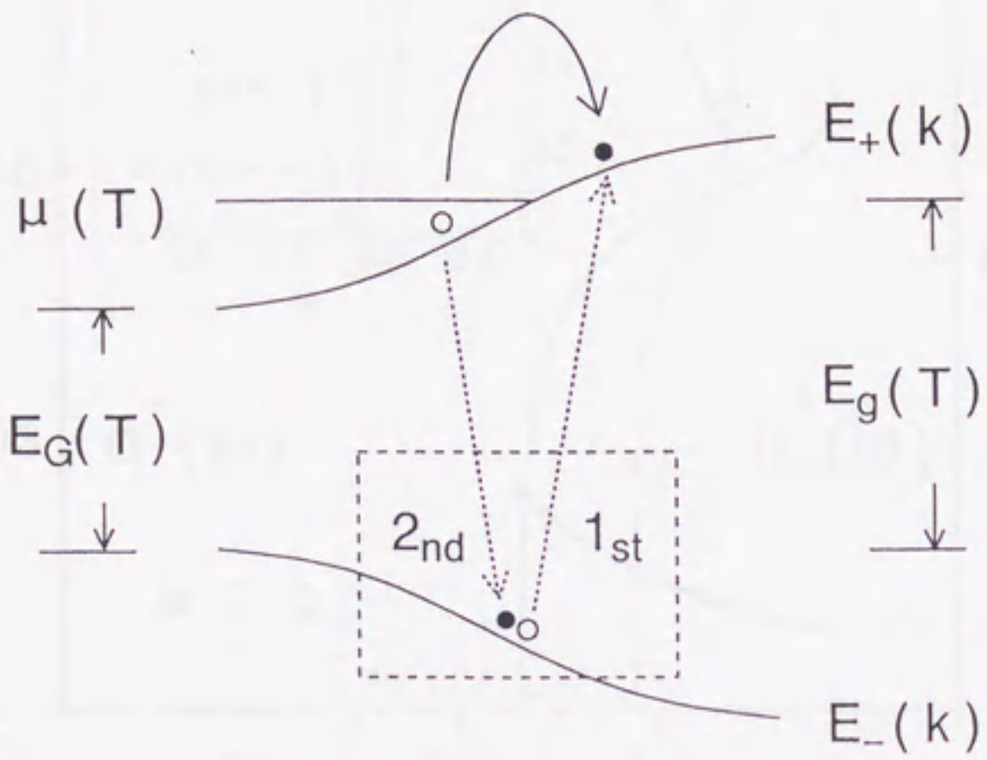

Fig.30 A schematic view of the resonant electronic Raman process, the process dominantly contributing to the scattering intensity through the $(\mathbf{p} \cdot \mathbf{A})^2$-term.

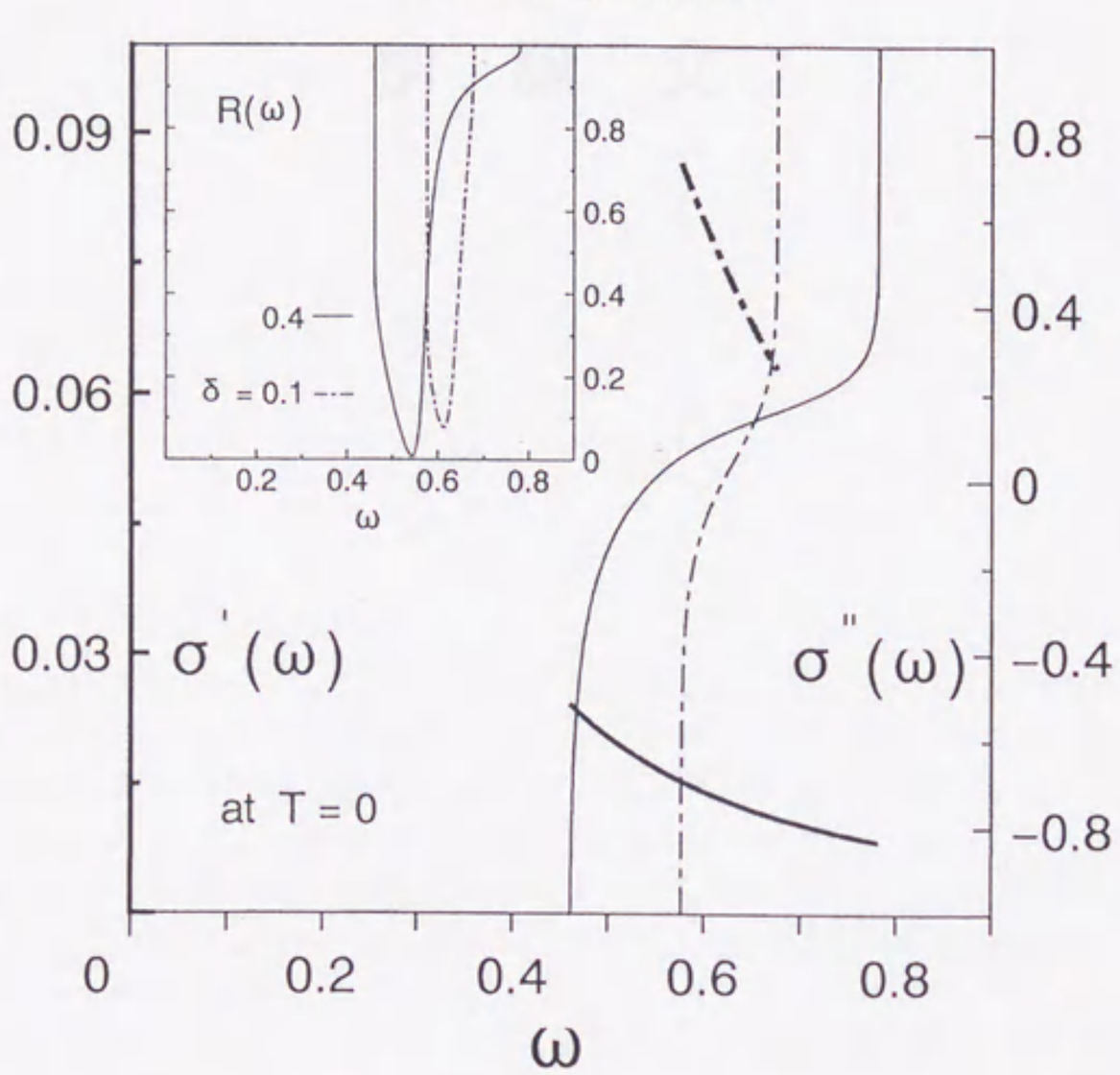

Fig.31 Transport coefficients for the interband transition for $\delta = 0.1$ and 0.4 at $T = 0$. The thick line denotes the real part of the conductivity and the thin line the imaginary part.